Insights into NAD homeostasis in the compartmentalized cell

Magali R. VanLinden

Dissertation for the degree of philosophiae doctor (PhD)
at the University of Bergen

2015

Dissertation date: August 24th, 2015

Year: 2015

Title: Insights into NAD homeostasis in the compartmentalized cell

Author: Magali R. VanLinden

Print: AIT OSLO AS / University of Bergen

Scientific environment

The work presented in this dissertation was carried out at the Faculty of Mathematics and Natural Sciences at the Department of Molecular Biology between May 2012 and May 2015 under the supervision of Professor Mathias Ziegler, and co-supervised by Professor Rein Aasland. This project was financed by Norges Forskningsråd and the Lauritz Meltzer Høyskolefond.

Acknowledgements

I consider myself extremely lucky to have been surrounded by amazing people during the journey that this PhD has been.

First and foremost, I want to express my deepest gratitude to my supervisor, Professor Mathias Ziegler. Your never-ending support and faith in me kept me on track, and your enthusiasm for Science was truly inspiring.

I would also like to thank my co-supervisor, Professor Rein Aasland for always being available, and keeping an eye on the progress of this work.

This experience would not have been the same without the present and former members of "Lab 5". In particular, I want to thank Renate (Bunny) Hvidsten Skoge, Christian Dölle, Marc Niere, Johannes Rack, and Charlotte Vandermeulen. I'm not always easy to deal with, and you all did a great job (especially Marc!). Coming to work every day was a real pleasure, and bad days in the lab were always better with you around. I will definitely miss the coffee breaks, Thanksgivings, meatballs, beers, lab retreats, poker nights, and so on and so forth. I would also like to thank the " better halves", Kari, Heike, and Luca, for always being part of the fun! I am glad to call you all Friends!

I would also like to thank everyone at MBI: group leaders, fellow PhD students, the administration, and the technical staff for contributing to a great working environment.

To my family and friends, near and far, thank you for always believing in me.

Cedric, the word "support" does not even start to describe what you have done for me. I would not have made it without you…Merci

Magali,

May 20th, 2015

Table of Contents

List of publications

Paper I: Rack, J. G., VanLinden, M. R., Lutter, T., Aasland, R., and Ziegler, M. (2014) Constitutive nuclear localization of an alternatively spliced sirtuin-2 isoform. *J. Mol. Biol.* **426**, 1677-1691

Paper II: VanLinden, M.R.*, Dölle, C.*, Pettersen, I.K.N., Kulikova, V.A., Niere, M., Agrimi, G., Palmieri, F., Nikiforov, A.A., Tronstad, K.J., and Ziegler, M. (2015) Subcellular distribution of NAD+ between cytosol and mitochondria determines the metabolic profile of human cells.

(Submitted Manuscript)

** Shared 1st authorship*

Paper III: Dölle, C., Skoge, R. H., VanLinden, M. R., and Ziegler, M. (2013) NAD biosynthesis in humans--enzymes, metabolites and therapeutic aspects. *Curr. Top. Med. Chem.* **13**, 2907-2917

(Review)

Abbreviations

2'/3' *O*AADPR	2'/3' *O*-acetyl ADP ribose
AceCS1/2	acetyl-coenzyme A synthase1/2
Acetyl-CoA	acetyl coenzyme A
AMP	adenosine monophosphate
AMPK	AMP kinase
ADP	adenosine diphosphate
ADPr	ADP-ribose
*At*NDT2:	*Arabidopsis thaliana* nicotinamide adenine dinucleotide transporter 2
ATP	adenosine triphosphate
BER	base excision repair
BMAL1	brain and muscle ARNT-like 1
cADPr	cyclic ADP-ribose
cAMP	cyclic AMP
CAS	CRISPR associated protein
cDNA	complementary DNA
CobB	prokaryotic sirtuin homolog
CPS1	carbamoylphosphate synthase 1
ChREBP	carbohydrate response element binding protein
CREB	cAMP response element binding
CRISPR	clustered regularly interspaced short palindromic repeats
CRM1	chromosome region maintenance 1 protein homolog
CtIP	DNA endonuclease RBBP8
DBC1	deleted in breast cancer 1
ETC	electron transport chain
FMN	flavin mononucleotide
FOXO1	forkhead box protein O1
GDH	glutamate dehydrogenase
H1	histone 1
H1K26	histone 1 lysine 26
H2B	histone 2B
H3K9	histone 3 lysine 9
H3K56	histone 3 lysine 56
H4K16	histone 4 lysine 16
H4K20	histone 4 lysine 20
HEK293	human embryonic kidney cells
HIF1α	hypoxia inducible factor 1-alpha
HMGCS2	3-hydroxy-3-methylglutaryl-coenzyme A synthase 2
IDH2	isocitrate dehydrogenase 2
KAT/HAT	lysine acetyltransferase
KDAC	lysine deacatylase
LCAD	long-chain acyl-coenzyme A dehydrogenase
LC-MS	liquid chromatography-mass spectrometry
LDH	lactate dehydrogenase

LXR	liver X receptor
MART	mono-ADP-ribosyl transferase
MCD	malonyl-coenzyme A decarboxylase
mRNA	messenger RNA
MnSOD	superoxide dismutase [Mn]
NA	nicotinic acid
NADK	NAD kinase
NA(A)D(P)	nicotinamide (nicotinic acid) adenine dinucleotide (phosphate)
Nam	nicotinamide
NADS	NAD synthase
N(A)MN	nicotinamide (nicotinic acid) mononucleotide
NAPRT	nicotinic acid phosphoribosyl transferase
NamPRT	nicotinamide phosphoribosyl transferase
NAR	nicotinic acid riboside
NFκB	nuclear factor kappa-light-chain-enhancer of activated B cells
NES	nuclear export signal
NLS	nuclear localization signal
NMNAT	nicotinamide mononucleotide adenylyltransferase
NR	nicotinamide riboside
NRK	nicotinamide riboside kinase
OTC	ornithine carbamoyltransferase
P53	cellular tumor antigen P53
P300	histone acetyltransferase p300
PAR	poly-ADP-ribose
PARAPLAY	PAR assisted protein localization assay
PARG	poly-ADP-ribose glycohydrolase
PARP1	poly-ADP-ribose polymerase 1
PARylation	poly-ADP-ribosylation
PCR	polymerase chain reaction
PDHE2	pyruvate dehydrogenase subunit E2
PEPCK1	phosphoenolpyruvate carboxykinase 1
PGC1α	peroxisome proliferator-activated receptor gamma coactivator 1-alpha
PRPP	phosphoribosyl pyrophosphate
PTEN	phosphatase and tensin homolog
QA	quinolinic acid
QAPRT	quinolinic acid phosphoribosyl transferase
rDNA	ribosomal DNA
*Sc*NDT1	*Saccharomyces cerevisiae* nicotinamide adenine dinucleotide transporter 1
SDH2	succinate dehydrogenase 2
SOD1	superoxide dismutase [Cu-Zn]
Sir2p	silent information regulator 2
SIRT	sirtuin
SLC25A17	peroxisomal membrane protein PMP34
SLC25A32	mitochondrial folate transporter

SLC25A33	solute carrier family 25 member 33
SLC25A36	solute carrier family 25 member 36
SSBR	single strand break repair
TAF_I68	RNA polymerase I-specific TBP-associated factor 68 kDa
TARG	terminal-ADP-ribose glycohydrolase
TCA	tricarboxylic acid
Tip60	histone acetyltransferase tip60
TNFα	tumor necrosis factor- alpha
UTR	untranslated region
VLCAD	very long-chain acyl-coenzyme A dehydrogenase

Abstract

The compartmentalized nature of eukaryotic cells requires the distribution of enzymes, metabolites, and cofactors among the organelles. This includes nicotinamide adenine dinucleotide (NAD), an essential coenzyme, precursor, and substrate to many cellular reactions. For instance, this dinucleotide is used by the NAD^+-dependent deacetylase sirtuin2 (SIRT2). The cytosolic location of this protein is in apparent contradiction to the nuclear location of some of its targets. In this study, whether a hitherto unidentified nuclear SIRT2 isoform could account for nuclear SIRT2-mediated deacetylation was investigated. A novel human SIRT2 isoform (SIRT2 isoform 5) was identified and shown to reside in the nucleus. Strikingly, this protein did not exhibit deacetylase activity towards several known SIRT2 targets. However, it retained the ability to interact with p300 in a NAD^+-dependent manner. These results suggest a non-catalytic function for SIRT2-isoform 5 in the nucleus of human cells.

The distribution of NAD^+-consuming enzymes in subcellular compartments highlights the necessity for the maintenance of the different NAD^+ pools. Mitochondria contain a substantial amount of the total cellular NAD^+. In yeast and plants, mitochondrial NAD^+ transporters ensure the maintenance of that pool, whereas in mammals such a transporter could not be identified so far. To address this problem, the closest human homologs to the *Arabidopsis thaliana* NAD^+ transporter NDT2 were expressed in human cells. None of them increased mitochondrial NAD^+ availability, indicating they do not function as NAD^+ carriers in humans. This finding argues for autonomous NAD biosynthesis in human mitochondria. Indeed, nicotinamide mononucleotide adenylyltransferase 3 (NMNAT3), an isoform of the enzyme that catalyzes the last step of NAD synthesis, was reported to be localized to the mitochondria. However, all previous studies were done with a recombinant protein, and the presence of the endogenous protein is still debated. This study conclusively demonstrates the presence of the endogenous NMNAT3 protein in human mitochondria, supporting the idea of autonomous biosynthesis within these organelles.

On the basis of the observation that the expression of plant and yeast NAD^+ transporters in human cells strongly increased mitochondrial NAD^+ content, the consequences of increased mitochondrial NAD^+ availability were investigated. Stable expression of the plant NAD^+ transporter NDT2 in HEK293 cells resulted in growth retardation as well as a metabolic shift from mitochondrial respiration to glycolysis, and conferred increased resistance towards cell death induced by NAD^+-depletion. These results suggest that distribution of NAD^+ between the cytosol and the mitochondria is a major determinant of the metabolic profile of human cells.

1. Introduction

A tremendous amount of research activities in molecular biology focuses on understanding both the function, and the dynamic interplay of proteins in living systems. Among this highly diverse class of biological macromolecules, enzymes are of particular interest owing to their ability to lower the activation energy required for a reaction to take place. No matter how important enzymes are, most of them are not capable of catalyzing their dedicated reactions on their own, and require additional cofactors referred to as coenzymes. The identification of these coenzymes thus opened up new directions, and their characterization revealed fascinating features. In 1906, roughly two centuries after the first description of enzymes, Arthur Harden and William Young identified, that besides enzymes, a low molecular weight compound was required for fermentation and alcohol production. In the late 1920's, Hans von Euler-Chelpin isolated this coenzyme, determined that it was composed of a sugar, adenine, and phosphate, and later described its dinucleotide nature. Finally, Arthur Kornberg described the synthesis of this coenzyme, namely nicotinamide adenine dinucleotide (NAD) [1].

NAD is a dinucleotide consisting of two mononucleotides, nicotinamide mononucleotide (NMN) and adenosine monophosphate (AMP), joined by their phosphate groups (Figure 1). NAD exists in the oxidized (NAD^+) and reduced (NADH) forms, which reflects its function as a major electron carrier in metabolic redox reactions. As such, it is involved in major metabolic pathways, including the tricarboxylic acid (TCA) cycle, β-oxidation of fatty acids, amino acid catabolism, and the urea cycle. Furthermore, the cleavage of NAD^+ in nicotinamide and ADP-ribose is the basis for post-translational protein regulation through ADP ribosylation, and deacetylation, and contributes to signaling events such as calcium signaling pathways and acetylation of histones in chromatin.

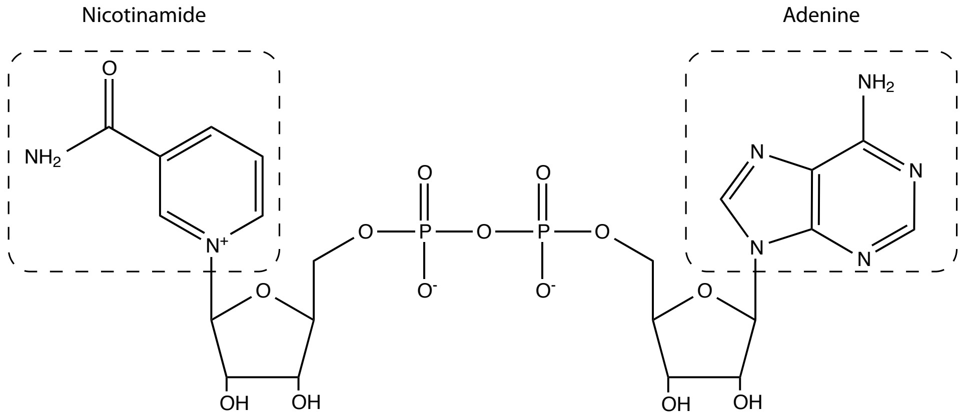

Figure 1: Structure of NAD. Nicotinamide adenine dinucleotide (NAD) consists of two nucleotides joined by phosphate groups. The nucleotides contain different bases: nicotinamide and adenine, respectively (boxed).

1.1 NAD and NADP as potent redox agents

The convertibility of the two forms, NAD^+ and NADH (Figure 2), is the cornerstone of the role of NAD as coenzyme to many catabolic reactions involving dehydrogenases. In these reversible reactions, NAD^+ accepts two electrons and a proton to be converted to NADH. For example, catabolism of glucose starts with glycolysis and the conversion of glucose to pyruvate. Pyruvate is subsequently transferred to the mitochondria where it is converted to acetyl coenzyme A (acetyl-CoA) and degraded during the TCA cycle. In glycolysis, oxidation of glyceraldehyde 3-phosphate is a dehydrogenation reaction involving the transfer of the hydrogen to NAD^+, thus reducing it to NADH. Similarly, the TCA cycle enzymes isocitrate dehydrogenase, α-ketoglutarate dehydrogenase, and malate dehydrogenase also reduce NAD^+ to NADH. In turn, complex I catalyzes the transfer of electrons from NADH generated in the mitochondria to a flavin mononucleotide (FMN)-containing flavoprotein of complex I of the electron transport chain (ETC). The transfer of electrons from one complex of the ETC to another is accompanied by the formation of a chemical and electrical gradient of protons across the mitochondrial inner membrane. This gradient constitutes the driving force of ATP synthesis.

Next to the NAD^+/NADH redox pair, their phosphorylated counterparts $NADP^+$ and NADPH constitute another redox couple that is largely involved in metabolic redox reactions. While many enzymes can use either, the presence of two similar but distinct redox pairs, with comparable redox potentials indicates that the two pairs are dedicated to different functions. While NAD is mostly present in the oxidized form and involved in catabolism, NADP is predominantly present as NADPH in cells and serves as the electron donor for reductive biosynthesis. For example, cholesterol is synthesized from acetyl-CoA in several steps. Among these reactions, those catalyzed by HMG-CoA reductase, squalene synthase and squalene monooxygenase convert NADPH to $NADP^+$. While oxidation and reduction of NAD is mainly involved in metabolic reactions, the NADP/NADPH couple fulfills a broader scope of functions. For example, oxidation of NADPH is required for the regeneration of reduced cytochrome P450 and glutathione involved in detoxification, and oxidative defense, respectively [2,3].

1.2 Signaling functions of NAD

In the late 1930's Otto Warburg characterized NAD as an electron carrier. This major discovery laid the ground for extensive research exploring this function, and for many years NAD was solely regarded as an electron carrier. However, the identification of NAD as the precursor to a new post-translation modification, namely poly-ADP-ribosylation [4], opened up the NAD field to new perspectives and since then, much research has been focusing on signaling events that are dependent on NAD and its derivatives. Remarkably, derivatives of both NAD and NADP have been associated with signaling pathways. For example, nicotinic acid adenine dinucleotide phosphate (NAADP), resulting from the exchange of the nicotinamide of NADP with nicotinic acid is considered to be the most potent intracellular calcium-mobilizing agent [1]. NAD^+ is also an important substrate for reversible post-translational modifications, as it serves as the ADP-ribose donor for ADP-ribosylation catalyzed by mono- and poly-ADP-ribosyltransferases. Moreover, deacetylation can be carried out by a group of NAD^+-dependent deacetylases known as sirtuins (Figure 2).

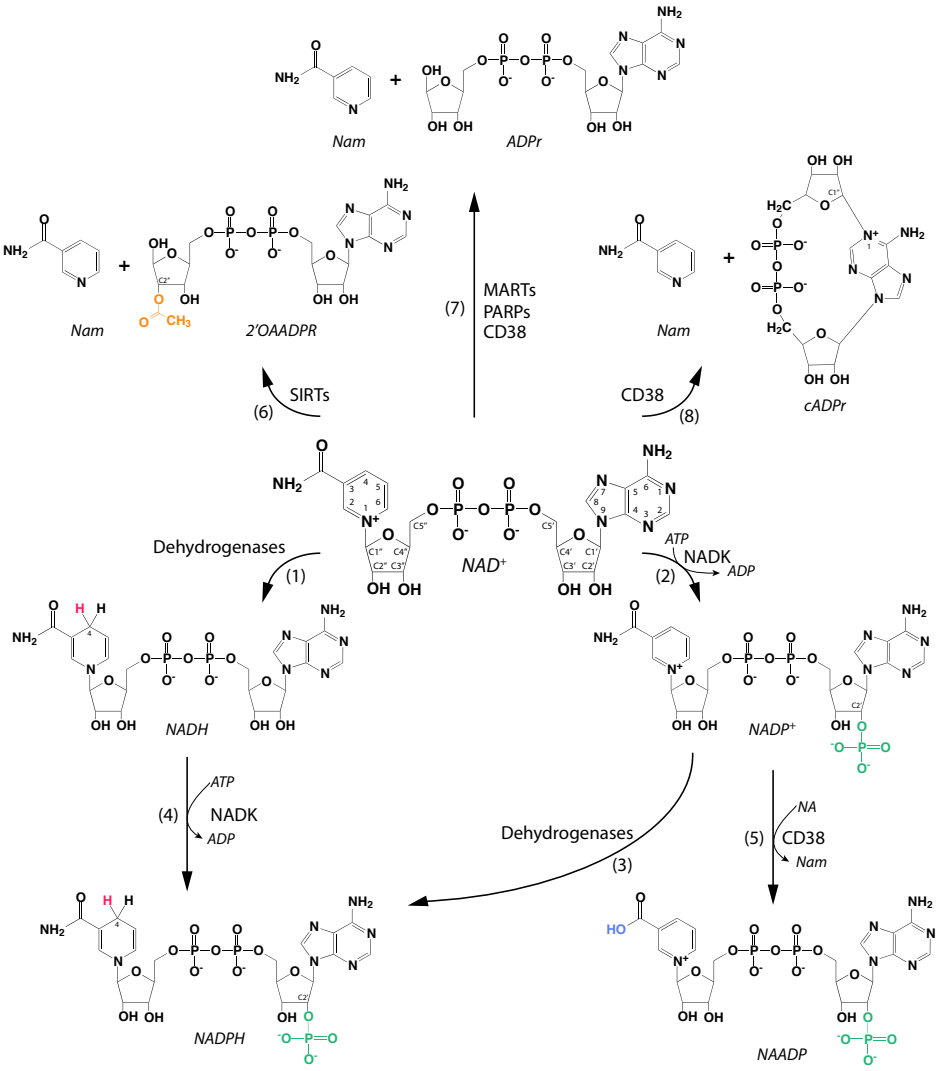

Figure 2: Metabolic and signaling conversions of NAD(P). (1) Nicotinamide adenine dinucleotide (NAD^+) is reduced at position 4 of the nicotinamide ring to NADH by dehydrogenases using NAD^+ as cofactor; (2) phosphorylated NAD^+ ($NADP^+$) is generated by phosphorylation at position C2' of the adenosine moiety, a reaction catalyzed by NAD Kinase (NADK), ATP is the phosphate donor; (3) NADP is reduced at position 4 of the nicotinamide ring to NADPH by dehydrogenases using $NADP^+$ as cofactor; (4) NADK phosphorylates NADH at position C2' (NADPH); (5) nicotinic acid adenine dinucleotide phosphate (NAADP) is generated from NADP by cyclic ADP-ribose hydrolase 1 (CD38) by exchange of the nicotinamide (Nam) with nicotinic acid (NA); (6) deacetylation by sirtuins (SIRTs) results in nicotinamide (Nam) and adenosine diphosphate-ribose (ADPr) acetylated at position C2" of the ribose formerly bound to Nam (2' OAADPR); (7) signaling reactions catalyzed by mono-ADP-ribosyl transferases (MARTs), poly-ADP-ribosyl transferases (PARPs) or CD38 cleave the glycosidic bond between Nam and ADPr; (8) CD38 can also generate cyclic ADPr (cADPr) by formation of a glycosidic bond between position C1" of the ribose formerly bound to Nam and position 1 of the adenine ring. Reductive hydrogen atoms highlighted in red; phosphate groups in green; hydroxyl group in blue and acetyl group in orange.

1.2.1 Poly-ADP-ribosylation.

Catalyzed by a group of enzymes known as poly-ADP-ribosyl polymerases (PARPs), poly-ADP-ribosylation (PARylation) is a reversible post-translational modification consisting in the cleavage of NAD^+ into nicotinamide and ADP-ribose, the ADP-ribose being subsequently transferred onto an acceptor protein, including PARP itself. Following attachment of an ADP-ribose unit onto the protein acceptor site, this ADP-ribose moiety serves in turn as the acceptor site for a subsequent ADP-ribose. By further elongation, polymers consist in either linear or branched structures of successive ADP-riboses linked by glycosidic bonds and varying in length (Figure 3). The negatively charged polymers will typically consist of 200 to 400 units of ADP-ribose with a branching point occurring every 20 to 50 units [5]. While NAD^+ concentration does not appear to play a major role in the activation of PARPs [6], the extent of PAR formation seems to depend on NAD^+ availability [7,8].

PARPs constitute a superfamily of 17 members sharing a conserved signature motif. Although the 17 members share some structural similarities, only a few members have been shown to catalyze PAR formation. Some other members can catalyze for example mono-ADP-ribosylation [9]. Owing to its abundance and activity, nuclear PARP1 is considered to be the major NAD^+-consuming enzyme in cells and has been extensively studied, especially with regards to its role in DNA single strand break repair (SSBR) [10]. Indeed, PARP1 recognizes DNA damages and modifies histones H1 and H2B, rendering chromatin more accessible to the repair machinery. Furthermore, PAR formation triggers cell-signaling events communicating the occurrence and extent of the damage to the cell. Based on these signals, the cell decides on the strategy (repair or suicide) to adopt. Finally, PARP activation leads to the recruitment of SSBR or base excision repair (BER) factors to the site of damage [9].

The NAD^+-consuming nature of PARP1, as well as its preference for auto-modification, can be exploited as a tool to enable visualization of cellular NAD^+ pools.

In this PAR Assisted Protein Localization AssaY approach (PARAPLAY), the catalytic domain of PARP1 is rendered constitutively active by deletion of the DNA binding domain and targeted to the compartment of interest. Whereas NAD^+ cannot be visualized by immunodetection methods, PAR can, and thus the extent of PAR formation reflects NAD^+ availability in any given organelle [11].

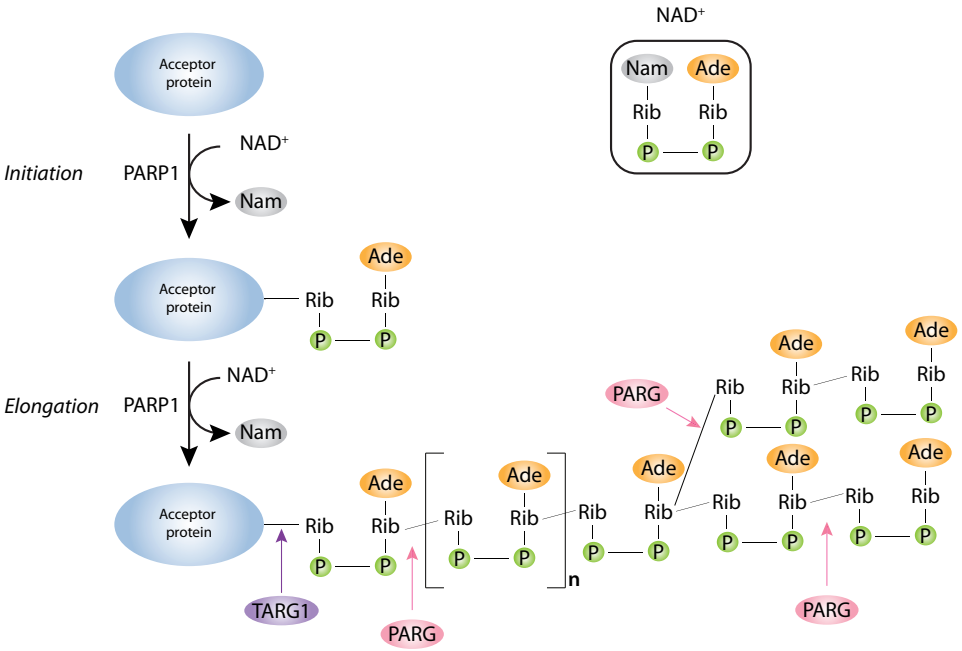

Figure 3: Poly-ADP-ribosylation catalyzed by PARP1. Poly-ADP-ribose polymerase 1 (PARP1) catalyzes the cleavage of oxidized nicotinamide adenine dinucleotide (NAD^+) (boxed) into nicotinamide (Nam) and ADP-ribose (ADPr), and subsequently transfers the ADP-ribose moiety onto the acceptor protein. Upon initiation, the first ADPr unit is transferred onto the acceptor protein. Polymer elongation results from the formation of glycosidic bonds between the riboses of two consecutive ADPr units (n, a number of ADPr units). Polymer branching occurs in the same way every 20 to 50 ADPr units. As it is a reversible modification, PAR can also be degraded: poly-ADP-ribose glycohydrolase (PARG) hydrolyzes the glycosidic bonds, except for the ester bond between the acceptor protein and the first ADPr unit, which is removed by terminal ADP-ribose glycohydrolase (TARG1). Nicotinamide: Nam; Adenine: orange; ribose: Rib; phosphate groups: P (adapted from [9]).

1.2.2 NAD^+-dependent deacetylation by sirtuins

Regulation of cellular processes through post-translational modifications is well known. Among these modifications, addition of the acetyl moiety of acetyl-CoA onto the ε-amino group of lysine residues is named acetylation and carried out by lysine acetyltransferases (KATs). Initially identified on histone tails, acetylation activates transcription by neutralizing the positive charge harbored by lysine residues. By doing so, the interaction between the negatively charged DNA backbone and histones is weakened, thereby resulting in euchromatin formation [12-14]. Moreover, acetylation also establishes binding sites for proteins harboring a bromodomain. These domains recognize acetylated lysines and contribute to processes such as transcription activation or repression, nucleosome rearrangement, and alteration of chromatin architecture [15,16]. Beyond histones, further investigations revealed that over 1700 non-histone proteins are also targets for acetylation, and that this modification regulates nearly all cellular processes [17].

Owing to the crucial role of acetylation, control of the acetylation state of the target proteins is of major importance. Hence, proteins catalyzing the removal of acetyl groups, namely deacetylases (KDACs), are equally important as KATs. KDACs can be divided in two superfamilies. The "classical" KDACs require a bivalent metal ion and hydrolyze the acetyl group releasing the deacetylated lysine and acetate [18]. In contrast, NAD^+-dependent deacetylases consume NAD^+ as a cofactor and release the deacetylated lysine and acetylated ADP-ribose [19].

The yeast silent information regulator 2 (Sir2p) was the first deacetylase identified to be NAD^+-dependent [19] and was demonstrated to participate, among others, in the silencing of the mating type loci and Ku-dependent double-strand DNA break repair [20,21]. Furthermore, Sir2p regulates transcriptional silencing of ribosomal DNA (rDNA), suppressing extrachromosomal rDNA circles arising from homologous recombination. This role in particular is believed to promote longevity in yeast. In line with this hypothesis, extra copies of *Sir2* increase yeast life span whereas deletion of *Sir2* has the opposite effect [22,23].

Seven homologs to Sir2p, named sirtuins (SIRTs), have been identified in mammals (SIRT1-7) [24,25]. Expressed ubiquitously in all tissues, they vary in their sub-cellular location and activity (Table 1). In spite of the fact that deacetylation activity has been reported for all SIRTs, the different members of the family favor different substrates. SIRT1, 2 and 3 have a strong deacetylase activity towards a wide variety of substrates, whereas SIRT 5 prefers the removal of malonyl and succinyl chains [26]. Recently, SIRT6 was found to cleave long-chain fatty acids, such as myristic acid, from lysine residues. Furthermore, the presence of free fatty acids appears to enhance the deacetylation activity of SIRT6 [27]. As for SIRT4 and SIRT7, the activities and substrates remain poorly understood.

Structure and catalytic mechanism of sirtuins

All sirtuins share a highly conserved catalytic domain, consisting of approximately 275 amino acids, but vary with regard to the lengths of their N- and C- terminal parts [24,28]. The 3D structure of the catalytic domain is highly similar for all sirtuins, including SIRT2, the sirtuin of interest in this study (Figure 4A). The overall SIRT2 structure consists of a large Rossman-fold domain, typical of NAD-binding enzymes, and a second smaller domain containing two modules: a zinc binding ribbon and a helical domain made of 3 or 4 α-helices [29,30]. The interface between the small domain and the large Rossman-fold domain forms a cleft where the target acetylated lysine and NAD^+ insert. Deacetylation of the target happens in two phases. First, NAD^+ is hydrolyzed and nicotinamide is released. Second, the acetyl moiety is transferred onto ADPr and the products, O-acetyl-ADPr (OAADPR) and the deacetylated lysine, are released. Entry of NAD^+ into the catalytic domain is followed by a nucleophilic attack of the acetylated target on the C1' of the nicotinamide ribose resulting in the formation of an alkylamidate intermediate. Next, the catalytic histidine activates the 2'OH, which in turn attacks the alkylamidate thus generating a cyclic intermediate. Finally, the cyclic intermediate is attacked by a water molecule, thus releasing the deacetylated target and 2'OAADPR or 3'OAADPR [31] (Figure 4B).

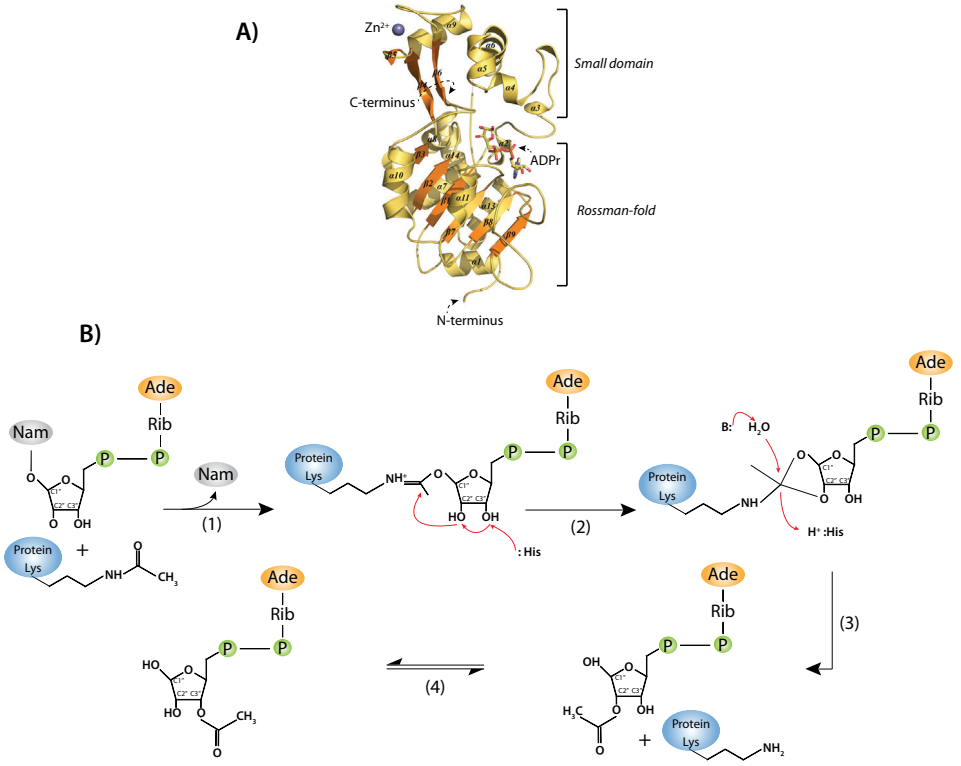

Figure 4: Structure and catalytic mechanism of SIRT2: A) Ribbon representation of the structure of the small domain and Rossman-fold of human sirtuin 2 (SIRT2) in complex with ADP-ribose (ADPr). The zinc ion (Zn^{2+}) is represented as a purple sphere; α-helices (yellow) and β-sheets (orange) are numbered from N- to C-terminal. N-terminus, C-terminus and ADPr are indicated with arrows (Adapted from [32]). B) Reaction mechanism of SIRT2. (1): The acetylated protein substitutes the nicotinamide (Nam) moiety of oxidized nicotinamide adenine dinucleotide (NAD^+) on C1' of the ribose. (2): Attack by the catalytic histidine (His) leads to the formation of the cyclic intermediate. (3): Release of the deacetylated target and (4) either 2'- or 3'-O-acetyl-ADP-ribose.

In contrast to the other deacetylases, the zinc ion does not directly participate in the catalysis but rather stabilizes the catalytic domain [33]. The involvement of sirtuins in a variety of important cellular processes underlines the necessity for a tight regulation of their activity. For example, regulation of transcription in response to external stimuli was reported for SIRT1. Following caloric restriction, binding of cyclic AMP (cAMP) response element binding (CREB) to the SIRT1 promoter increases its transcription. In turn, SIRT1 can take part in the adenosine monophosphate protein kinase (AMPK) pathway: as a consequence to lower energy levels, the increased

AMP concentration activates AMPK, which in turn phosphorylates cytosolic PGC1α thereby triggering the translocation of the latter to the nucleus.

There, PGC1α can be activated by SIRT1-mediated deacetylation, and enhance transcription of genes implicated in the regulation of mitochondrial functions and mobilization of energy reserves. Upon refeeding of the cells, the carbohydrate response element binding protein (ChREBP) will bind to the SIRT1 promoter, thereby inhibiting its transcription [34-36]. Other regulatory mechanisms of sirtuin activity include post-translational modification (e.g. phosphorylation), complex formation with endogenous inhibitors (e.g. deleted in breast cancer 1 (DBC1)) and NAD^+ availability (e.g. competition with PARP1) [37,38].

Sirtuins: NAD+-dependent enzymes with different activities and localization

Of the seven human sirtuins, SIRT1, SIRT6 and SIRT7 are localized to the nucleus (Table 1). SIRT1 is the most extensively studied member of the SIRT family and its deacetylase activity has been linked to many cellular processes and diseases. Generally, activation of SIRT1 is associated with repression of transcription in situations of energetic stress such as calorie restriction, and thus SIRT1 is considered to be a key player in metabolic homeostasis. SIRT1 can repress transcription of metabolic genes by directly deacetylating histone 1 lysine 26 (H1K26), histone 3 lysine 9 (H3K9) and histone 4 lysine 16 (H4K16) [39]. By removing the ε-acetyl group from the residues, SIRT1 promotes formation of heterochromatin, which is little accessible to the transcription machinery ("silent chromatin"). Besides histones, SIRT1 can also deacetylate a number of transcription factors such as P300/CBP, PGC1α, FOXO1, NFκB, HIF1α, HIF2α, all of them being involved in metabolic regulation [40].

Displaying a much weaker deacetylase activity, SIRT6 also has fewer targets than SIRT1. Involved in genomic DNA stability and repair, SIRT6 also has a role in metabolism. Consistent with these functions, SIRT6 knockout mice exhibit aging-like phenotypes and shorter lifespan [41].

Table 1: Functions and targets of sirtuins (Adapted from [42])

Sirtuin	Localization[a]	Reaction	Targets[b]	Pathways	References
SIRT1	Nucleus [Cytosol]	Deacetylation	Many, e.g. H3K9Ac, H4K16Ac, Hif1α, NFκB, PGC1α, FOXO1, LXR, p53, BMAL1, AceCS1, β-catein, PTEN TAF_I68, Tip60	Many, e.g. transcription regulation, gluconeogenesis, circadian rhythm, apoptosis	[19,43-54]
SIRT2	Cytosol [Nucleus]	Deacetylation	Several, e.g. p300, H4K16Ac, H3K56Ac, α-tubulin, PEPCK1, FOXO1	Several, e.g., transcription regulation, microtubule organization, cell cycle progression, gluconeogenesis	[55-60]
SIRT3	Mitochondria [Nucleus]	Deacetylation	Many, e.g. AceCS2, GDH, HMGCS2, IDH2, LCAD, VLCAD, MnSOD, OTC, SDH2	Many, e.g. Krebs cycle, acetylCoA metabolism, fatty acid oxidation, ROS response, amino acid catabolism, urea cycle	[47,61-73]
SIRT4	Mitochondria	Mono-ADP-ribosylation Deacetylation Lipoamidase	GDH, MCD, PDHE2	Amino acid catabolism, fatty acid oxidation	[74-76]
SIRT5	Mitochondria [Cytosol]	Deacetylation Demalonylation Desuccinylation Deglutarylation	CPS1, SOD1	Urea cycle, fatty acid oxidation	[26,77-79]
SIRT6	Nucleus	Deacetylation Demyristoylation Depalmitoylation Mono-ADP-ribosylation	H3K9Ac, H3K56Ac, CtIP, TNFα, PARP1	Genomic stability, glucose homeostasis, cell signaling	[80-86]
SIRT7	Nucleolus [Nucleus]	Deacetylation	H3K18Ac, PAF53, NPM1, GABP-β1, p53 (debated)	rDNA transcription, mitochondrial homeostasis	[87-91]

[a] Primary subcellular localization is given first, additionally described localization is given in brackets.

[b] Abbreviations: α-tubulin, alpha-tubulin; AceCS1/2, acetyl-coenzyme A synthase1/2;B-catein, beta-catein; BMAL1, brain and muscle ARNT-like 1; CPS1, carbamoylphosphate synthase 1; CtIP, DNA endonuclease RBBP8; FOXO1, forkhead box protein O1; GABP-β1, GA- binding protein subunit beta-1; GDH,glutamate; dehydrogenase; H3K9, histone 3 lysine 9; H3K18, histone 3 lysine 18; H3K56, histone 3 lysine 56; H4K16, histone 4 lysine 16; HIF1α, hypoxia inducible factor 1-alpha; HMGCS2, 3-hydroxy-3-methylglutaryl-coenzyme A synthase 2; IDH2, isocitrate dehydrogenase 2; LCAD, long-chain acyl-coenzyme A dehydrogenase; LXR, liver X receptor; MCD, malonyl-coenzyme A decarboxylase; MnSOD, superoxide dismutase [Mn]; NFκB, nuclear factor kappa-light-chain-enhancer of activated B cells; NPM1, nucleophosmin; OTC, ornithine carbamoyltransferase; P53, cellular tumor antigen P53; P300, histone acetyltransferase p300; PAF53, DNA-directed RNA polymerase I subunit RPA49; PARP1, poly-ADP-ribose polymerase 1; PDHE2, pyruvate dehydrogenase subunit E2; PEPCK1, phosphoenolpyruvate carboxykinase 1; PGC1α, peroxisome proliferator-activated receptor gamma coactivator 1-alpha; PTEN, phosphatase and tensin homolog; SDH2, succinate dehydrogenase 2; SOD1, superoxide dismutase [Cu-Zn]; TAF_I68, RNA polymerase I-specific TBP-associated factor 68 kDa; Tip60, histone acetyltransferase tip60; TNFα, tumor necrosis factor- alpha; VLCAD, very long-chain acyl-coenzyme A dehydrogenase.

Enriched in the nucleolus, SIRT7 exhibits deacetylase activity towards a limited set of targets, which are primarily involved in ribosomal DNA transcription [88,92], stabilization of cancer cell phenotypes [87,93-95], and mitochondrial biogenesis and function [91].

Of the remaining sirtuins, SIRT3, SIRT4 and SIRT5 reside in mitochondria due to the presence of mitochondrial targeting sequences. Among these, SIRT3 is the only one possessing a strong deacetylase activity, and is actually considered to be the major (and possibly sole) mitochondrial deacetylase [96]. Given that approximately 50% of all mitochondrial proteins involved in metabolic pathways possess at least one acetylation site [97], SIRT3 appears to be a key regulator of mitochondrial metabolism. SIRT5 also has the ability to deacetylate, however, to a much lesser extent than SIRT3. So far, only carbamoyl-phosphate synthase 1 (CPS1), involved in ammonia detoxification through the urea cycle, is found to be a target of SIRT5 for deacetylation. Instead, SIRT5 displays demalonylase, desuccinylase, and deglutarylation activities regulating among others urea production, fatty acid oxidation, TCA cycle, and glycolysis [26,77-79]. SIRT4 was proposed to act as mono ADP ribosyltransferase inhibiting glutamate dehydrogenase (GDH) thereby blocking amino acid-induced insulin secretion [74], and recently, deacetylation and delipoylation activities were detected towards malonyl-CoA decarboxylase (MCD) and pyruvate dehydrogenase (PDH), respectively [75,76].

SIRT2 is predominantly localized to the cytosol where, among other functions, it acts as a regulator of microtubule-associated events through the deacetylation of α-tubulin [55]. Although the role of tubulin acetylation remains unclear, it is generally regarded as a stabilizing factor involved in the recruitment of kinesin-1 and dynein, two motor proteins moving along the microtubules [98,99]. In addition, SIRT2 also carries out the deacetylation of several other targets including H4K16, p300 and FOXO1 and plays a role in processes such as gluconeogenesis, adipogenesis, and chromatin compaction [38,40,100].

Remarkably, several nuclear events also require the activity of SIRT2. During the G2/M transition, SIRT2 accumulates and associates with chromatin to globally deacetylate H4K16 thereby facilitating H4K20 methylation and subsequent chromatin compaction. Whereas accumulation of SIRT2 appears to play a major role in the early mitotic events, a decrease of SIRT2 is important for mitotic exit, as demonstrated by the fact that SIRT2 overexpression delays reentry in the cell cycle [56,101,102]. Furthermore, SIRT2 is involved in other nuclear reactions independent of the cell cycle such as the inactivation of the transcription factor P300 [58] or deacetylation of H3K56 involved in DNA repair [59].

Topological paradox of sirtuins

As mentioned above, sirtuins are preferentially localized to specific compartments. However, the target proteins of some sirtuins are not confined to a single subcellular compartment, and sirtuins themselves can exhibit alternative localization. Little is known about the mechanisms and physiological relevance of these different cellular distributions. For example, the predominantly nuclear protein SIRT1 was also detected in the cytoplasm of myoblast cells. This shuttling event is regulated by the phosphoinositie 3-Kinase (PI3K) signal cascade, which controls the two nuclear localization signals (NLS) and two nuclear export signals (NES) by post-translational modifications [103,104]. Furthermore, SIRT1 was shown to deacetylate the cytosolic acetyl-CoA synthase 1 (AceCS1) [47].

Two of the mitochondrial sirtuins may also exhibit alternative localization: SIRT3 has been reported in the nucleus whereas alternative splicing of SIRT5 leads to the alteration of the C-terminal end of isoform 1 resulting in its retention in the cytoplasm [105-107]. Nevertheless, to date, no substrates outside the mitochondria have been reported for SIRT3 and SIRT5.

The question as to how SIRT2-mediated nuclear processes are regulated is critical due to the non-negligible number of nuclear targets. While the breakdown of the nuclear envelope is likely to explain how SIRT2 associates with nuclear targets during mitosis, it is still unclear how SIRT2 mediates nuclear events during the interphase.

Prior to this work, four transcript variants of SIRT2 had been deposited in the GenBANK[a] database. Analysis of the primary structure of SIRT2 isoforms 1 and 2, which differ by the use of an alternative start codon, revealed the presence of a chromosome region maintenance 1 protein homolog (CRM1)-dependent nuclear export signal encoded by exon 4 [108] (Figure 5). However, no nuclear import signal has so far been identified thus suggesting a passive import of SIRT2 and raising the question as to how SIRT2-mediated nuclear processes are regulated.

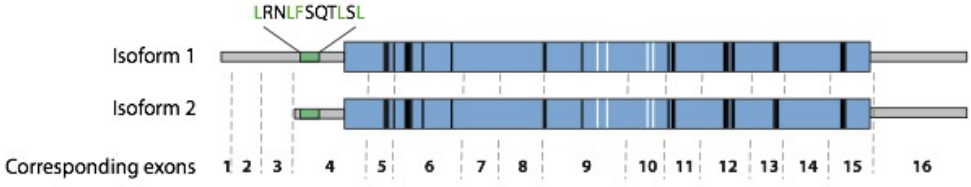

Figure 5: Primary structure of SIRT2 isoforms 1 and 2. Isoforms 1 and 2 differ by the usage of an alternative start codon located at the junction between exons 3 and 4 resulting in a protein lacking the first 37 amino acids. The SIRT2 catalytic domain is indicated in blue, the N- terminal and C-terminal flanking regions are in grey and the nuclear export signal is in green. Black bars represent residues involved in substrate binding whereas white bars represent zinc-coordinating residues. Exon junctions corresponding to the primary structure are indicated by dotted lines.

[a] GenBank accession numbers for the SIRT2 transcript variants (TV): TV1: NM_012237.3; TV2: NM_030593.2; TV3 NM_001193286.1; TV4. NR034146.1. Experimental evidence is missing for isoforms 3 and 4 and thus, they will not be addressed

1.3 NAD biosynthetic pathways and enzymes

As opposed to redox reactions, utilization of NAD^+ as a signaling molecule leads to a net consumption of the dinucleotide. Consequently, perpetual biosynthesis of NAD^+ is required to maintain physiological cellular concentrations (~300 μM) [109,110]. Several routes can lead to the synthesis of NAD, differing by the nature of the precursor used. Irrespective of which route is favored (e.g., depending on the organism), the first step of NAD biosynthesis is always the generation of a mononucleotide (Figure 6).

De novo synthesis of NAD relies on the degradation of an amino acid precursor that can be aspartate in plants and bacteria or tryptophan in humans. Tryptophan, an essential amino acid, is mainly catabolized by the kynurenine pathway leading to quinolinic acid (QA), the substrate for quinolinic acid phosphoribosyl transferase (QAPRT). QAPRT yields nicotinic acid mononucleotide (NAMN) by catalyzing the decarboxylation and phosphoribosylation of QA using phosphoribosyl pyrophosphate (PRPP) as a co-substrate [111,112].

The relatively low contribution of *de novo* synthesis to NAD generation underlines the importance of the alternative biosynthetic route, the salvage pathway. As opposed to the *de novo* synthesis, the salvage pathway relies on recycling of the cleaved nicotinamide (Nam) moiety originating from NAD^+-degrading activities such as PARylation and deacetylation performed by sirtuins. The resulting free Nam can be NMN by the rate-limiting enzyme nicotinamide phosphorybosyl transferase (NamPRT), which transfers the phosphoribosyl unit from PRPP onto Nam. Alternatively, the acid form of Nam, namely nicotinic acid (NA) may also serve as precursor in a biosynthetic route known as the Preiss-Handler pathway [113,114]. In this route, NA is converted to nicotinic acid mononucleotide (NAMN) by addition of phosphoribose provided by PRPP, a reaction catalyzed by nicotinic acid phosphoribosyl transferase (NAPRT). Interestingly, some organisms such as flies and worms do not display QAPRT activity, showing that the *de novo* pathway is not absolutely required for NAD synthesis [115].

Furthermore, it was shown for yeast that *de novo* synthesis contributes to a very small extent to NAD synthesis as long as the salvage pathways are functional [116], whereas QAPRT knock-out mice are viable provided a nicotinic acid diet [117].

In addition to QA, NA and Nam, two additional precursors were more recently discovered: the riboside forms of NA and NAM, nicotinic acid riboside (NAR) and nicotinamide riboside, respectively [118,119]. The riboside forms of NA and Nam are phosphorylated to NAMN and NMN, respectively, by nicotinamide ribose kinases (NRKs), where ATP serves as the phosphate donor. Alternatively, NR can be cleaved, liberating Nam that can in turn enter the salvage pathways [120-123].

After generation of the mononucleotide, the second step of NAD synthesis is the reversible condensation of the adenylyl moiety from ATP with the mononucleotide (generated either from NA, NAR, Nam, QA or NR), a reaction accompanied by the release of pyrophosphate. Well conserved among species, this reaction is catalyzed by nicotinic acid/nicotinamide mononucleotide adenylyltransferases (NMNATs), the final product being either nicotinic acid adenine dinucleotide (NAAD) or NAD. When the biosynthetic pathway originates from the acidic mononucleotide, an additional step is required for the amidation of NAAD to NAD. This reaction is catalyzed by NAD synthase (NADS), and is dependent on glutamine as an ammonia donor in eukaryotes.

Humans express three different NMNATs, which differ by their sub-cellular localization. NMNAT1 is the predominant isoform with regards to both activity, and tissue distribution. It is found in the nucleus [124] where it is involved in many NAD-dependent nuclear processes. For example, PARP1 localized at target gene promoters recruits and interacts with NMNAT1 to regulate its activity by enhancing local NAD^+ availability [125,126]. Similar observations have been made for the other major nuclear NAD^+- consuming enzyme, namely SIRT1 [127]. NMNAT2 is localized to the Golgi apparatus and axonal vesicles [124,128,129], whereas overexpressed NMNAT3 reportedly co-localizes with mitochondrial structures [8,124] (Figure 6).

1.4 Compartmentalization of NAD^+: biosynthesis and importance of the mitochondrial pool.

The membranes in eukaryotic cells constitute impermeable barriers thereby creating distinct environments. This compartmentalized character allows for tremendous possibilities for regulation (e.g. by the spatial separation of anabolic and catabolic pathways). Control of pathways at this level requires metabolites, enzymes, and cofactors to cross the physical barrier that membranes are, a process often depending on proteins dedicated to the transport across membranes. The mechanisms underlying the cellular distribution of metabolites and cofactors are still the center of attention for many research groups. For example, although much was already known about the role of pyruvate in metabolism, it was only recently that a mitochondrial pyruvate carrier was identified [130,131].

The variety of reactions involving NAD highlights the central position of this coenzyme in cellular functions and the requirement for tight regulatory mechanisms. The compartmentalization of the eukaryotic cell provides an additional level of regulation by segregating NAD^+-dependent enzymes as well as biosynthetic enzymes to specific compartments.

In accordance with the wide cellular distribution of NAD^+-dependent enzymes and processes, it is not surprising that NAD^+ was also found to be distributed in several subcellular pools. A large proportion of NAD-dependent events takes place in the cytosol and nucleus and, although experimental evidence is still missing, it is generally believed that NAD^+ can freely diffuse through the nuclear pores and thus, that these two pools are interchangeable and of equal concentration. Beside the nucleo-cytoplasmic pool, NAD^+ was detected in the peroxisomes, Golgi, endoplasmic reticulum, and mitochondria [11], which may contain up to 70% of the total cellular NAD pool where it plays a vital role in multiple redox and signaling reactions [132].

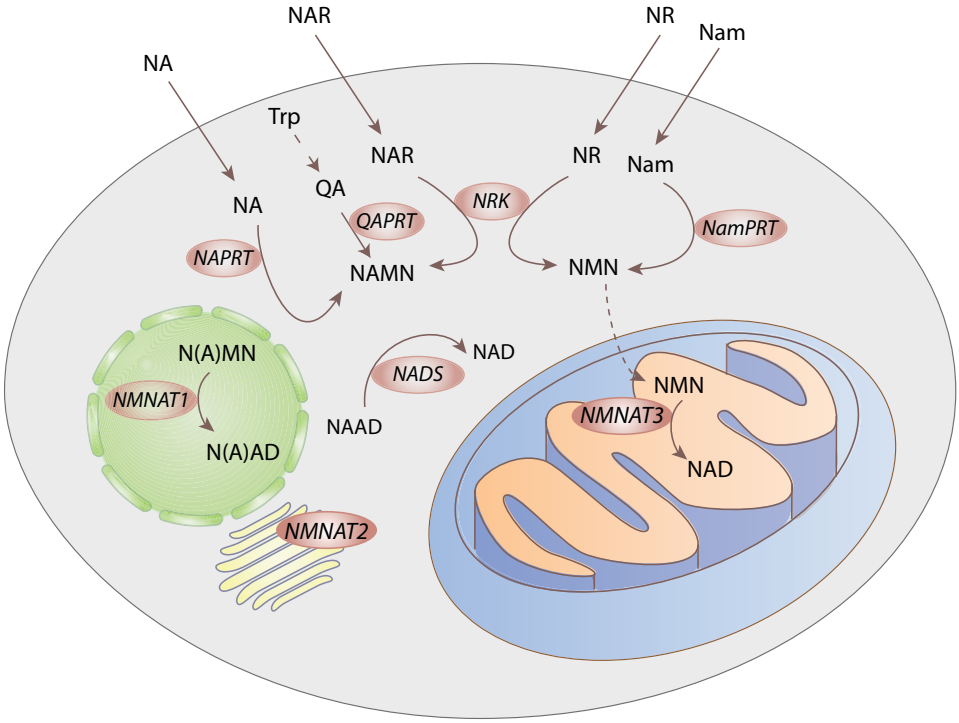

Figure 6: Subcellular localization and reactions of the different NAD biosynthetic enzymes. The different entry points use extracellular precursors containing the pyridine moiety or tryptophan (Trp) as a precursor to quinolinic acid (QA). QA and nicotinic acid (NA) are converted to nicotinic acid mononucleotide (NAMN) by their respective phosphoribosyl transferase QAPRT and NAPRT. Nicotinamide phosphoribosyl transferase (NamPRT) catalyzes the conversion of nicotinamide (Nam) to nicotinamide mononucleotide (NMN). The riboside forms of Nam and NA, nicotinamide riboside [86] and nicotinic acid riboside (NAR), respectively, may also serve as precursors for NMN and NAMN. These reactions are catalyzed by nicotinamide riboside kinases (NRKs). Nicotinamide mononucleotide adenylyltransferases (NMNATs) catalyze the formation of nicotinamide/ nicotinic acid adenine dinucleotide (N(A)AD) and localize to the nucleus (NMNAT1, green), the Golgi apparatus (NMNAT2, yellow) or the mitochondria (NMNAT3, blue). NAD synthase (NADS) converts NAAD to NAD. The hypothetical import of NMN into mitochondria is represented by the dotted line.

Owing to the importance of mitochondria in metabolic reactions and the role played by NAD^+ in these reactions, several studies have recently highlighted the crucial role of mitochondrial NAD^+ maintenance. For example, genotoxic stress resulting in the activation of PARP1 leads to severe cellular NAD^+ depletion. However, mitochondrial NAD^+ concentrations are maintained and promote cell survival, an effect depending on SIRT3 and SIRT4 [109].

Similarly, incubation of cells with the NamPRT inhibitor FK866 depletes cytosolic NAD^+ whereas the mitochondrial NAD^+ pool remains unaffected [133].

Conversely, consumption of mitochondrial NAD^+ was demonstrated to affect mitochondrial respiration, lactate production and mitochondrial membrane potential [134]. Reduction of mitochondrial NAD^+ availability may even lead to cell death: upon activation of the mitochondrial permeability transition pore, depletion of mitochondrial NAD^+ and subsequent degradation by NAD^+ catabolic enzymes can result in the loss of cellular metabolic integrity and potentially cell death [135].

Whereas much is known about NAD^+-dependent processes in the mitochondria, information regarding establishment and maintenance of the mitochondrial NAD^+ pool is rather scarce. Two possible mechanisms may explain how mitochondrial NAD^+ is brought about. On the one hand, a dedicated carrier could directly import NAD^+. An alternative to direct import is intra-organellar biosynthesis. In *Saccharomyces cerevisiae* and *Arabidopsis thaliana*, *Sc*NDT1 and *At*NDT2, respectively, were identified as membrane carriers mediating NAD^+ transport across the inner mitochondrial membrane [136,137]. In contrast to yeast and plants, the only human NAD^+ carrier identified is SLC25A17 [138], which mediates the transport of NAD^+ across the peroxisomal membrane, and to date, no mitochondrial NAD^+ transporter has been identified in humans or other mammals [74,109,139].

While all the other biosynthetic enzymes are localized to the nucleus and cytoplasm, the suggested presence of NMNAT3 within the mitochondria implies that generation of mitochondrial NAD^+ may rely on the import of NMN and subsequent conversion of the mononucleotide to NAD^+. Nevertheless, the hypothesis of mitochondrial NAD biosynthesis is debated, mostly due to the lack of experimental evidence for the presence of the endogenous NMNAT3 protein. Several studies have indicated the presence of the mRNA whereas the overexpressed protein has been detected in mitochondria [8,124,140-142]. Nevertheless, conclusive evidence for the protein within mitochondria is still missing.

Therefore, given the uncertainties regarding the presence of NMNAT3 in mitochondria of human cells, it has remained an open question whether there is an autonomous biosynthesis of NAD within these organelles.

2. Aims of the study

In the light of the compartmentalization of human cells, it is obvious that complex mechanisms must regulate not only the activity of NAD metabolic enzymes, but also the distribution of these enzymes and of NAD^+ itself. Thus, understanding the mechanisms underlying these events is of critical importance and provided the basis to the scientific problems addressed in this dissertation.

The ability of SIRT2 to deacetylate nuclear targets is an apparent contradiction to its predominantly cytosolic location. One major aim was to provide further insights into the regulatory mechanisms involved in nuclear deacetylation by SIRT2. Sirtuins may exhibit alternative localization due to alternative splicing, and the recent identification of a new SIRT2 splice variant in mice, lacking the nuclear export signal and thus localized to the nucleus, shed new light on the topic of SIRT2 localization. Whether such an isoform existed in human remained to be elucidated. The objective of this part of the study was therefore to establish if a nuclear splice variant of SIRT2 existed and if it could account for nuclear deacetylation.

Owing to the major importance and observed segregated nature of mitochondrial NAD^+, modulations of that pool may result in dramatic changes in cellular processes such as metabolic pathways. In accordance with this, it has been previously reported that the decrease of mitochondrial NAD^+ availability affects metabolism, lactate production, and mitochondrial membrane potential. A second aim of this study was thus to analyze the consequences arising from the subcellular redistribution of NAD^+. More specifically, the intent was to increase mitochondrial NAD^+ availability and assess the cellular response to this change, especially with regards to metabolic functions.

Another challenge arising from the isolation of the mitochondrial NAD^+ pool lies in its establishment. Whereas mitochondrial NAD^+ carriers have been characterized in yeast and *Arabidopsis thaliana*, no human homolog has so far been identified.

The localization of an NMNAT isoform (NMNAT3) to the mitochondria suggests that mitochondrial NAD^+ is synthesized within these organelles. However, experimental proof of the endogenous protein is still missing. Another goal of this study was thus to address the question of whether a NAD^+ carrier exists for human mitochondria, or if NAD^+ is synthesized within these organelles.

3. Summary of the results

3.1 Constitutive nuclear localization of an alternatively spliced Sirtuin2 protein isoform

Paper I investigated the possibility that a not yet identified nuclear isoform of the SIRT2 protein may be responsible for deacetylation of SIRT2 nuclear targets. PCR analyses performed on cDNA from several human cell lines led to the identification of a new *SIRT2* transcript variant linking exon 1 to exon 5. Given that SIRT2 protein isoforms 1, 2, 3 and 4 were already deposited in the GenBank database, the new isoform was named isoform 5. Compared to SIRT2 isoform 1, this new isoform is characterized by the substitution of amino acids 6 to 76 by an arginine residue. The alternative splicing of SIRT2 leads to the exclusion of the NES encoded by exon 4 in SIRT2 isoform 1. Expression of the open reading frame of SIRT2 isoform 5 in the context of its endogenous 5'UTR resulted in a protein product of expected size. The absence of the NES suggested that this isoform could be localized to a different sub-cellular compartment than the cytosol. Immunocytochemistry as well as western blot analysis following cell fractionation determined that SIRT2 isoform 5 is indeed predominantly localized to the nucleus. To investigate the possibility that SIRT2 isoform 5 accounts for nuclear deacetylation events carried out by SIRT2, its activity towards several acetylated targets was assessed both by *in vitro* and *in vivo* approaches. Surprisingly, isoform 5 failed to deacetylate all targets tested (HAT domain of P300, chemically acetylated histones and α-tubulin). A possible reason for this could be that, due to the splicing event, the catalytic domain of SIRT2 isoform 5 is slightly truncated, and α-helix α1 of the Rossman-fold is missing. Molecular modeling analysis with homology modeling and threading suggested that, in spite of the changes in the catalytic domain, SIRT2 isoform 5 adopts a fold similar to that of isoforms 1 and 2, which was further confirmed by protein denaturation and intrinsic tryptophan fluorescence shift assay. Finally, although unable to deacetylate it, SIRT2 isoform 5 retained the ability to interact with P300, which may suggest a non-catalytic function for this isoform.

3.2 Subcellular distribution of NAD^+ between cytosol and mitochondria determines the metabolic profile of human cells

It was previously shown that a diminished mitochondrial NAD^+ pool affects mitochondrial metabolism. Paper II aimed at understanding the impact of increased mitochondrial NAD^+ availability and the consequences of the redistribution of NAD^+ between the cytosol and the mitochondria. Mitochondrial NAD^+ availability was successfully increased by expressing mitochondrial NAD^+ transporters from yeast or plants (*Sc*NDT1 and *At*NDT2 respectively) but overexpression of the closest human homologs (SLC25A32, SLC25A33 and SLC25A36) failed to do so. A cell line stably expressing *At*NDT2 (293*At*NDT2) was established, and the elevation of mitochondrial NAD^+ availability in these cells was confirmed. The redistribution of cellular NAD^+ had several physiological consequences for the cells. 293*At*NDT2 cells proliferated at a slower rate compared to the control cells, a phenotype that could not be rescued by addition of nicotinic acid, indicating that the slow growth did not result from impaired total NAD^+ availability. Incubation with NamPRT inhibitor FK866 revealed that the 293*At*NDT2 cells were less sensitive towards NAD biosynthesis inhibition. It has been previously reported that consumption of mitochondrial NAD^+ reduced mitochondrial respiration and increased lactate production with accelerated acidification of the cell culture medium [134]. Surprisingly, the stable expression of *At*NDT2 also resulted in increased lactate production accompanied by a drop of pH of the cell culture medium. To further understand the metabolic consequences of increased mitochondrial NAD^+ availability, mitochondrial respiration and glycolytic function were assessed using a SeaHorse XF analyzer. Redistribution of NAD^+ from the cytosol to the mitochondria led to a metabolic shift from respiration to glycolysis. The dramatic phenotypes displayed by 293*At*NDT2 cells indicate that the presence of such a transporter in human mitochondria might be harmful and that intra-organellar NAD biosynthesis is likely to be the source for mitochondrial NAD^+. This hypothesis was substantiated by western blot analysis providing evidence for the existence of endogenous NMNAT3 protein in human mitochondria.

4. General Discussion

NAD holds a central position in cells due to its involvement not only in metabolic redox reactions, but also in major signaling events including PARylation, Sirtuin-mediated deacetylation, and calcium signaling. As such, this co-substrate influences virtually every cellular function, and understanding of NAD^+-dependent processes is of vital importance. In the present study, key questions relative to NAD^+ metabolism and distribution, in the frame of subcellular compartmentalization, were addressed.

Compartmentalization of eukaryotic cells provides an additional level of regulation. Indeed the confinement of enzymes to specific locations, as well as the maintenance of different concentrations of cofactors results in local environments influencing the functions of these compartments. However, the membranes constitute obstacles to the free distribution of biomolecules thus raising several questions as to how the distribution of enzymes and cofactors is regulated.

4.1 Compartmentation of NAD metabolic enzymes

4.1.1 The nuclear isoform of SIRT2 does not deacetylate nuclear targets

The first aspect of this study consisted in investigating the topological paradox of SIRT2 activity. As mentioned in the previous sections, SIRT2 mainly resides in the cytosol, but is able to deacetylate a considerable number of nuclear targets and participates in the control of, among others, cell division and transcriptional events (Table 1). Whereas the rupture of the nuclear envelope can explain the interaction between SIRT2 and nuclear partners during mitosis, how deacetylation of nuclear proteins during the interphase is regulated remains poorly understood. A previous study has identified a CRM1-dependent NES, but no functional NLS has so far been identified in SIRT2. The authors thus suggested that nuclear import of SIRT2 happens passively by a “piggy-back” mechanism [108].

However, nuclear deacetylation events mediated by SIRT2 ought to be tightly regulated. Thus, it is unlikely that the regulation of these deacetylation events depends on passive nuclear import of SIRT2.

In paper I, analysis of cDNA from several human cell lines revealed the existence of a new splice variant and confirmed the previously reported data from mice [143,144]. This new isoform, named SIRT2 isoform 5, results in an “in frame” mRNA excluding exons 2 to 4. Owing to the splicing event, isoform 5 lacks the NES present in SIRT2 isoforms 1 and 2 [108] and predominantly resides in the nucleus. Furthermore, computational NLS prediction indicated the presence of a candidate weak bipartite non-canonical NLS in the C-terminal region of SIRT2 (residues 342-375 in isoform 1).

The particular localization of isoform 5 suggested that it could be responsible for SIRT2-mediated deacetylation occurring in the nucleus. As outlined by several experimental approaches in Paper I, SIRT2 isoform 5 surprisingly failed to deacetylate any of the reported targets tested. In order to determine whether the lack of activity was the result of structural impairments, further attention was given to the structural features of isoform 5. Beyond the deletion of the NES, 12 residues from the conserved catalytic domain are also absent in SIRT2 isoform 5. Importantly, all amino acids reported as essential for SIRT2 activity are still present in isoform 5 [32,145]. The data presented in this paper further indicate that the removal of this stretch of residues is unlikely to affect the overall structure of SIRT2. In fact, all three isoforms tested (isoforms 1, 2 and 5) displayed very similar denaturation profiles. Furthermore threading and homology modeling predicted a structure resembling that of isoforms 1 and 2 for SIRT2 isoform 5. In spite of these similarities, the Rossman-fold of isoform 5 could still be affected by the absence of α-helix 1. This is however unlikely given the remote position of this helix compared to the catalytic pocket. In line with this, the bacterial sirtuin CobB was also shown to lack the corresponding helix but remained an active sirtuin [146]. Interestingly, SIRT2 isoform 5 retained the ability to associate with P300, a known target of SIRT2 [58,147].

The strength of this interaction appears to be dependent on the concentration of NAD^+ indicating that both substrate binding and NAD^+ binding pockets remain intact. Thus, the apparent inactivity of SIRT2 isoform 5 may result from very subtle changes in the overall structure of this isoform.

Although the results presented in this study indicate that SIRT2 isoform 5 is not responsible for nuclear deacetylation of SIRT2 targets, the possibility that this isoform would deacetylate other targets cannot be ruled out. Moreover, it is possible that the newly discovered SIRT2 isoform 5 exhibits other functions than protein deacetylation, as described for other sirtuins. For example, SIRT4 acts as mono-ADP-ribosyl transferase and was recently also characterized as a lipoamidase targeting subunit E2 (dehydrolipoyl dehydrogenase) of the pyruvate dehydrogenase complex, thereby inhibiting its activity [76]. Another example is the recent discovery of lysine glutarylation, a new five-carbon posttranslational modification found on CPS1 and inhibiting this enzyme. SIRT5 was identified as the enzyme responsible for removal of lysine glutarylation on CPS1.

Alternatively, SIRT2 isoform 5 may have functions independent of any catalytic activities. Such roles have previously been described for SIRT1. Proteolytic cleavage of SIRT1 generates an inactive form of SIRT1, which can in turn be exported to the cytoplasm. In the cytoplasm, the fragment of SIRT1 associates with the outer mitochondrial membrane and blocks the assembly of cytochrome c with the apoptosome complex, thus protecting cells from apoptosis [148]. SIRT1 was also found to promote neuroprotection independently of its catalytic activity. Indeed overexpression of SIRT1 protects neurons from cell death, an effect still visible when catalytically dead mutant SIRT1 is overexpressed, or in presence of SIRT1 inhibitors [149].

Whether the hereby-presented new isoform of SIRT2 deacetylates other targets, or has alternative functions will have to be clarified by future investigations.

4.1.2 NAD biosynthetic enzyme NMNAT3 is localized to the mitochondria

Another aspect of this study was to examine the question of NAD biosynthesis within mitochondria. While NAD^+ is generally considered to freely distribute between the nucleus and cytoplasm, the presence of an impermeable inner membrane in mitochondria prevents that NAD^+ freely distributes from the cytosol to this organelle. Thus, two options may explain how the mitochondrial NAD^+ pool is established and maintained: either a mitochondrial carrier imports NAD^+, or it is synthesized within the mitochondria.

To test the possibility that mitochondrial NAD^+ is imported by a transporter, the ability of three human candidate proteins to increase mitochondrial NAD^+ was compared to that of previously described NAD^+ carriers. Such mitochondrial NAD^+ transporters have been identified in yeast (*Sc*NDT1) [136] and in plants (*At*NDT2) [137]. When overexpressed, none of these three human candidate proteins could increase mitochondrial NAD^+ availability suggesting that they do not exhibit NAD^+ transporter activities. These results are in accordance with a previous publication reporting that SLC25A32 has no influence on mitochondrial NAD^+ [109]. Furthermore, during the preparation of Paper II, SLC25A33 or SLC25A36 were characterized as pyrimidine nucleotide transporters unable to transport NAD^+ [150].

The existence of a human mitochondrial NAD^+ transporter cannot completely be ruled out. SLC25A32 could still be the human NAD^+ carrier but may already be expressed at a very high level, in which case its overexpression may not result in any detectable changes in mitochondrial NAD^+ availability. Furthermore, NAD^+ could be imported into mitochondria by a transporter sharing little homology with the yeast and plant proteins, which could explain the difficulties encountered in the course of its identification. For example, the mitochondrial pyruvate carrier (MPC) was initially believed to be a member of the mitochondrial carrier family, which led to its misidentification [136,151,152].

Only later, it was found that the MPC is a heterocomplex formed by two members of a family of previously uncharacterized membrane proteins that are conserved from yeast to mammals [130,131].

The alternative to direct import is intra-mitochondrial NAD^+ biosynthesis. Previous work demonstrated that all NAD^+ biosynthetic enzymes reside in the cytoplasm and nucleus, with the exception of the overexpressed recombinant NMNAT3, which is localized to the mitochondrial matrix [8]. The existence of human NMNAT3 protein in mitochondria was debated, mostly due to the challenges encountered in its specific immunodetection within these organelles. Whereas the mRNA has been detected in several studies [140,142,153], the mitochondrial localization of NMNAT3 had only been demonstrated for the overexpressed protein [8,141,142,153,154] and conclusive evidence of the presence of human endogenous NMNAT3 protein within the mitochondrial matrix was still lacking. The low expression levels of NMNAT3, combined with a possible low sensitivity of the antibodies used in those studies, may explain why the endogenous protein could not be detected.

In this study, the presence in mitochondria of endogenous NMNAT3 protein was confirmed in HEK293 cells, and the protein could be readily immunodetected in extracts from different human cell lines (data not shown). Interestingly, comparison of NMNAT3 expression in 293mitoPARP and 293*At*NDT2 showed that mitochondrial NAD^+ availability appears to have no effect on NMNAT3 levels. Furthermore, preliminary experiments suggest that overexpression of NMNAT3 does not increase mitochondrial NAD^+ availability (data not shown). Although these findings may be surprising, they are in line with previous studies showing that overexpression of NMNAT1 does not increase cellular NAD^+ content [155-157].

Taken together, these data strongly argue in favor of intra-mitochondrial biosynthesis. Interestingly, yeast and *Arabidopsis thaliana* express mitochondrial NAD^+ transporters but lack an NMNAT3 homolog. Conversely, *Helianthus tuberosus L* (Jersualem artichoke) has a mitochondrial NMNAT [158], but a BLAST search failed to identify a putative gene coding for a NAD^+ transporter of the *Arabidopsis thaliana*

type. This may suggest that mitochondrial NAD^+ import and biosynthesis are two evolutionary separate mechanisms to establish the mitochondrial NAD^+ pool, but may be mutually exclusive.

Finally, given that all other NAD biosynthetic enzymes are located outside the mitochondria, if the mitochondrial NAD^+ pool depends on autonomous biosynthesis, it still requires the substrate for NMNAT3, namely NMN. The absence of NamPRT from the mitochondria [8,133] indicates that NMN would have to be imported by a dedicated transporter. However, such a transporter remains to be identified.

4.2 Distribution of NAD^+ between cellular compartments affects the metabolic profile of human cells

Previous work in our group demonstrated that a cell line stably expressing the catalytic domain of PARP1 targeted to the mitochondria exhibits a decrease of NAD^+, resulting in cells far more dependent on glycolysis than the controls [134]. These findings raised the question as to what repercussions the opposite modulation, namely increased mitochondrial NAD^+ availability, would have.

Mitochondrial NAD^+ availability was successfully increased by expression of mitochondrial NAD^+ carriers *Sc*NDT1 and *At*NDT2, and a cell line stably expressing *At*NDT2 (293*At*NDT2) was established. Strikingly, the presence of the plant transporter strongly reduced cell proliferation and led to shift from oxidative phosphorylation to glycolysis as demonstrated both by lactate measurements, and determination of glycolytic rate and oxygen consumption. The finding that increasing mitochondrial NAD^+ availability appeared to be harmful to human cells was unexpected, especially in the light of several reports highlighting the protective nature of mitochondrial NAD^+. For example, mitochondrial NAD^+ was shown to protect against genotoxic stess-induced cell death [109] whereas maintenance of mitochondrial NAD^+ protects myocytes from death in the context if postischemic reperfusion of the heart [159].

Furthermore, inhibition of NAD biosynthesis with the NamPRT inhibitor FK866 appears to have no effect on the mitochondrial NAD^+ pool [133]. All these observations would thus suggest that increasing mitochondrial NAD^+ availability would be beneficial for the cells.

To understand this apparent contradiction, one should consider that the increase of mitochondrial NAD^+ might be at the expense of the cytosolic pool. Should cytosolic NAD^+ levels be lowered, maintenance of glycolysis would require a higher oxidation of NADH to NAD^+, a reaction catalyzed by lactate dehydrogenase (LDH) and accompanied by the increased lactate formation measured in these cells. Moreover, oxidation of NADH would also require pyruvate as the substrate for LDH. Hence, it is reasonable to argue that under such conditions, pyruvate would serve as substrate to LDH rather than mitochondrial respiration, which would translate into the low oxygen consumption rate of these cells. In line with this hypothesis, recent findings linked PARP1 activation in response to DNA damage to inhibition of glycolysis and mitochondrial respiratory failure, a phenotype reversed by the addition of pyruvate. These results indicated that impaired mitochondrial respiration was the consequence of lower pyruvate availability in response to glycolysis inhibition [160,161].

Whereas the results presented here are in accordance with such a mechanism, one aspect that has to be considered is the nature of the transporter. *At*NDT2 was characterized as a member of the mitochondrial carrier family working in a counter-exchange mode. This type of exchange implies that when NAD^+ accumulates in the mitochondria, the counter substrate should accumulate in the cytosol. In plants, AMP and ADP are the most efficient counter substrates for the antiporter *At*NDT2 [137]. Redistribution of these nucleotides could also affect the metabolic profile of 293AtNDT2 cells. For example, higher concentrations of AMP in the cytosol could activate the AMPK pathway resulting in the activation of glycolysis [162]. Whereas AMPK activation may contribute to the increased glycolytic rate, this hypothesis fails to explain the failure in mitochondrial respiration and the increased lactate production. Furthermore, activation of glucose catabolism by AMPK is a feature of insulin-dependent tissues such as liver, adipose tissue and muscle.

Thus, it is unlikely to contribute significantly to the effects observed in HEK293 cells, a cell line likely originating from transformation of an embryonic adrenal gland cell, and sharing many features with neuronal cells [163,164].

As ADP is the substrate for ATP synthase, a putative ADP withdrawal from the mitochondria may also lower basal mitochondrial respiration and favor glycolysis. However, mitochondrial ADP shortage would not affect the oxygen consumption rate in the presence of the uncoupler, an effect observed in the 293*At*NDT2 cells.

A similar shift from respiration towards glycolysis also occurred upon increased consumption of mitochondrial NAD^+ (293mitoPARP). Although both mitochondrial NAD^+ modulations result in the same phenotype, in 293mitoPARP, the decrease in mitochondrial NAD^+ availability is likely to be responsible for reduced mitochondrial respiration, which in turn would be compensated for by increasing the glycolytic rate. Though it was surprising that seemingly opposite mitochondrial NAD^+ modulations resulted in similar metabolic profiles, comparable observations have been reported in yeast: overexpression as well as deletion of mitochondrial NAD^+ carriers lowers ATP production, and upon complete respiratory growth conditions both mutants exhibited a low biomass yield indicating impaired respiratory functions [165].

Although similar with regards to their metabolic profiles, 293mitoPARP cells and 293*At*NDT2 cells exhibited different behaviors in several aspects. One of the most striking phenotype of the 293*At*NDT2 cells is their substantially impaired growth rate. Possibly, the continuous drainage of NAD^+ from the cytosol and the necessity to replenish that pool may affect the ability of cells to produce acetyl-CoA from pyruvate, and this to an extent severely affecting cell proliferation. Moreover, a decrease in cytosolic NAD^+ would in turn reduce the ability of SIRT1 to deacetylate and activate AceCS1 thus also lowering acetyl-CoA production in the cytosol [47]. Reducing acetyl-CoA availability would subsequently affect acetylation of histones and transcription factors involved in cell proliferation but also negatively affect lipid biosynthesis, hence lowering the availability of “building blocks” necessary for cell proliferation.

On the other hand, mitochondrial NAD^+ consumption in 293mitoPARP might be sufficiently compensated for to maintain the proliferation, and would not affect the cytosolic NAD^+ content.

Importantly, mitochondrial NAD^+ levels appear to dictate the extent of cell survival upon treatment with the NamPRT inhibitor FK866. As previously reported, NamPRT inhibition leads to severe NAD^+ depletion and subsequent cell death [8,166], an effect enhanced when mitochondrial NAD^+ is lowered. On the contrary, accumulation of NAD^+ within the mitochondria in 293*At*NDT2 cells conferred a protective effect towards NAD^+-depletion-mediated cell death. The slow proliferation of these cells could translate into lower NAD^+ consumption enabling longer survival in presence of FK866. In line with this hypothesis, inhibition of PARP1 also increases tolerance to inhibition of NAD^+ biosynthesis [8,133,167].

Reshuffling of NAD^+ from the cytosol to the mitochondria thus resulted in dramatic changes in the metabolic profile of human cells, characterized by severe deleterious effects on mitochondrial respiration and cell proliferation. As such, the data obtained here demonstrate that appropriate distribution of cellular NAD^+ is important to maintain healthy metabolism in human cells.

5. Concluding remarks and future perspectives

The results presented in this dissertation have significantly extended our knowledge of NAD^+- related processes in the context of a compartmentalized cell, but also raised a significant amount of exciting questions.

This work led to the identification and characterization of a new human splice variant of SIRT2 but further investigations will be required to understand the physiological relevance of this isoform. In the frame of this study, deacetylation activity of SIRT2 isoform 5 could not be detected. However, the scope of targets and activities tested could be enlarged in order to further verify the activity of the isoform 5. Although the expression was rather weak, the presence of the mRNA coding for isoform 5 was confirmed in several cell lines. It will be interesting to screen more cell lines in order to determine if some cell lines, or tissues, express isoform 5 at higher levels, and if the endogenous protein can be detected. If such samples can be identified, specific knockdown by interfering RNA may bring important information with regards to the role played by this isoform. Given that the new nuclear SIRT2 isoform exhibited no apparent activity, the mechanisms underlying the deacetylation of nuclear targets by the cytosolic SIRT2 could not be solved. The contribution of the predicted nuclear localization signal will have to be further investigated. Indeed, mutations and/or deletion of the NLS in SIRT2 isoform 5 should determine whether the prediction is accurate. Upon confirmation of the NLS, it will be interesting to determine whether the absence of the NLS in SIRT2 isoforms 1 or 2 affects deacetylation of nuclear targets.

Regarding mitochondrial NAD metabolism, the work presented here provides conclusive evidence of the existence of a mitochondrial NMNAT protein. This finding sheds new light on the topic of how the mitochondrial NAD^+ pool is established and suggests several interesting experiments.

According to the hypothesis that NMNAT3 is responsible for NAD biosynthesis within the mitochondrial matrix, knockout of this protein, for example, by means of the CRISPR-cas9 method, should affect mitochondrial NAD^+ availability to a great extent. In turn, the putative NAD^+-depletion could affect, among others, the metabolic profile, cell survival, or mitochondrial acetylation. For example, NMNAT3 knockout cells and 293mitoPARP cells may exhibit similar metabolic phenotypes. If such observations can be made, it will be interesting to test whether the presence of the plant transporter *At*NDT2 results in desensitization of cells towards the knockout of NMNAT3. Additional work will also be required to understand how the substrate of NMNAT3, namely NMN, enters the mitochondria. It is generally accepted that NamPRT, the enzyme generating NMN, resides in the cytoplasm, suggesting that NMN is imported in mitochondria by a transporter. To date, this carrier remains to be identified.

The results obtained in this work thus support the conclusion that NAD is synthesized within mitochondria rather than imported by a transporter. While the possibility that a human NAD^+ transporter exists cannot be ruled out based on these data, the necessity for human mitochondrial NAD^+ import might be alleviated by the presence of NMNAT3 inside these organelles.

Finally, this study reveals that modulation of mitochondrial NAD^+ has severe consequences on important cellular processes, and opens up new perspectives. First, the hypothesis that pyruvate is diverted away from mitochondrial respiration towards lactate dehydrogenase will have to be tested. Failure of mitochondrial respiration resulting from PARP1 activation is rescued by addition of pyruvate [160,161]. Seahorse experiments could be performed to verify whether the oxygen consumption rate of the 293*At*NDT2 cells can be rescued by addition of pyruvate. Moreover, supplementation with pyruvate may also have beneficial effects on the cell proliferation. Second, modulating mitochondrial NAD^+ availability may result in changes in mitochondrial sirtuin activity, and for example, acetylation levels of mitochondrial proteins may be altered.

Preliminary results indicate that global mitochondrial acetylation does not, however, change upon consumption or increase in mitochondrial availability. Future experimental approaches will have to determine whether acetylation or ADP-ribosylation of specific targets is affected by changes in mitochondrial NAD^+ concentrations.

Third, a major challenge in the future will be to accurately determine the concentration of NAD^+, for example in the mitochondria and the cytosol. Such measurements are critical and rendered difficult by the need for a method sensitive enough for cell samples. In this context, high performance liquid chromatography coupled to mass spectrometry (LC-MS) is becoming the leading analytical method in the measurement of nucleotides in cell extracts [110]. This method will surely enable the quantification not only of NAD but also of other nucleotides such as ADP-ribose, ATP, and ADP in organelles and compartments.

6. References

[1] Berger, F., Ramirez-Hernandez, M. H., and Ziegler, M. (2004) The new life of a centenarian: signalling functions of NAD(P). *Trends Biochem. Sci.* **29**, 111-118

[2] Wu, G., Fang, Y. Z., Yang, S., Lupton, J. R., and Turner, N. D. (2004) Glutathione metabolism and its implications for health. *J. Nutr.* **134**, 489-492

[3] Iyanagi, T. (2005) Structure and function of NADPH-cytochrome P450 reductase and nitric oxide synthase reductase domain. *Biochem. Biophys. Res. Commun.* **338**, 520-528

[4] Chambon, P., Weill, J. D., and Mandel, P. (1963) Nicotinamide mononucleotide activation of new DNA-dependent polyadenylic acid synthesizing nuclear enzyme. *Biochem. Biophys. Res. Commun.* **11**, 39-43

[5] Hassa, P. O., Haenni, S. S., Elser, M., and Hottiger, M. O. (2006) Nuclear ADP-ribosylation reactions in mammalian cells: where are we today and where are we going? *Microbiol. Mol. Biol. Rev.* **70**, 789-829

[6] Ueda, K., Ogata, N., Kawaichi, M., Inada, S., and Hayaishi, O. (1982) ADP-ribosylation reactions. *Current topics in cellular regulation* **21**, 175-187

[7] Alvarez-Gonzalez, R., and Mendoza-Alvarez, H. (1995) Dissection of ADP-ribose polymer synthesis into individual steps of initiation, elongation, and branching. *Biochimie* **77**, 403-407

[8] Nikiforov, A., Dölle, C., Niere, M., and Ziegler, M. (2011) Pathways and subcellular compartmentation of NAD biosynthesis in human cells: from entry of extracellular precursors to mitochondrial NAD generation. *J. Biol. Chem.* **286**, 21767-21778

[9] Schreiber, V., Dantzer, F., Ame, J. C., and de Murcia, G. (2006) Poly(ADP-ribose): novel functions for an old molecule. *Nat. Rev. Mol. Cell Biol.* **7**, 517-528

[10] Shieh, W. M., Ame, J. C., Wilson, M. V., Wang, Z. Q., Koh, D. W., Jacobson, M. K., and Jacobson, E. L. (1998) Poly(ADP-ribose) polymerase null mouse cells synthesize ADP-ribose polymers. *J. Biol. Chem.* **273**, 30069-30072

[11] Dölle, C., Niere, M., Lohndal, E., and Ziegler, M. (2010) Visualization of subcellular NAD pools and intra-organellar protein localization by poly-ADP-ribose formation. *Cell. Mol. Life Sci.* **67**, 433-443

[12] Phillips, D. M. (1963) The presence of acetyl groups of histones. *Biochem. J.* **87**, 258-263

[13] Allfrey, V. G., Faulkner, R., and Mirsky, A. E. (1964) Acetylation and Methylation of Histones and Their Possible Role in the Regulation of Rna Synthesis. *Proceedings of the National Academy of Sciences of the United States of America* **51**, 786-794

[14] Allfrey, V. G., and Mirsky, A. E. (1964) Structural Modifications of Histones and their Possible Role in the Regulation of RNA Synthesis. *Science* **144**, 559

[15] Yang, X. J. (2004) Lysine acetylation and the bromodomain: a new partnership for signaling. *Bioessays* **26**, 1076-1087

[16] Musselman, C. A., and Kutateladze, T. G. (2011) Handpicking epigenetic marks with PHD fingers. *Nucleic Acids Res.* **39**, 9061-9071

[17] Choudhary, C., Kumar, C., Gnad, F., Nielsen, M. L., Rehman, M., Walther, T. C., Olsen, J. V., and Mann, M. (2009) Lysine acetylation targets protein complexes and co-regulates major cellular functions. *Science* **325**, 834-840

[18] Lombardi, P. M., Cole, K. E., Dowling, D. P., and Christianson, D. W. (2011) Structure, mechanism, and inhibition of histone deacetylases and related metalloenzymes. *Curr. Opin. Struct. Biol.* **21**, 735-743

[19] Imai, S., Armstrong, C. M., Kaeberlein, M., and Guarente, L. (2000) Transcriptional silencing and longevity protein Sir2 is an NAD-dependent histone deacetylase. *Nature* **403**, 795-800

[20] Rine, J., and Herskowitz, I. (1987) Four genes responsible for a position effect on expression from HML and HMR in Saccharomyces cerevisiae. *Genetics* **116**, 9-22

[21] Tsukamoto, Y., Kato, J., and Ikeda, H. (1997) Silencing factors participate in DNA repair and recombination in Saccharomyces cerevisiae. *Nature* **388**, 900-903

[22] Sinclair, D. A., and Guarente, L. (1997) Extrachromosomal rDNA circles--a cause of aging in yeast. *Cell* **91**, 1033-1042

[23] Kaeberlein, M., McVey, M., and Guarente, L. (1999) The SIR2/3/4 complex and SIR2 alone promote longevity in Saccharomyces cerevisiae by two different mechanisms. *Genes Dev.* **13**, 2570-2580

[24] Frye, R. A. (1999) Characterization of five human cDNAs with homology to the yeast SIR2 gene: Sir2-like proteins (sirtuins) metabolize NAD and may have protein ADP-ribosyltransferase activity. *Biochem. Biophys. Res. Commun.* **260**, 273-279

[25] Frye, R. A. (2000) Phylogenetic classification of prokaryotic and eukaryotic Sir2-like proteins. *Biochem. Biophys. Res. Commun.* **273**, 793-798

[26] Du, J., Zhou, Y., Su, X., Yu, J. J., Khan, S., Jiang, H., Kim, J., Woo, J., Kim, J. H., Choi, B. H., He, B., Chen, W., Zhang, S., Cerione, R. A., Auwerx, J., Hao, Q., and Lin, H. (2011) Sirt5 is a NAD-dependent protein lysine demalonylase and desuccinylase. *Science* **334**, 806-809

[27] Feldman, J. L., Baeza, J., and Denu, J. M. (2013) Activation of the protein deacetylase SIRT6 by long-chain fatty acids and widespread deacylation by mammalian sirtuins. *The Journal of biological chemistry* **288**, 31350-31356

[28] Brachmann, C. B., Sherman, J. M., Devine, S. E., Cameron, E. E., Pillus, L., and Boeke, J. D. (1995) The SIR2 gene family, conserved from bacteria to humans, functions in silencing, cell cycle progression, and chromosome stability. *Genes Dev.* **9**, 2888-2902

[29] Min, J., Landry, J., Sternglanz, R., and Xu, R. M. (2001) Crystal structure of a SIR2 homolog-NAD complex. *Cell* **105**, 269-279

[30] Yuan, H., and Marmorstein, R. (2012) Structural basis for sirtuin activity and inhibition. *J. Biol. Chem.* **287**, 42428-42435

[31] Feldman, J. L., Dittenhafer-Reed, K. E., and Denu, J. M. (2012) Sirtuin catalysis and regulation. *J. Biol. Chem.* **287**, 42419-42427

[32] Moniot, S., Schutkowski, M., and Steegborn, C. (2013) Crystal structure analysis of human Sirt2 and its ADP-ribose complex. *Journal of structural biology* **182**, 136-143

[33] Chakrabarty, S. P., and Balaram, H. (2010) Reversible binding of zinc in Plasmodium falciparum Sir2: structure and activity of the apoenzyme. *Biochimica et biophysica acta* **1804**, 1743-1750

[34] Canto, C., and Auwerx, J. (2009) PGC-1alpha, SIRT1 and AMPK, an energy sensing network that controls energy expenditure. *Current opinion in lipidology* **20**, 98-105

[35] Canto, C., Gerhart-Hines, Z., Feige, J. N., Lagouge, M., Noriega, L., Milne, J. C., Elliott, P. J., Puigserver, P., and Auwerx, J. (2009) AMPK regulates energy expenditure by modulating NAD+ metabolism and SIRT1 activity. *Nature* **458**, 1056-1060

[36] Noriega, L. G., Feige, J. N., Canto, C., Yamamoto, H., Yu, J., Herman, M. A., Mataki, C., Kahn, B. B., and Auwerx, J. (2011) CREB and ChREBP oppositely regulate SIRT1 expression in response to energy availability. *EMBO reports* **12**, 1069-1076

[37] Flick, F., and Luscher, B. (2012) Regulation of sirtuin function by posttranslational modifications. *Frontiers in pharmacology* **3**, 29

[38] Houtkooper, R. H., Pirinen, E., and Auwerx, J. (2012) Sirtuins as regulators of metabolism and healthspan. *Nature reviews. Molecular cell biology* **13**, 225-238

[39] Vaquero, A., Scher, M., Lee, D., Erdjument-Bromage, H., Tempst, P., and Reinberg, D. (2004) Human SirT1 interacts with histone H1 and promotes formation of facultative heterochromatin. *Mol. Cell* **16**, 93-105

[40] Nakagawa, T., and Guarente, L. (2011) Sirtuins at a glance. *J. Cell Sci.* **124**, 833-838

[41] Mostoslavsky, R., Chua, K. F., Lombard, D. B., Pang, W. W., Fischer, M. R., Gellon, L., Liu, P., Mostoslavsky, G., Franco, S., Murphy, M. M., Mills, K. D., Patel, P., Hsu, J. T., Hong, A. L., Ford, E., Cheng, H. L., Kennedy, C., Nunez, N., Bronson, R., Frendewey, D., Auerbach, W., Valenzuela, D., Karow, M., Hottiger, M. O., Hursting, S., Barrett, J. C., Guarente, L., Mulligan, R., Demple, B., Yancopoulos, G. D., and Alt, F. W. (2006) Genomic instability and aging-like phenotype in the absence of mammalian SIRT6. *Cell* **124**, 315-329

[42] Dölle, C., Rack, J. G., and Ziegler, M. (2013) NAD and ADP-ribose metabolism in mitochondria. *FEBS J.* **280**, 3530-3541

[43] Luo, J., Nikolaev, A. Y., Imai, S., Chen, D., Su, F., Shiloh, A., Guarente, L., and Gu, W. (2001) Negative control of p53 by Sir2alpha promotes cell survival under stress. *Cell* **107**, 137-148

[44] Muth, V., Nadaud, S., Grummt, I., and Voit, R. (2001) Acetylation of TAF(I)68, a subunit of TIF-IB/SL1, activates RNA polymerase I transcription. *EMBO J.* **20**, 1353-1362

[45] Vaziri, H., Dessain, S. K., Ng Eaton, E., Imai, S. I., Frye, R. A., Pandita, T. K., Guarente, L., and Weinberg, R. A. (2001) hSIR2(SIRT1) functions as an NAD-dependent p53 deacetylase. *Cell* **107**, 149-159

[46] Yeung, F., Hoberg, J. E., Ramsey, C. S., Keller, M. D., Jones, D. R., Frye, R. A., and Mayo, M. W. (2004) Modulation of NF-kappaB-dependent transcription and cell survival by the SIRT1 deacetylase. *EMBO J.* **23**, 2369-2380

[47] Hallows, W. C., Lee, S., and Denu, J. M. (2006) Sirtuins deacetylate and activate mammalian acetyl-CoA synthetases. *Proceedings of the National Academy of Sciences of the United States of America* **103**, 10230-10235

[48] Li, X., Zhang, S., Blander, G., Tse, J. G., Krieger, M., and Guarente, L. (2007) SIRT1 deacetylates and positively regulates the nuclear receptor LXR. *Mol. Cell* **28**, 91-106

[49] Firestein, R., Blander, G., Michan, S., Oberdoerffer, P., Ogino, S., Campbell, J., Bhimavarapu, A., Luikenhuis, S., de Cabo, R., Fuchs, C., Hahn, W. C., Guarente, L. P., and Sinclair, D. A. (2008) The SIRT1 deacetylase suppresses intestinal tumorigenesis and colon cancer growth. *PloS one* **3**, e2020

[50] Ikenoue, T., Inoki, K., Zhao, B., and Guan, K. L. (2008) PTEN acetylation modulates its interaction with PDZ domain. *Cancer Res.* **68**, 6908-6912

[51] Nakahata, Y., Kaluzova, M., Grimaldi, B., Sahar, S., Hirayama, J., Chen, D., Guarente, L. P., and Sassone-Corsi, P. (2008) The NAD+-dependent deacetylase SIRT1 modulates CLOCK-mediated chromatin remodeling and circadian control. *Cell* **134**, 329-340

[52] Lim, J. H., Lee, Y. M., Chun, Y. S., Chen, J., Kim, J. E., and Park, J. W. (2010) Sirtuin 1 modulates cellular responses to hypoxia by deacetylating hypoxia-inducible factor 1alpha. *Mol. Cell* **38**, 864-878

[53] Wang, J., and Chen, J. (2010) SIRT1 regulates autoacetylation and histone acetyltransferase activity of TIP60. *J. Biol. Chem.* **285**, 11458-11464

[54] Stunkel, W., and Campbell, R. M. (2011) Sirtuin 1 (SIRT1): the misunderstood HDAC. *J. Biomol. Screen.* **16**, 1153-1169

[55] North, B. J., Marshall, B. L., Borra, M. T., Denu, J. M., and Verdin, E. (2003) The human Sir2 ortholog, SIRT2, is an NAD+-dependent tubulin deacetylase. *Molecular cell* **11**, 437-444

[56] Vaquero, A., Scher, M. B., Lee, D. H., Sutton, A., Cheng, H. L., Alt, F. W., Serrano, L., Sternglanz, R., and Reinberg, D. (2006) SirT2 is a histone deacetylase with preference for histone H4 Lys 16 during mitosis. *Genes Dev.* **20**, 1256-1261

[57] Wang, F., Nguyen, M., Qin, F. X., and Tong, Q. (2007) SIRT2 deacetylates FOXO3a in response to oxidative stress and caloric restriction. *Aging cell* **6**, 505-514

[58] Black, J. C., Mosley, A., Kitada, T., Washburn, M., and Carey, M. (2008) The SIRT2 deacetylase regulates autoacetylation of p300. *Molecular cell* **32**, 449-455

[59] Vempati, R. K., Jayani, R. S., Notani, D., Sengupta, A., Galande, S., and Haldar, D. (2010) p300-mediated acetylation of histone H3 lysine 56 functions in DNA damage response in mammals. *J. Biol. Chem.* **285**, 28553-28564

[60] Jiang, W., Wang, S., Xiao, M., Lin, Y., Zhou, L., Lei, Q., Xiong, Y., Guan, K. L., and Zhao, S. (2011) Acetylation regulates gluconeogenesis by promoting PEPCK1 degradation via recruiting the UBR5 ubiquitin ligase. *Mol. Cell* **43**, 33-44

[61] Shi, T., Wang, F., Stieren, E., and Tong, Q. (2005) SIRT3, a mitochondrial sirtuin deacetylase, regulates mitochondrial function and thermogenesis in brown adipocytes. *J. Biol. Chem.* **280**, 13560-13567

[62] Schwer, B., Bunkenborg, J., Verdin, R. O., Andersen, J. S., and Verdin, E. (2006) Reversible lysine acetylation controls the activity of the mitochondrial enzyme acetyl-CoA synthetase 2. *Proceedings of the National Academy of Sciences of the United States of America* **103**, 10224-10229

[63] Schlicker, C., Gertz, M., Papatheodorou, P., Kachholz, B., Becker, C. F., and Steegborn, C. (2008) Substrates and regulation mechanisms for the human mitochondrial sirtuins Sirt3 and Sirt5. *J. Mol. Biol.* **382**, 790-801

[64] Cimen, H., Han, M. J., Yang, Y., Tong, Q., Koc, H., and Koc, E. C. (2010) Regulation of succinate dehydrogenase activity by SIRT3 in mammalian mitochondria. *Biochemistry* **49**, 304-311

[65] Hirschey, M. D., Shimazu, T., Goetzman, E., Jing, E., Schwer, B., Lombard, D. B., Grueter, C. A., Harris, C., Biddinger, S., Ilkayeva, O. R., Stevens, R. D., Li, Y., Saha, A. K., Ruderman, N. B., Bain, J. R., Newgard, C. B., Farese, R. V., Jr., Alt, F. W., Kahn, C. R., and Verdin, E. (2010) SIRT3 regulates mitochondrial fatty-acid oxidation by reversible enzyme deacetylation. *Nature* **464**, 121-125

[66] Shimazu, T., Hirschey, M. D., Hua, L., Dittenhafer-Reed, K. E., Schwer, B., Lombard, D. B., Li, Y., Bunkenborg, J., Alt, F. W., Denu, J. M., Jacobson, M. P., and Verdin, E. (2010) SIRT3 deacetylates mitochondrial 3-hydroxy-3-methylglutaryl CoA synthase 2 and regulates ketone body production. *Cell metabolism* **12**, 654-661

[67] Sol, E. M., Wagner, S. A., Weinert, B. T., Kumar, A., Kim, H. S., Deng, C. X., and Choudhary, C. (2012) Proteomic investigations of lysine acetylation identify diverse substrates of mitochondrial deacetylase sirt3. *PloS one* **7**, e50545

[68] Hebert, A. S., Dittenhafer-Reed, K. E., Yu, W., Bailey, D. J., Selen, E. S., Boersma, M. D., Carson, J. J., Tonelli, M., Balloon, A. J., Higbee, A. J., Westphall, M. S., Pagliarini, D. J., Prolla, T. A., Assadi-Porter, F., Roy, S., Denu, J. M., and Coon, J. J. (2013) Calorie restriction and SIRT3 trigger global reprogramming of the mitochondrial protein acetylome. *Mol. Cell* **49**, 186-199

[69] Chegary, M., Brinke, H., Ruiter, J. P., Wijburg, F. A., Stoll, M. S., Minkler, P. E., van Weeghel, M., Schulz, H., Hoppel, C. L., Wanders, R. J., and Houten, S. M. (2009) Mitochondrial long chain fatty acid beta-oxidation in man and mouse. *Biochim. Biophys. Acta* **1791**, 806-815

[70] Bell, E. L., and Guarente, L. (2011) The SirT3 divining rod points to oxidative stress. *Mol. Cell* **42**, 561-568

[71] Finley, L. W., Haas, W., Desquiret-Dumas, V., Wallace, D. C., Procaccio, V., Gygi, S. P., and Haigis, M. C. (2011) Succinate dehydrogenase is a direct target of sirtuin 3 deacetylase activity. *PloS one* **6**, e23295

[72] Hallows, W. C., Yu, W., Smith, B. C., Devries, M. K., Ellinger, J. J., Someya, S., Shortreed, M. R., Prolla, T., Markley, J. L., Smith, L. M., Zhao, S., Guan, K. L., and Denu, J. M. (2011) Sirt3 promotes the urea cycle and fatty acid oxidation during dietary restriction. *Mol. Cell* **41**, 139-149

[73] Giralt, A., and Villarroya, F. (2012) SIRT3, a pivotal actor in mitochondrial functions: metabolism, cell death and aging. *Biochem. J.* **444**, 1-10

[74] Haigis, M. C., Mostoslavsky, R., Haigis, K. M., Fahie, K., Christodoulou, D. C., Murphy, A. J., Valenzuela, D. M., Yancopoulos, G. D., Karow, M., Blander, G., Wolberger, C., Prolla, T. A., Weindruch, R., Alt, F. W., and Guarente, L. (2006) SIRT4 inhibits glutamate dehydrogenase and opposes the effects of calorie restriction in pancreatic beta cells. *Cell* **126**, 941-954

[75] Laurent, G., German, N. J., Saha, A. K., de Boer, V. C., Davies, M., Koves, T. R., Dephoure, N., Fischer, F., Boanca, G., Vaitheesvaran, B., Lovitch, S. B., Sharpe, A. H., Kurland, I. J., Steegborn, C., Gygi, S. P., Muoio, D. M., Ruderman, N. B., and Haigis, M. C. (2013) SIRT4 coordinates the balance between lipid synthesis and catabolism by repressing malonyl CoA decarboxylase. *Mol. Cell* **50**, 686-698

[76] Mathias, R. A., Greco, T. M., Oberstein, A., Budayeva, H. G., Chakrabarti, R., Rowland, E. A., Kang, Y., Shenk, T., and Cristea, I. M. (2014) Sirtuin 4 is a lipoamidase regulating pyruvate dehydrogenase complex activity. *Cell* **159**, 1615-1625

[77] Nakagawa, T., Lomb, D. J., Haigis, M. C., and Guarente, L. (2009) SIRT5 Deacetylates carbamoyl phosphate synthetase 1 and regulates the urea cycle. *Cell* **137**, 560-570

[78] Peng, C., Lu, Z., Xie, Z., Cheng, Z., Chen, Y., Tan, M., Luo, H., Zhang, Y., He, W., Yang, K., Zwaans, B. M., Tishkoff, D., Ho, L., Lombard, D., He, T. C., Dai, J., Verdin, E., Ye, Y., and Zhao, Y. (2011) The first identification of lysine malonylation substrates and its regulatory enzyme. *Mol. Cell. Proteomics* **10**, M111 012658

[79] Tan, M., Peng, C., Anderson, K. A., Chhoy, P., Xie, Z., Dai, L., Park, J., Chen, Y., Huang, H., Zhang, Y., Ro, J., Wagner, G. R., Green, M. F., Madsen, A. S., Schmiesing, J., Peterson, B. S., Xu, G., Ilkayeva, O. R., Muehlbauer, M. J., Braulke, T., Muhlhausen, C., Backos, D. S., Olsen, C. A., McGuire, P. J., Pletcher, S. D., Lombard, D. B., Hirschey, M. D., and Zhao, Y. (2014) Lysine glutarylation is a protein posttranslational modification regulated by SIRT5. *Cell metabolism* **19**, 605-617

[80] Michishita, E., McCord, R. A., Berber, E., Kioi, M., Padilla-Nash, H., Damian, M., Cheung, P., Kusumoto, R., Kawahara, T. L., Barrett, J. C., Chang, H. Y., Bohr, V. A., Ried, T., Gozani, O., and Chua, K. F. (2008) SIRT6 is a histone H3 lysine 9 deacetylase that modulates telomeric chromatin. *Nature* **452**, 492-496

[81] Kawahara, T. L., Michishita, E., Adler, A. S., Damian, M., Berber, E., Lin, M., McCord, R. A., Ongaigui, K. C., Boxer, L. D., Chang, H. Y., and Chua, K. F. (2009) SIRT6 links histone H3 lysine 9 deacetylation to NF-kappaB-dependent gene expression and organismal life span. *Cell* **136**, 62-74

[82] Yang, B., Zwaans, B. M., Eckersdorff, M., and Lombard, D. B. (2009) The sirtuin SIRT6 deacetylates H3 K56Ac in vivo to promote genomic stability. *Cell cycle* **8**, 2662-2663

[83] Kaidi, A., Weinert, B. T., Choudhary, C., and Jackson, S. P. (2010) Human SIRT6 promotes DNA end resection through CtIP deacetylation. *Science* **329**, 1348-1353

[84] Mao, Z., Hine, C., Tian, X., Van Meter, M., Au, M., Vaidya, A., Seluanov, A., and Gorbunova, V. (2011) SIRT6 promotes DNA repair under stress by activating PARP1. *Science* **332**, 1443-1446

[85] Jiang, H., Khan, S., Wang, Y., Charron, G., He, B., Sebastian, C., Du, J., Kim, R., Ge, E., Mostoslavsky, R., Hang, H. C., Hao, Q., and Lin, H. (2013) SIRT6 regulates TNF-alpha secretion through hydrolysis of long-chain fatty acyl lysine. *Nature* **496**, 110-113

[86] Zhong, L., D'Urso, A., Toiber, D., Sebastian, C., Henry, R. E., Vadysirisack, D. D., Guimaraes, A., Marinelli, B., Wikstrom, J. D., Nir, T., Clish, C. B., Vaitheesvaran, B., Iliopoulos, O., Kurland, I., Dor, Y., Weissleder, R., Shirihai, O. S., Ellisen, L. W., Espinosa, J. M., and Mostoslavsky, R. (2010) The histone deacetylase Sirt6 regulates glucose homeostasis via Hif1alpha. *Cell* **140**, 280-293

[87] Barber, M. F., Michishita-Kioi, E., Xi, Y., Tasselli, L., Kioi, M., Moqtaderi, Z., Tennen, R. I., Paredes, S., Young, N. L., Chen, K., Struhl, K., Garcia, B. A., Gozani, O., Li, W., and Chua, K. F. (2012) SIRT7 links H3K18 deacetylation to maintenance of oncogenic transformation. *Nature* **487**, 114-118

[88] Chen, S., Seiler, J., Santiago-Reichelt, M., Felbel, K., Grummt, I., and Voit, R. (2013) Repression of RNA polymerase I upon stress is caused by inhibition of RNA-dependent deacetylation of PAF53 by SIRT7. *Mol. Cell* **52**, 303-313

[89] Karim, M. F., Yoshizawa, T., Sato, Y., Sawa, T., Tomizawa, K., Akaike, T., and Yamagata, K. (2013) Inhibition of H3K18 deacetylation of Sirt7 by Myb-binding protein 1a (Mybbp1a). *Biochem. Biophys. Res. Commun.* **441**, 157-163

[90] Lee, N., Kim, D. K., Kim, E. S., Park, S. J., Kwon, J. H., Shin, J., Park, S. M., Moon, Y. H., Wang, H. J., Gho, Y. S., and Choi, K. Y. (2014) Comparative interactomes of SIRT6 and SIRT7: Implication of functional links to aging. *Proteomics* **14**, 1610-1622

[91] Ryu, D., Jo, Y. S., Lo Sasso, G., Stein, S., Zhang, H., Perino, A., Lee, J. U., Zeviani, M., Romand, R., Hottiger, M. O., Schoonjans, K., and Auwerx, J. (2014) A SIRT7-dependent acetylation switch of GABPbeta1 controls mitochondrial function. *Cell metabolism* **20**, 856-869

[92] Ford, E., Voit, R., Liszt, G., Magin, C., Grummt, I., and Guarente, L. (2006) Mammalian Sir2 homolog SIRT7 is an activator of RNA polymerase I transcription. *Genes Dev.* **20**, 1075-1080

[93] De Nigris, F., Cerutti, J., Morelli, C., Califano, D., Chiariotti, L., Viglietto, G., Santelli, G., and Fusco, A. (2002) Isolation of a SIR-like gene, SIR-T8, that is overexpressed in thyroid carcinoma cell lines and tissues. *Br. J. Cancer* **87**, 1479

[94] Frye, R. (2002) "SIRT8" expressed in thyroid cancer is actually SIRT7. *Br. J. Cancer* **87**, 1479

[95] Ashraf, N., Zino, S., Macintyre, A., Kingsmore, D., Payne, A. P., George, W. D., and Shiels, P. G. (2006) Altered sirtuin expression is associated with node-positive breast cancer. *Br. J. Cancer* **95**, 1056-1061

[96] Lombard, D. B., Alt, F. W., Cheng, H. L., Bunkenborg, J., Streeper, R. S., Mostoslavsky, R., Kim, J., Yancopoulos, G., Valenzuela, D., Murphy, A., Yang, Y., Chen, Y., Hirschey, M. D., Bronson, R. T., Haigis, M., Guarente, L. P., Farese, R. V., Jr., Weissman, S., Verdin, E., and Schwer, B. (2007) Mammalian Sir2 homolog SIRT3 regulates global mitochondrial lysine acetylation. *Mol. Cell. Biol.* **27**, 8807-8814

[97] Anderson, K. A., and Hirschey, M. D. (2012) Mitochondrial protein acetylation regulates metabolism. *Essays in biochemistry* **52**, 23-35

[98] Reed, N. A., Cai, D., Blasius, T. L., Jih, G. T., Meyhofer, E., Gaertig, J., and Verhey, K. J. (2006) Microtubule acetylation promotes kinesin-1 binding and transport. *Curr. Biol.* **16**, 2166-2172

[99] Dompierre, J. P., Godin, J. D., Charrin, B. C., Cordelieres, F. P., King, S. J., Humbert, S., and Saudou, F. (2007) Histone deacetylase 6 inhibition compensates for the transport deficit in Huntington's disease by increasing tubulin acetylation. *J. Neurosci.* **27**, 3571-3583

[100] Houtkooper, R. H., Canto, C., Wanders, R. J., and Auwerx, J. (2010) The secret life of NAD+: an old metabolite controlling new metabolic signaling pathways. *Endocrine reviews* **31**, 194-223

[101] Dryden, S. C., Nahhas, F. A., Nowak, J. E., Goustin, A. S., and Tainsky, M. A. (2003) Role for human SIRT2 NAD-dependent deacetylase activity in control of mitotic exit in the cell cycle. *Mol. Cell. Biol.* **23**, 3173-3185

[102] Serrano, L., Martinez-Redondo, P., Marazuela-Duque, A., Vazquez, B. N., Dooley, S. J., Voigt, P., Beck, D. B., Kane-Goldsmith, N., Tong, Q., Rabanal, R. M., Fondevila, D., Munoz, P., Kruger, M., Tischfield, J. A., and Vaquero, A. (2013) The tumor suppressor SirT2 regulates cell cycle progression and genome stability by modulating the mitotic deposition of H4K20 methylation. *Genes Dev.* **27**, 639-653

[103] Tanno, M., Sakamoto, J., Miura, T., Shimamoto, K., and Horio, Y. (2007) Nucleocytoplasmic shuttling of the NAD+-dependent histone deacetylase SIRT1. *J. Biol. Chem.* **282**, 6823-6832

[104] Hisahara, S., Chiba, S., Matsumoto, H., Tanno, M., Yagi, H., Shimohama, S., Sato, M., and Horio, Y. (2008) Histone deacetylase SIRT1 modulates neuronal differentiation by its nuclear translocation. *Proceedings of the National Academy of Sciences of the United States of America* **105**, 15599-15604

[105] Scher, M. B., Vaquero, A., and Reinberg, D. (2007) SirT3 is a nuclear NAD+-dependent histone deacetylase that translocates to the mitochondria upon cellular stress. *Genes Dev.* **21**, 920-928

[106] Matsushita, N., Yonashiro, R., Ogata, Y., Sugiura, A., Nagashima, S., Fukuda, T., Inatome, R., and Yanagi, S. (2011) Distinct regulation of mitochondrial localization and stability of two human Sirt5 isoforms. *Genes Cells* **16**, 190-202

[107] Iwahara, T., Bonasio, R., Narendra, V., and Reinberg, D. (2012) SIRT3 functions in the nucleus in the control of stress-related gene expression. *Mol. Cell. Biol.* **32**, 5022-5034

[108] North, B. J., and Verdin, E. (2007) Interphase nucleo-cytoplasmic shuttling and localization of SIRT2 during mitosis. *PloS one* **2**, e784

[109] Yang, H., Yang, T., Baur, J. A., Perez, E., Matsui, T., Carmona, J. J., Lamming, D. W., Souza-Pinto, N. C., Bohr, V. A., Rosenzweig, A., de Cabo, R., Sauve, A. A., and Sinclair, D. A. (2007) Nutrient-sensitive mitochondrial NAD+ levels dictate cell survival. *Cell* **130**, 1095-1107

[110] Trammell, S. A., and Brenner, C. (2013) Targeted, LCMS-based Metabolomics for Quantitative Measurement of NAD(+) Metabolites. *Computational and structural biotechnology journal* **4**, e201301012

[111] Nishizuka, Y., and Hayaishi, O. (1963) Studies on the Biosynthesis of Nicotinamide Adenine Dinucleotide. I. Enzymic Synthesis of Niacin Ribonucleotides from 3-Hydroxyanthranilic Acid in Mammalian Tissues. *J. Biol. Chem.* **238**, 3369-3377

[112] Nishizuka, Y., and Hayaishi, O. (1963) Enzymic synthesis of niacin nucleotides from 3-hydroxyanthranilic acid in mammalian liver. *J. Biol. Chem.* **238**, 483-485

[113] Preiss, J., and Handler, P. (1958) Biosynthesis of diphosphopyridine nucleotide. II. Enzymatic aspects. *J. Biol. Chem.* **233**, 493-500

[114] Preiss, J., and Handler, P. (1958) Biosynthesis of diphosphopyridine nucleotide. I. Identification of intermediates. *J. Biol. Chem.* **233**, 488-492

[115] Rongvaux, A., Andris, F., Van Gool, F., and Leo, O. (2003) Reconstructing eukaryotic NAD metabolism. *Bioessays* **25**, 683-690

[116] Sporty, J., Lin, S. J., Kato, M., Ognibene, T., Stewart, B., Turteltaub, K., and Bench, G. (2009) Quantitation of NAD+ biosynthesis from the salvage pathway in Saccharomyces cerevisiae. *Yeast* **26**, 363-369

[117] Terakata, M., Fukuwatari, T., Sano, M., Nakao, N., Sasaki, R., Fukuoka, S., and Shibata, K. (2012) Establishment of true niacin deficiency in quinolinic acid phosphoribosyltransferase knockout mice. *J. Nutr.* **142**, 2148-2153

[118] Bieganowski, P., and Brenner, C. (2004) Discoveries of nicotinamide riboside as a nutrient and conserved NRK genes establish a Preiss-Handler independent route to NAD+ in fungi and humans. *Cell* **117**, 495-502

[119] Tempel, W., Rabeh, W. M., Bogan, K. L., Belenky, P., Wojcik, M., Seidle, H. F., Nedyalkova, L., Yang, T., Sauve, A. A., Park, H. W., and Brenner, C. (2007) Nicotinamide riboside kinase structures reveal new pathways to NAD+. *PLoS Biol.* **5**, e263

[120] Rowen, J. W., and Kornberg, A. (1951) The phosphorolysis of nicotinamide riboside. *J. Biol. Chem.* **193**, 497-507

[121] Grossman, L., and Kaplan, N. O. (1958) Nicotinamide riboside phosphorylase from human erythrocytes. II. Nicotinamide sensitivity. *J. Biol. Chem.* **231**, 727-740

[122] Grossman, L., and Kaplan, N. O. (1958) Nicotinamide riboside phosphorylase from human erythrocytes. I. Phosphorolytic activity. *J. Biol. Chem.* **231**, 717-726

[123] Wielgus-Kutrowska, B., Kulikowska, E., Wierzchowski, J., Bzowska, A., and Shugar, D. (1997) Nicotinamide riboside, an unusual, non-typical, substrate of purified purine-nucleoside phosphorylases. *Eur. J. Biochem.* **243**, 408-414

[124] Berger, F., Lau, C., Dahlmann, M., and Ziegler, M. (2005) Subcellular compartmentation and differential catalytic properties of the three human nicotinamide mononucleotide adenylyltransferase isoforms. *The Journal of biological chemistry* **280**, 36334-36341

[125] Berger, F., Lau, C., and Ziegler, M. (2007) Regulation of poly(ADP-ribose) polymerase 1 activity by the phosphorylation state of the nuclear NAD biosynthetic enzyme NMN adenylyl transferase 1. *Proceedings of the National Academy of Sciences of the United States of America* **104**, 3765-3770

[126] Zhang, T., Berrocal, J. G., Yao, J., DuMond, M. E., Krishnakumar, R., Ruhl, D. D., Ryu, K. W., Gamble, M. J., and Kraus, W. L. (2012) Regulation of poly(ADP-ribose) polymerase-1-dependent gene expression through promoter-directed recruitment of a nuclear NAD+ synthase. *J. Biol. Chem.* **287**, 12405-12416

[127] Zhang, T., Berrocal, J. G., Frizzell, K. M., Gamble, M. J., DuMond, M. E., Krishnakumar, R., Yang, T., Sauve, A. A., and Kraus, W. L. (2009) Enzymes in the NAD+ salvage pathway regulate SIRT1 activity at target gene promoters. *J. Biol. Chem.* **284**, 20408-20417

[128] Raffaelli, N., Sorci, L., Amici, A., Emanuelli, M., Mazzola, F., and Magni, G. (2002) Identification of a novel human nicotinamide mononucleotide adenylyltransferase. *Biochem. Biophys. Res. Commun.* **297**, 835-840

[129] Gilley, J., and Coleman, M. P. (2010) Endogenous Nmnat2 is an essential survival factor for maintenance of healthy axons. *PLoS Biol.* **8**, e1000300

[130] Bricker, D. K., Taylor, E. B., Schell, J. C., Orsak, T., Boutron, A., Chen, Y. C., Cox, J. E., Cardon, C. M., Van Vranken, J. G., Dephoure, N., Redin, C., Boudina, S., Gygi, S. P., Brivet, M., Thummel, C. S., and Rutter, J. (2012) A mitochondrial pyruvate carrier required for pyruvate uptake in yeast, Drosophila, and humans. *Science* **337**, 96-100

[131] Herzig, S., Raemy, E., Montessuit, S., Veuthey, J. L., Zamboni, N., Westermann, B., Kunji, E. R., and Martinou, J. C. (2012) Identification and functional expression of the mitochondrial pyruvate carrier. *Science* **337**, 93-96

[132] Di Lisa, F. (2001) Mitochondrial Contribution in the Progression of Cardiac Ischemic Injury. *IUBMB Life* **52**, 255-261

[133] Pittelli, M., Formentini, L., Faraco, G., Lapucci, A., Rapizzi, E., Cialdai, F., Romano, G., Moneti, G., Moroni, F., and Chiarugi, A. (2010) Inhibition of nicotinamide phosphoribosyltransferase: cellular bioenergetics reveals a mitochondrial insensitive NAD pool. *J. Biol. Chem.* **285**, 34106-34114

[134] Niere, M., Kernstock, S., Koch-Nolte, F., and Ziegler, M. (2008) Functional localization of two poly(ADP-ribose)-degrading enzymes to the mitochondrial matrix. *Mol. Cell. Biol.* **28**, 814-824

[135] Kristian, T., Balan, I., Schuh, R., and Onken, M. (2011) Mitochondrial dysfunction and nicotinamide dinucleotide catabolism as mechanisms of cell death and promising targets for neuroprotection. *J. Neurosci. Res.* **89**, 1946-1955

[136] Todisco, S., Agrimi, G., Castegna, A., and Palmieri, F. (2006) Identification of the mitochondrial NAD+ transporter in Saccharomyces cerevisiae. *J. Biol. Chem.* **281**, 1524-1531

[137] Palmieri, F., Rieder, B., Ventrella, A., Blanco, E., Do, P. T., Nunes-Nesi, A., Trauth, A. U., Fiermonte, G., Tjaden, J., Agrimi, G., Kirchberger, S., Paradies, E., Fernie, A. R., and Neuhaus, H. E. (2009) Molecular identification and functional characterization of Arabidopsis thaliana mitochondrial and chloroplastic NAD+ carrier proteins. *J. Biol. Chem.* **284**, 31249-31259

[138] Agrimi, G., Russo, A., Scarcia, P., and Palmieri, F. (2012) The human gene SLC25A17 encodes a peroxisomal transporter of coenzyme A, FAD and NAD+. *Biochem. J.* **443**, 241-247

[139] Palmieri, F. (2013) The mitochondrial transporter family SLC25: identification, properties and physiopathology. *Molecular aspects of medicine* **34**, 465-484

[140] Zhang, X., Kurnasov, O. V., Karthikeyan, S., Grishin, N. V., Osterman, A. L., and Zhang, H. (2003) Structural characterization of a human cytosolic NMN/NaMN adenylyltransferase and implication in human NAD biosynthesis. *J. Biol. Chem.* **278**, 13503-13511

[141] Lau, C., Dolle, C., Gossmann, T. I., Agledal, L., Niere, M., and Ziegler, M. (2010) Isoform-specific targeting and interaction domains in human nicotinamide mononucleotide adenylyltransferases. *J. Biol. Chem.* **285**, 18868-18876

[142] Felici, R., Lapucci, A., Ramazzotti, M., and Chiarugi, A. (2013) Insight into molecular and functional properties of NMNAT3 reveals new hints of NAD homeostasis within human mitochondria. *PloS one* **8**, e76938

[143] Maxwell, M. M., Tomkinson, E. M., Nobles, J., Wizeman, J. W., Amore, A. M., Quinti, L., Chopra, V., Hersch, S. M., and Kazantsev, A. G. (2011) The Sirtuin 2 microtubule deacetylase is an abundant neuronal protein that accumulates in the aging CNS. *Hum. Mol. Genet.* **20**, 3986-3996

[144] Zhu, H., Zhao, L., Wang, E., Dimova, N., Liu, G., Feng, Y., and Cambi, F. (2012) The QKI-PLP pathway controls SIRT2 abundance in CNS myelin. *Glia* **60**, 69-82

[145] Finnin, M. S., Donigian, J. R., and Pavletich, N. P. (2001) Structure of the histone deacetylase SIRT2. *Nat. Struct. Biol.* **8**, 621-625

[146] Zhao, K., Chai, X., and Marmorstein, R. (2004) Structure and substrate binding properties of cobB, a Sir2 homolog protein deacetylase from Escherichia coli. *J. Mol. Biol.* **337**, 731-741

[147] Han, Y., Jin, Y. H., Kim, Y. J., Kang, B. Y., Choi, H. J., Kim, D. W., Yeo, C. Y., and Lee, K. Y. (2008) Acetylation of Sirt2 by p300 attenuates its deacetylase activity. *Biochem. Biophys. Res. Commun.* **375**, 576-580

[148] Oppenheimer, H., Gabay, O., Meir, H., Haze, A., Kandel, L., Liebergall, M., Gagarina, V., Lee, E. J., and Dvir-Ginzberg, M. (2012) 75-kd sirtuin 1 blocks tumor necrosis factor alpha-mediated apoptosis in human osteoarthritic chondrocytes. *Arthritis Rheum.* **64**, 718-728

[149] Pfister, J. A., Ma, C., Morrison, B. E., and D'Mello, S. R. (2008) Opposing effects of sirtuins on neuronal survival: SIRT1-mediated neuroprotection is independent of its deacetylase activity. *PloS one* **3**, e4090

[150] Di Noia, M. A., Todisco, S., Cirigliano, A., Rinaldi, T., Agrimi, G., Iacobazzi, V., and Palmieri, F. (2014) The human SLC25A33 and SLC25A36 genes of solute carrier family 25 encode two mitochondrial pyrimidine nucleotide transporters. *The Journal of biological chemistry* **289**, 33137-33148

[151] Hildyard, J. C., and Halestrap, A. P. (2003) Identification of the mitochondrial pyruvate carrier in Saccharomyces cerevisiae. *Biochem. J.* **374**, 607-611

[152] Schell, J. C., Olson, K. A., Jiang, L., Hawkins, A. J., Van Vranken, J. G., Xie, J., Egnatchik, R. A., Earl, E. G., DeBerardinis, R. J., and Rutter, J. (2014) A role for the mitochondrial pyruvate carrier as a repressor of the Warburg effect and colon cancer cell growth. *Mol. Cell* **56**, 400-413

[153] Berger, F., Lau, C., Dahlmann, M., and Ziegler, M. (2005) Subcellular compartmentation and differential catalytic properties of the three human nicotinamide mononucleotide adenylyltransferase isoforms. *J. Biol. Chem.* **280**, 36334-36341

[154] Zhang, H., Zhou, T., Kurnasov, O., Cheek, S., Grishin, N. V., and Osterman, A. (2002) Crystal structures of E. coli nicotinate mononucleotide adenylyltransferase and its complex with deamido-NAD. *Structure* **10**, 69-79

[155] Revollo, J. R., Grimm, A. A., and Imai, S. (2004) The NAD biosynthesis pathway mediated by nicotinamide phosphoribosyltransferase regulates Sir2 activity in mammalian cells. *J. Biol. Chem.* **279**, 50754-50763

[156] Sasaki, Y., Vohra, B. P., Baloh, R. H., and Milbrandt, J. (2009) Transgenic mice expressing the Nmnat1 protein manifest robust delay in axonal degeneration in vivo. *J. Neurosci.* **29**, 6526-6534

[157] Sasaki, Y., Vohra, B. P., Lund, F. E., and Milbrandt, J. (2009) Nicotinamide mononucleotide adenylyl transferase-mediated axonal protection requires enzymatic activity but not increased levels of neuronal nicotinamide adenine dinucleotide. *J. Neurosci.* **29**, 5525-5535

[158] Di Martino, C., and Pallotta, M. L. (2011) Mitochondria-localized NAD biosynthesis by nicotinamide mononucleotide adenylyltransferase in Jerusalem artichoke (Helianthus tuberosus L.) heterotrophic tissues. *Planta* **234**, 657-670

[159] Di Lisa, F., Menabo, R., Canton, M., Barile, M., and Bernardi, P. (2001) Opening of the mitochondrial permeability transition pore causes depletion of mitochondrial and cytosolic NAD+ and is a causative event in the death of myocytes in postischemic reperfusion of the heart. *J. Biol. Chem.* **276**, 2571-2575

[160] Andrabi, S. A., Umanah, G. K., Chang, C., Stevens, D. A., Karuppagounder, S. S., Gagne, J. P., Poirier, G. G., Dawson, V. L., and Dawson, T. M. (2014) Poly(ADP-ribose) polymerase-dependent energy depletion occurs through inhibition of glycolysis. *Proceedings of the National Academy of Sciences of the United States of America* **111**, 10209-10214

[161] Fouquerel, E., Goellner, E. M., Yu, Z., Gagne, J. P., Barbi de Moura, M., Feinstein, T., Wheeler, D., Redpath, P., Li, J., Romero, G., Migaud, M., Van Houten, B., Poirier, G. G., and Sobol, R. W. (2014) ARTD1/PARP1 negatively regulates glycolysis by inhibiting hexokinase 1 independent of NAD+ depletion. *Cell reports* **8**, 1819-1831

[162] Hardie, D. G., Ross, F. A., and Hawley, S. A. (2012) AMPK: a nutrient and energy sensor that maintains energy homeostasis. *Nat. Rev. Mol. Cell Biol.* **13**, 251-262

[163] Shaw, G., Morse, S., Ararat, M., and Graham, F. L. (2002) Preferential transformation of human neuronal cells by human adenoviruses and the origin of HEK 293 cells. *FASEB J.* **16**, 869-871

[164] Lin, Y. C., Boone, M., Meuris, L., Lemmens, I., Van Roy, N., Soete, A., Reumers, J., Moisse, M., Plaisance, S., Drmanac, R., Chen, J., Speleman, F., Lambrechts, D., Van de Peer, Y., Tavernier, J., and Callewaert, N. (2014) Genome dynamics of the human embryonic kidney 293 lineage in response to cell biology manipulations. *Nature communications* **5**, 4767

[165] Agrimi, G., Brambilla, L., Frascotti, G., Pisano, I., Porro, D., Vai, M., and Palmieri, L. (2011) Deletion or overexpression of mitochondrial NAD+ carriers in Saccharomyces cerevisiae alters cellular NAD and ATP contents and affects mitochondrial metabolism and the rate of glycolysis. *Appl. Environ. Microbiol.* **77**, 2239-2246

[166] Hasmann, M., and Schemainda, I. (2003) FK866, a highly specific noncompetitive inhibitor of nicotinamide phosphoribosyltransferase, represents a novel mechanism for induction of tumor cell apoptosis. *Cancer Res.* **63**, 7436-7442

[167] Bruzzone, S., Fruscione, F., Morando, S., Ferrando, T., Poggi, A., Garuti, A., D'Urso, A., Selmo, M., Benvenuto, F., Cea, M., Zoppoli, G., Moran, E., Soncini, D., Ballestrero, A., Sordat, B., Patrone, F., Mostoslavsky, R., Uccelli, A., and Nencioni, A. (2009) Catastrophic NAD+ depletion in activated T lymphocytes through Nampt inhibition reduces demyelination and disability in EAE. *PloS one* **4**, e7897

I

Constitutive Nuclear Localization of an Alternatively Spliced Sirtuin-2 Isoform

Johannes G.M. Rack, Magali R. VanLinden, Timo Lutter, Rein Aasland and Mathias Ziegler

Department of Molecular Biology, *University of Bergen, Postbox 7803, 5020 Bergen, Norway*

Correspondence to Mathias Ziegler: *mathias.ziegler@mbi.uib.no.*
http://dx.doi.org/10.1016/j.jmb.2013.10.027
Edited by S. Khorasanizadeh

Abstract

Sirtuin-2 (SIRT2), the cytoplasmic member of the sirtuin family, has been implicated in the deacetylation of nuclear proteins. Although the enzyme has been reported to be located to the nucleus during G_2/M phase, its spectrum of targets suggests functions in the nucleus throughout the cell cycle. While a nucleocytoplasmic shuttling mechanism has been proposed for SIRT2, recent studies have indicated the presence of a constitutively nuclear isoform. Here we report the identification of a novel splice variant (isoform 5) of SIRT2 that lacks a nuclear export signal and encodes a predominantly nuclear isoform. This novel isoform 5 fails to show deacetylase activity using several assays, both *in vitro* and *in vivo*, and we are led to conclude that this isoform is catalytically inactive. Nevertheless, it retains the ability to interact with p300, a known interaction partner. Moreover, changes in intrinsic tryptophan fluorescence upon denaturation indicate that the protein is properly folded. These data, together with computational analyses, confirm the structural integrity of the catalytic domain. Our results suggest an activity-independent nuclear function of the novel isoform.

Introduction

Members of the sirtuin family of NAD^+-dependent deacetylases are modulators of various cellular processes including metabolic homeostasis, cell cycle control, development and chromatin organization [1–6]. Consequently, the regulation of sirtuin activity, for example, by alteration of expression levels, posttranslational modifications or subcellular compartmentation [7–12], is a key issue for normal cellular function. A total of seven human sirtuin homologues (SIRT1–SIRT7) with distinct cellular locations have been identified.

SIRT1, SIRT6 and SIRT7 are primarily localized to the nucleus, while SIRT3, SIRT4 and SIRT5 are mitochondrial proteins, and SIRT2 has a predominant cytosolic localization [13–15]. Moreover, several reports suggest that the presence of some sirtuins is not confined to a single subcellular compartment. Localization of SIRT1 was found to be tissue specific in mice with either nuclear, cytoplasmic or nucleocytoplasmic distribution [16,17]. SIRT3 contains a mitochondrial targeting signal and, hence, localizes predominantly to the mitochondria but also displays a partial nuclear localization [18,19]. Similarly, SIRT5 does not only localize to the mitochondria but can be retained in the cytoplasm [9], while a cell cycle-dependent shuttling from the cytosol to the nucleus has been reported for SIRT2 [20].

The molecular mechanisms and functional consequences underlying the different cellular distributions of sirtuins are so far poorly understood. It has been shown that the activation of the phosphatidylinositol 3-kinase pathway in myoblast cells leads to alteration in the subcellular localization of SIRT1 [16,17]. This is achieved by control of the two nuclear localization signals (NLSs) and two nuclear export signals (NESs) in the primary structure of SIRT1 via posttranslational modifications [17]. For SIRT5, subcellular localization is regulated by alternative splicing, affecting the amino acid composition at the C-terminal end of the protein. One of the SIRT5 splice variants contains a GPCG motif that is required for retaining the protein in the cytoplasm, whereas the C-terminus of the other may anchor the protein in the outer mitochondrial membrane [9].

For *SIRT2*, four different human splice variants are deposited in the GenBank sequence database. However, only transcript variants 1 and 2 have confirmed protein products of physiological relevance. A leucine-rich NES within the N-terminal region of these two isoforms was identified. Since deletion of the NES led to nucleocytoplasmic distribution, it was suggested to mediate their cytosolic localization [21]. Cytosolic functions of SIRT2 include the regulation of microtubule acetylation, control of myelination in the central and peripheral nervous system and gluconeogenesis [15,22–24]. There is growing evidence for additional functions of SIRT2 in the nucleus. During the G_2/M transition, nuclear SIRT2 is responsible for global deacetylation of H4K16, facilitating H4K20 methylation and subsequent chromatin compaction [3,20,25]. This process links SIRT2 to maintenance of genomic integrity and may thus explain, at least in part, why SIRT2-deficient mice show elevated rates of tumorigenesis. In response to DNA damage, SIRT2

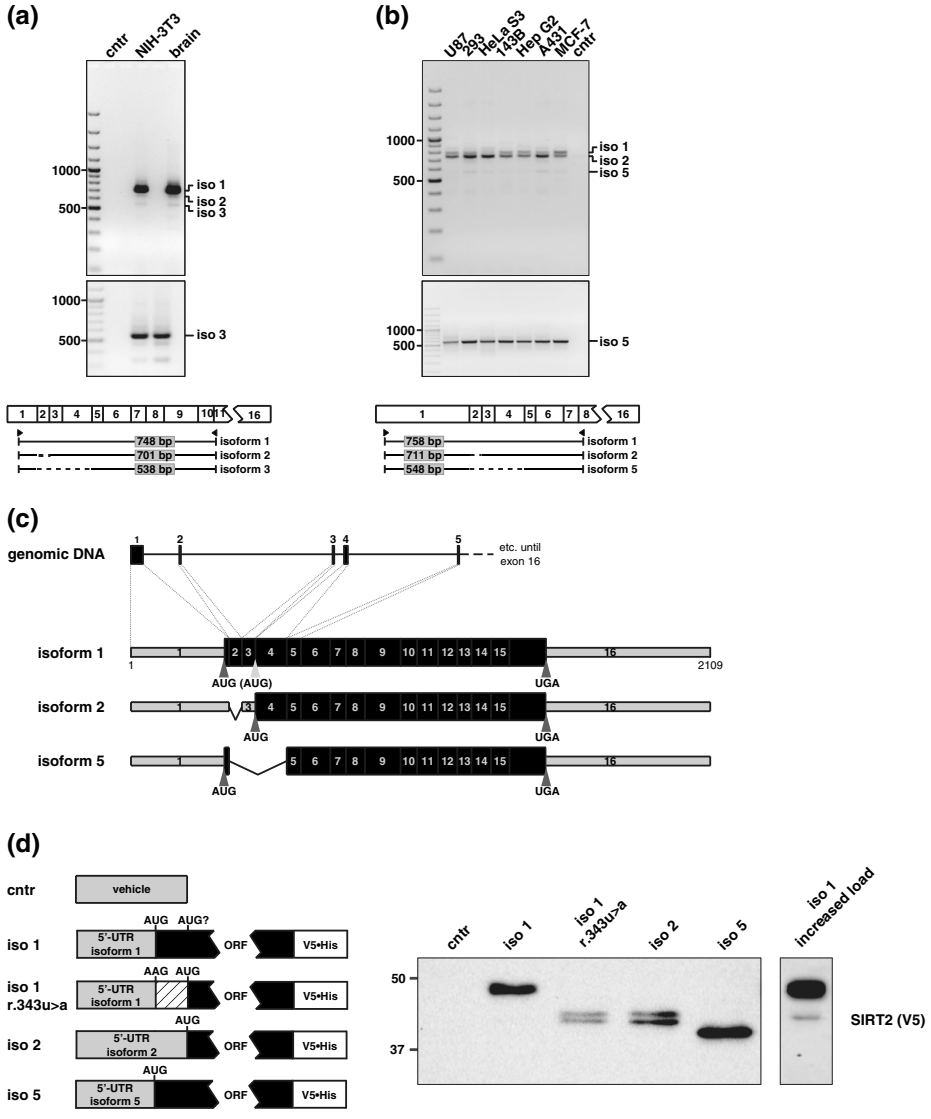

was also found to deacetylate H3K56 *in vivo* [26]. Finally, SIRT2 negatively regulates the acetyltransferase activity of the transcriptional co-activator p300 via deacetylation of an automodification loop within its catalytic domain [26–28].

The characterization of SIRT2 isoforms as cytosolic proteins is in apparent contradiction with the reported nuclear functions. Earlier studies, which indicated the nuclear accumulation of SIRT2 after CRM1 inhibition of protein export from the nucleus, suggested the presence of a nucleocytoplasmic shuttling mechanism for SIRT2 [21,29]. However, a functional NLS has not been detected in the SIRT2 primary structure [21]. Additionally, the NES is present in both known isoforms, which indicates a passive form of nuclear accumulation. This raises the question as to how the nuclear presence of SIRT2 is brought about. In mice, another *Sirt2* splice variant was demonstrated [24,30]. Interestingly, the corresponding protein would lack the amino acids that constitute the NES in the human isoforms.

On the basis of these findings, we asked whether additional isoforms for human SIRT2 that result from alternative splicing of the primary transcript exist. We here demonstrate the identification of an alternatively spliced transcript, which results from skipping of exons 2–4 and encodes a novel SIRT2 isoform that we have designated as isoform 5. The new isoform is predominantly localized in the nucleus and does not exhibit any detectable deacetylase activity as demonstrated in several assays. However, the protein appears to be properly folded and retains the ability to bind p300. Unless isoform 5 requires other, as yet unidentified, cofactors for activity, our data suggest a non-catalytic, nuclear function for SIRT2 isoform 5.

Results

Alternative splicing of the primary transcript results in a hitherto unrecognized human SIRT2 splice variant

First we verified the presence of the reported murine splice variant that lacks the NES encoding sequence [30] in complementary DNA (cDNA) preparations from murine brain tissue and NIH-3T3 cells by PCR using primers specific for sequences in exon 1 and exon 10 of the *Sirt2* gene. We amplified three DNA fragments of approximately 750, 700 and 550 bp in length (Fig. 1a, top panel). The isolated ~550 bp fragment was reamplified (Fig. 1a, middle panel). DNA sequence analysis confirmed these DNA fragments to originate from the reported splice events containing all exons (isoform 1), leading to skipping of exon 2 (isoform 2) or exons 2–4 (isoform 3) (Fig. 1a, bottom panel). To investigate whether the human primary *SIRT2* transcript is subject to a similar splicing event, we performed PCRs with primers spanning exons 1–8 using cDNAs derived from seven human cell lines as templates. DNA fragments of ~800 bp and ~750 bp were amplified, which correspond to the known *SIRT2* isoforms 1 and 2 (Fig. 1b, top panel). An additional fragment of ~550 bp in length was consistently co-amplified in all reactions (Fig. 1b, top panel) and was reamplified after gel purification (Fig. 1b, middle panel). DNA sequencing analysis showed that this

Fig. 1. Identification of a novel human *SIRT2* splice variant. PCR analyses of cDNAs derived from mouse (a) and human (b) sources. The exon composition and length of the amplified DNA fragments is shown below the agarose gels, and triangles indicate the location of primer sequences. The size of selected marker bands (bp) is indicated. Control reactions (cntr) were run in the absence of cDNA. (a) PCR analysis of cDNA preparations from murine brain tissue and NIH-3T3 cells. Samples were run in 2% ethidium bromide-stained agarose gels. The major product of the reactions from both templates was a 748-bp fragment derived from the transcript encoding isoform 1 (iso 1), and a second product of 701 bp resulted from the isoform 2-specific mRNA (iso 2). A third DNA fragment running at ~550 bp could be specifically reamplified after gel purification (middle panel) and was identified as specific 538-bp sequence originating from a murine *Sirt2*-transcript variant (iso 3) lacking exons 2–4. (b) PCR analysis of cDNA preparations from seven human cell lines. Amplified fragments were separated in a 2% agarose gel. The two major products of the amplification corresponded to human *SIRT2* isoforms 1 and 2 (758 bp and 711 bp, respectively). A third DNA fragment running at ~550 bp could be specifically reamplified after gel purification (middle panel) and was identified as specific 548-bp sequence originating from a novel human *SIRT2*-transcript variant (iso 5) lacking exons 2–4. (c) Overview of the isoform-specific *SIRT2* splicing events occurring on the human primary transcript. Exon 1 is linked via a common splice donor site with the common splice acceptor sites in exon 3 (to process transcript variant 2) and to exon 5 (for maturation of transcript variant 5). Exons 1 and 3 constitute the 5′-UTR of transcript variant 2. The ORF starts at an AUG triplet that is formed directly at the transition from exon 3 to exon 4. Alternative splicing of exons 1 and 5 leads to the substitution of the codons for amino acids 6–76 of the full-length ORF of isoform 1 by an arginine codon in isoform 5. (d) The ORFs of the different SIRT2 isoforms were expressed as C-terminal V5-His-tagged proteins in the context of the endogenous 5′-UTRs of the corresponding mRNAs. The molecular masses of the different SIRT2 isoforms (including V5-His tag) were predicted to be 46.7 kDa (isoform 1), 43 kDa (isoform 2) and 39.1 kDa (isoform 5). The V5-epitope was used for immunodetection. Expression of isoform 1 from a transcript harboring its physiological 5′-UTR (iso 1) leads to detection of an additional weakly expressed protein that corresponds in size to SIRT2 isoform 2 (right panel). In the context of the endogenous 5′-UTR, mutation of the start codon of the isoform 1- specific transcript (iso 1 r.343u > a) leads to translation of isoform 2 as the sole protein. Lysates from cells transfected with the vector backbone were used as control (cntr).

third PCR product originated from a splicing event that links exon 1 to exon 5 (Fig. 1b, bottom panel).[†] The presence of this splicing event was further supported by analyses of expressed sequence tags (GenBank) from human and Sumatran orangutan tissues.

We then asked whether there are further alternative splicing events downstream of exon 5 in the identified transcript. Nested PCRs were performed in order to amplify the full-length messenger RNA (mRNA) of the novel transcript variant. cDNA preparations from 293 and SH-SY5Y cells were subjected to primary PCRs using primers spanning exons 1–16. Three secondary PCRs were carried out using (i) a primer pair spanning the 5′-untranslated region (UTR) to the exon 1/5 junction, (ii) a primer pair spanning the exon 1/5 junction to exon 16 and (iii) a primer pair spanning exons 1–16 (Fig. S1, bottom panel). All reactions led to amplification of specific products. DNA sequence analysis revealed no further alternative splicing events downstream of exon 5 of the novel human *SIRT2* splice variant. Thus, the novel human *SIRT2* transcript is composed of exon 1 and exons 5–16 (Fig. S1). The open reading frame (ORF) starts from the same AUG triplet in exon 1 that is used to initiate

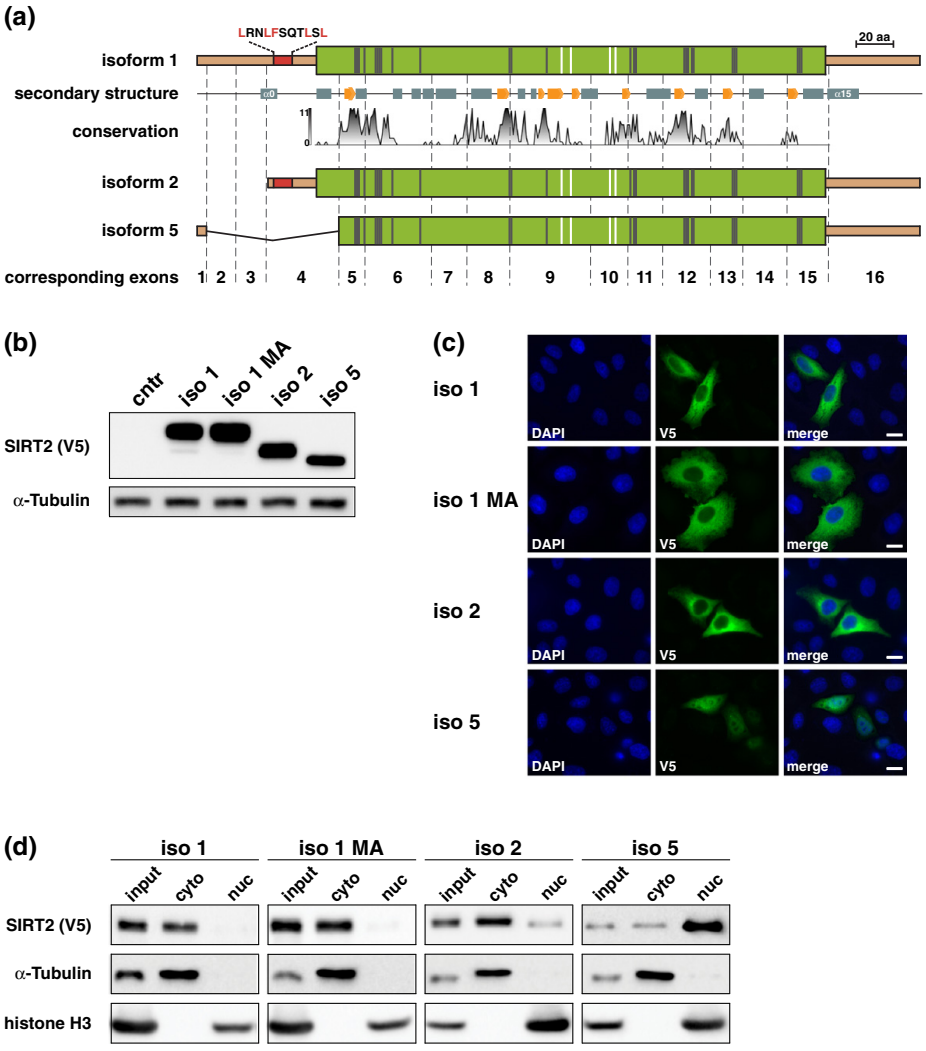

translation of SIRT2 isoform 1 and terminates in exon 16 at the common stop codon for all (known) SIRT2 isoforms (Fig. 1c). As transcripts variants 3 and 4 are already deposited in GenBank database,[‡] the novel human SIRT2 isoform encoded by the alternative splicing events reported here is designated isoform 5. Since we could not identify sequences corresponding to transcript variants 3 and 4, all subsequent experiments were carried out using the three identified transcript variants 1, 2 and 5.

Next, we analyzed whether the composition of the 5′-UTRs of the three human *SIRT2* mRNAs may affect the translation into proteins. To this end, we expressed C-terminally V5-His-tagged SIRT2 isoforms 1, 2 and 5 in the context of their endogenous 5′-UTRs in 293 cells. Immunoblot analyses showed expression of C-terminally V5-tagged proteins of expected size (Fig. 1d). We also observed a weak band corresponding in size to isoform 2 in cells transfected with the plasmid encoding isoform 1 (Fig. 1d, right panel). When the start codon of isoform 1 was mutated (r.343u > a), we observe a band pattern identical with the one seen for wild-type (wt) isoform 2 (Fig. 1d, r.343u > a). This observation suggests that the second AUG triplet within the ORF of isoform 1 may be used as alternative start codon leading to leaky co-translation of isoform 2. Thus, co-translation of SIRT2 isoform 2 from the transcript encoding isoform 1 may be of relevance *in vivo*.

Predominant nuclear localization of human SIRT2 isoform 5

Compared to isoform 1, alternative splicing events of the *SIRT2* primary transcript result in N-terminal truncation (residues 1–37) of isoform 2 and, for isoform 5, in the substitution of residues 6–76 by an arginine residue (Fig. 2a and Fig. S2). As a consequence, the catalytic domain (defined here as residues 64–336 by multiple sequence alignment and structure analysis) is slightly truncated. However, a conservation analysis using the phylogenetic dataset described by Frye [31] indicated that neither highly conserved residues nor amino acids involved in co-substrate binding would be affected by the changes in the primary structure (Fig. 2a). Importantly, N-terminal amino acids that are absent from isoform 5 represent the reported NES found in the other isoforms. Therefore, isoform 5 may display a different cellular distribution than SIRT2 isoforms 1 and 2. To address this question, we investigated subcellular localization of C-terminally V5-His-tagged SIRT2 isoforms in HeLa S3 and 293 cells. To avoid expression of isoform 2 from the construct encoding isoform 1, we included a mutant form of isoform 1 (M38A) to eliminate the alternative translational start site for isoform 2 (Fig. 2b). As expected, V5 immunocytochemistry showed predominant cytoplasmic localizations of isoforms 1 (wt and M38A) and 2. In contrast, isoform 5 localized primarily to the nucleus (Fig. 2c). This finding was substantiated by immunoblot analyses of subcellular fractions from 293 cells (Fig. 2d).

SIRT2 isoform 5 is catalytically inactive *in vitro* and *in vivo*

Next, we asked whether the lack of amino acids encoded by exons 2–4 in isoform 5 might change the catalytic properties of this protein. The deacetylase activities of purified SIRT2 isoforms were measured using the CycLex SIRT2 fluorometric activity kit. Isoform 5 showed no detectable activity, whereas isoforms 1 (wt and M38A) and 2 showed a robust deacetylase activity toward the fluoro-peptide (Fig. 3a). Lack of activity when measuring mutant proteins (H > Y) in which the essential proton acceptor histidine 187 (isoform 1) was replaced by tyrosine confirmed the specificity of the reactions.

Given that isoform 5 contains all residues predicted to be required for catalysis, the lack of deacetylation activity of this isoform was a rather unexpected

Fig. 2. SIRT2 isoform 5 predominantly localizes to the nucleus. (a) Alternative splicing of the human *SIRT2* pre-mRNA leads to three distinct proteins. The ORF of isoform 2 starts at a methionine codon formed at the exon 3/4 transition, thereby shortening isoform 2 by the first 37 amino acids relative to isoform 1. In SIRT2 isoform 5, amino acids 6–76 of isoform 1 are exchanged by an arginine leading to the removal of the NES (indicated by the red box). Secondary structure is given with gray rectangles representing α-helices and orange arrows representing β-sheets. The degree of conservation was calculated from multiple sequence alignment (gaps matching non-SIRT2 residue were removed) with a score range from 1 to 10 reflecting conservation of biophysical properties of residues and a maximum score of 11 for absolute conservation. The catalytic domain is indicated in green; flanking N- and C-terminal regions, in brown; residues involved in co-substrate coordination and catalysis, in gray; zinc-coordinating residues, in white. All annotation correspond to the reported structures (PDB IDs: 3ZGO and 3ZGV) [42]. (b) V5-immunoblot analysis of lysates from 293 cells transiently expressing SIRT2 isoforms. Overexpression of SIRT2 isoform 1 results in co-expression of isoform 2 by alternative translational start from the second in frame AUG triplet. Mutation of methionine at position 38 to alanine (MA) in the ORF of SirtT2 isoform 1 leads to sole detection of isoform 1. (c) The different SIRT2 isoforms were expressed in HeLa S3 cells and cell lysates subjected to V5 immunocytochemistry. SIRT2 isoforms 1 (wt and MA) and 2 localize to the cytoplasm, whereas isoform 5 is predominantly found in the nucleus. The bar represents 10 μm. (d) Cell fractionation of 293 cells transiently overexpressing SIRT2 isoforms. Isoforms 1 (wt and MA) and 2 are detected in cytoplasmic fractions, whereas isoform 5 is predominantly detected in the nuclear fraction. The purity of the cellular fractions was tested by probing the membranes with α-tubulin and histone H3 antibodies.

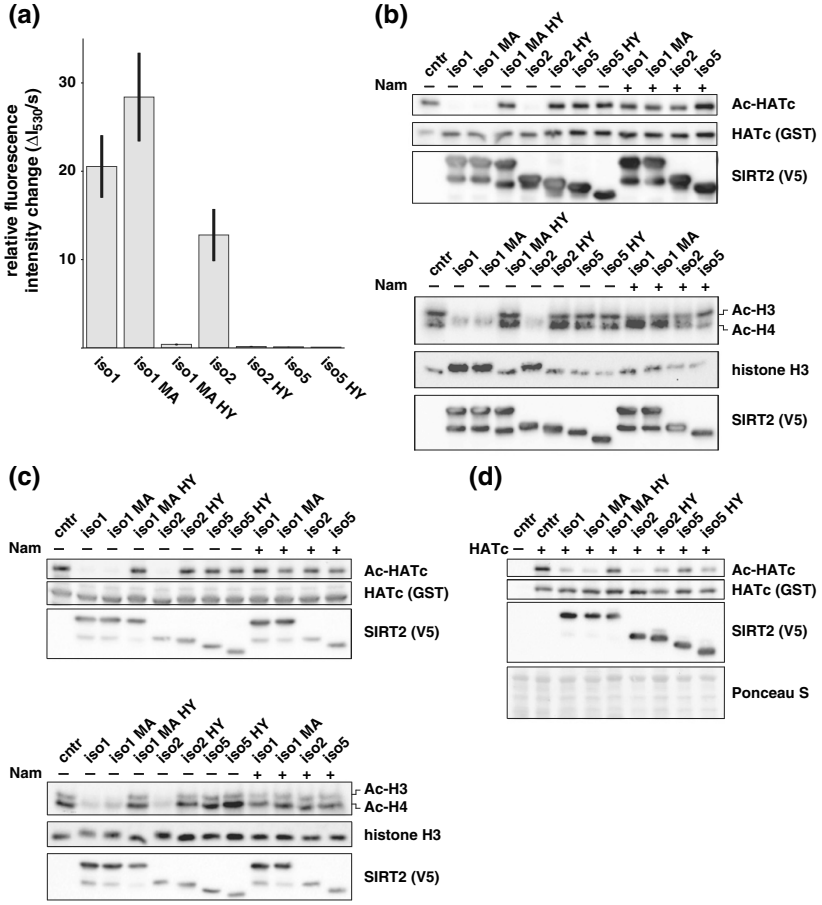

Fig. 3. SIRT2 isoform 5 is inactive for protein deacetylation *in vitro*. The deacetylation activity of recombinant SIRT2 isoforms was determined by four individual experimental approaches. Proteins carrying a mutation of the catalytic important histidine residue (H > Y) were used as negative controls. The mutant SIRT2 isoform 1 (MA) was used to exclude co-expression of isoform 2 from the recombinant DNA. (a) Deacetylase activity of purified SIRT2 isoforms toward an acetylated peptide using CycLex SIRT2 Deacetylation Fluorometric Assay Kit (excitation, 485 nm; emission, 530 nm). Data are background corrected and represent mean of relative fluorescence intensity changes ± SD of triplicate measurements. (b) Purified SIRT2 isoforms were incubated with either recombinant HATc or chemically acetylated histones in the presence and absence of 20 mM nicotinamide (Nam). The acetylation state of HATc and histone H3 and H4 as determined by immunoblot analyses was used as readout. Control reactions (cntr) were performed in the absence of any SIRT2 isoform. (c) Deacetylation activity in lysates from bacteria expressing the SIRT2 isoforms. The activity was tested toward the same acetylated targets as in (b). Control reactions (cntr) were performed using lysates from bacteria harboring the "empty" SIRT2 expression vector. (d) Deacetylation activity of SIRT2 isoforms in living cells. Bacteria were transformed with prokaryotic HATc expression plasmid along with different vectors encoding SIRT2 isoforms. After expression, the acetylation state of HATc in whole bacterial lysates was assessed by immunoblot analysis. Bacteria harboring the "empty" HATc expression vector as well as cells co-transformed with the "empty" SIRT2 and the "empty" HATc expression vector were used as controls.

observation. Therefore, we extended our study to include alternative activity assays. We analyzed purified recombinant proteins for NAD^+-dependent deacetylase activity using nuclear targets such as the hyperacetylated catalytic domain of p300 (HATc) or chemically acetylated histones as substrates. Immunoblot analysis with an acetyllysine antibody showed a clear decrease in acetylation of both

targets when using isoform 1 (wt and M38A) or 2 in the reactions. In contrast, no deacetylation activity was detected for isoform 5 (Fig. 3b).

To rule out inactivation of isoform 5 by the purification procedure, we performed deacetylation assays using lysates from bacteria expressing the different SIRT2 isoforms. Similar to the experiments with isolated proteins, bacterial lysates containing isoforms 1 (wt and M38A) or 2 deacetylated HATc and histones, whereas no activity was observed in lysates from bacteria expressing recombinant isoform 5 (Fig. 3c).

HATc is hyperacetylated when expressed in bacteria [32]. Since NAD^+ is also freely available in prokaryotic cells, co-expression with SIRT2 may reduce the degree of HATc acetylation [33]. As shown in Fig. 3d, co-expression with SIRT2 isoforms 1 (wt and M38A) and 2 substantially reduced HATc self-acetylation. In contrast, co-expressed SIRT2 isoform 5 had no effect on the acetylation state of HATc (Fig. 3d).

Together, these data suggest that SIRT2 isoform 5 is inactive *in vitro*. To exclude the possibility of suboptimal assay condition, for example, the lack of endogenous cofactors, we overexpressed the different SIRT2 isoforms in HeLa S3 and monitored the acetylation status of α-tubulin. In the presence of isoforms 1 (wt and M38A) and 2, acetylation of α-tubulin at lysine 40 was substantially reduced. In contrast, expression of SIRT2 isoform 5, which is partially located in the cytosol (Fig. 2c and d), did not affect the acetylation status of α-tubulin (Fig. 4).

SIRT2 isoform 5 is properly folded and interacts with HATc

To determine whether the alteration of the N-terminal region of SIRT2 isoform 5 led to a structural impairment of the catalytic domain and thus could account for the apparent lack of deacetylase activity, we first performed molecular modeling analyses using homology and threading approaches. All models generated are consistent with SIRT2 isoform 5 adopting a fold very similar to the solved structure of SIRT2 isoform 1 (RMSD values between 0.1 and 0.9 Å over 249–274 residues) (Fig. 5a and Fig. S3). Examination of the electrostatic surface potential indicated no alterations of the peptide or NAD^+ binding surfaces. The most striking difference was a charge inversion near the Rossmann fold due to the absence of α-helix α1 (Fig. 5a, dotted circle). However, given the relatively large distance to the catalytic region, it appears rather unlikely that this charge inversion would severely influence the enzymatic activity. These analyses suggest that the overall fold of isoform 5 is unlikely to be significantly different from those of isoforms 1 and 2.

To substantiate these models, we compared the sensitivity of the purified isoforms for denaturation by

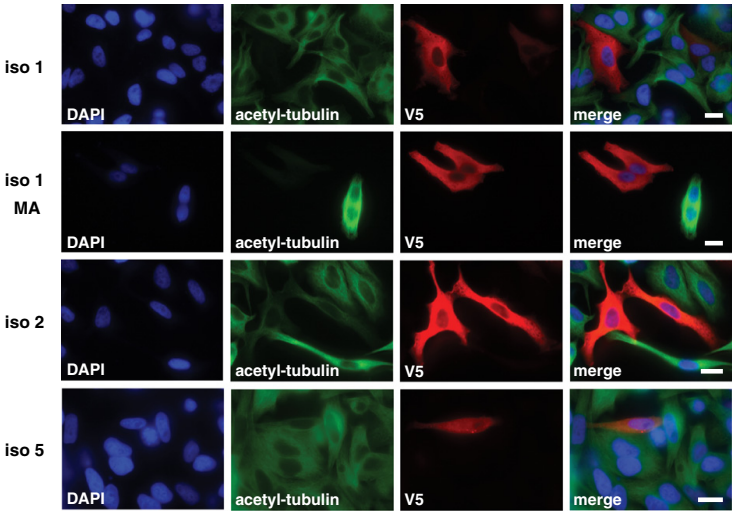

Fig. 4. SIRT2 isoform 5 is inactive for protein deacetylation *in vivo*. HeLa S3 cells expressing the different SIRT2 isoforms for 24 h were subsequently incubated with 400 nM TSA for 12 h. The cells were subjected to co-immunocytochemistry to detect the V5-epitope and lysine 40-acetylated α-tubulin. Overexpressed SIRT2 isoforms 1 (wt and MA) and 2 show reduces immunoreactivity for acetylated α-tubulin, whereas isoform 5 causes no change in the α-tubulin (K40) acetylation. The bar represents 10 μm.

increasing concentrations of guanidinium hydrochloride (GdmCl) by monitoring changes in the intrinsic fluorescence of tryptophan residues. There are three tryptophan residues in SIRT2, all within or near the catalytic domain (W208, W320 and W337, isoform 1; Fig. S2). Complete denaturation (at a GdmCl concentration of 6 M) was accompanied by a red shift, indicating exposure to more polar environment, and changes in intensity (Fig. 5b). The spectra for isoforms 1 and 2 indicate the reduction of a quenching influence on at least one of the tryptophans and, hence, an increase in fluorescence intensity during denaturation.

The denaturation profiles, obtained by measurements at various GdmCl concentrations, are shown as the ratios between the fluorescence intensity at 330 and 360 nm (Fig. 5c). Calculation of I_{330}/I_{360} ratios effectively filters off whole spectrum influences (such as concentration differences) [34]. The denaturation profiles indicate that unfolding occurs in at least two steps. The lower initial I_{330}/I_{360} ratio calculated for isoforms 2 and 5, in comparison to isoform 1, points toward an influence of the N-terminus in the first denaturation step (Fig. 5c). The subsequent denaturation profiles are comparable for all isoforms; thus, a

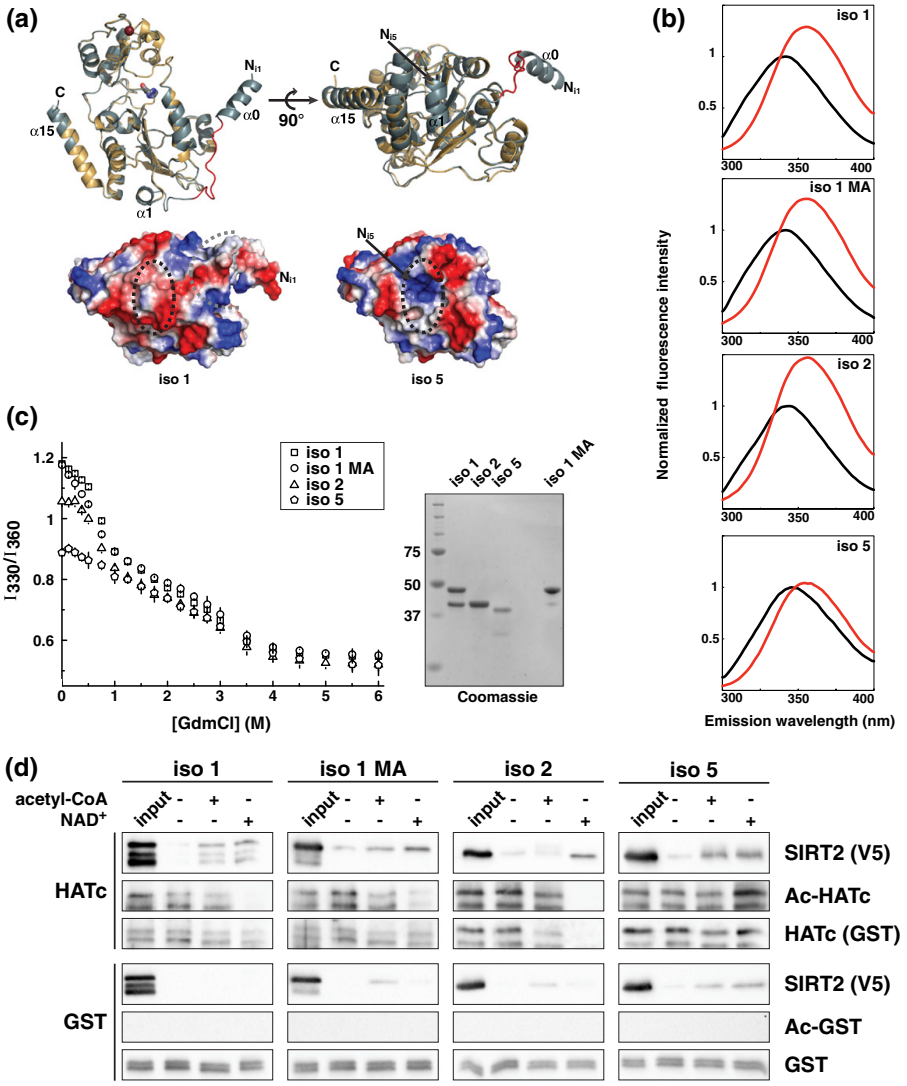

similar ordered structure of all isoforms can be assumed (Fig. 5c). The increase in fluorescence intensity, and hence the release of the quenching effect, coincides with the first denaturation event (data not shown). The observed quenching may be due to electron transfer or static quenching of the tryptophans within the structure (W208 and W337) or a result of an interaction between the C- or the N-terminal regions with the surface tryptophan W330, or both.

These observations support the results of the modeling approaches suggesting that the overall structure of isoform 5 is not severely perturbed. Therefore, we considered the possibility that isoform 5 might still possess the ability to interact with SIRT2 binding partners. A previous study demonstrated an interaction of SIRT2 isoform 1 with the C-terminal part of p300 including the HAT domain [28]. We investigated whether the SIRT2 isoforms 2 and 5 retained this property. Indeed, as shown in Fig. 5d, all SIRT2 isoforms specifically interacted with the core catalytic domain of p300 *in vitro*. We occasionally observed weak binding of SIRT2 isoforms to GST (*g*lutathione *S*-*t*ransferase). However, the specific interaction with p300 was invariably far stronger for all isoforms. Interestingly, an increase in the interaction was observed in the presence of co-substrates (either acetyl-CoA or NAD^+). Since p300 is a substrate for SIRT2 and vice versa [27,28], stronger binding in the presence of co-substrate may indicate that the interaction partially results from an enzyme–substrate relationship. Noteworthy, the interaction of HATc and isoform 5 is also strengthened by the addition of NAD^+ indicating that isoform 5 retained the structural features to bind this nucleotide.

Discussion

In the present study, we have identified the novel isoform 5 of human SIRT2. Our analyses show that it is an evolutionarily conserved isoform that corresponds to a previously reported splice variant, designated isoform 3, in mouse. As isoform 5 lacks the NES, it localizes predominantly to the nucleus. Despite the presence of an apparently intact SIRT2 catalytic domain, isoform 5 does not deacetylate known targets of SIRT2 isoforms 1 and 2. Nevertheless, it retains the overall protein fold and the ability to interact with p300. These results suggest a non-enzymatic function for this isoform, which remains to be elucidated. Alternatively, the novel isoform 5 might have a substrate specificity that is different from that of the known SIRT2 isoforms 1 and 2 or may require a hitherto unidentified cofactor.

Generation of SIRT2 isoforms by alternative splicing and translation

The alternatively spliced transcript encoding isoform 5 has been detected in all human cell lines analyzed. Additionally, the existence of a similar splice variant in mice has been reported recently [24,30] and was confirmed in this study. The discovery of this splice variant in primates and rodents suggests that isoform 5 is the result of an evolutionary selection and not a coincidental "slippage" of the splicing machinery.

In addition to alternative splicing, our results point toward utilization of an internal start codon as a second mechanism to regulate the presence of isoforms 1 and 2. Earlier, it was shown that isoform 2 is expressed from plasmid carrying isoform 1 in the presence of an artificial 5′-UTR [35]. Our experiments utilizing the endogenous 5′-UTR of *SIRT2* showed expression of isoform 2 from the plasmid encoding isoform 1. Moreover, mutation of the isoform 1 start codon showed efficient expression of isoform 2. In the context of the endogenous 5′-UTR, isoform 1 has a moderately strong Kozak sequence (position −3: cytosine; position +4: guanine), whereas the start codon of isoform 2 is surrounded by a strong Kozak sequence (positions −3 and +4: guanine) [36]. Consequently, the expression of isoform 2 in the

Fig. 5. SIRT2 isoform 5 is structurally intact and can interact with p300-HATc. (a) Comparison of the SIRT2 isoforms 1 and 5 structure predictions (upper panel). Models were generated using homology modeling (Swiss-Model: isoform 1, yellow; M4T: isoform 5, blue gray). Model of isoform 1 differs from the solved structure (PDB ID: 3ZGO, RMSD: 0.069 Å) only in the presence of a connection loop (red) between α-helices α0 and α1. Both α0 and α1 are absent in isoform 5. Note that α0 is only resolved in chains A and B of the asymmetric unit of 3ZGO. The C- and N-termini (N_{i1}: isoform 1, N_{i5}: isoform 5) are indicated, and the catalytic histidine (H187, isoform 1) is given in stick representation. Absence of α1 from the structure leads to an alteration in the electrostatic surface potential at the lower site of the Rossmann fold, but not to an exposure of hydrophobic patches (lower panel). In the surface potential map, blue represents positively charged, red represents negatively charged and white represents neutral areas. The black dotted circle indicates the position of α1, and the gray dotted line indicates the beginning of the modeled loop. The structures were prepared with PyMOL. (b) Fluorescence emission spectra for SIRT2 isoforms in the absence (black) or presence (red) of 6 M GdmCl (excitation at 290 nm). Values were normalized to the maximal emission of the folded protein. Spectra represent the average of four measurements and are buffer corrected. (c) GdmCl denaturation of SIRT2 isoforms as monitored by intrinsic tryptophan fluorescence. The denaturation profile of the SIRT2 isoforms in response to increased GdmCl concentration is shown as the ratios of fluorescence intensities at 330 and 360 nm (excitation at 290 nm) (left panel). Data represent means ± SD of quadruple measurements. The right panel shows Coomassie-stained gel of SIRT2 isoforms used in the denaturation shift assay. (d) GST-pulldown assay using the GST-fused catalytic domain of p300 (HATc) and SIRT2 isoforms. Prior to the pulldown, samples were incubated in the absence or presence of co- substrates (acetyl-CoA or NAD^+). The molar ratio of proteins (HATc/GST: SIRT2) was 1:5. SIRT2 binding to HATc was monitored by acetyllysine and HATc immunoblot analyses. Recombinant GST was used as negative control.

context of isoform 1 could be a result of leaky ribosome scanning. That is, isoform 2 may be generated from the isoform 1 transcript *in vivo* and thus might contribute to the differences in isoform expression observed in murine tissues [30]. However, the favored expression of isoform 1 from its endogenous 5′-UTR indicates that isoform 2 originates predominantly from an isoform-specific alternatively spliced mRNA. Since the isoform 5 was detectable when overexpressed in context of its endogenous 5′-UTR, it is more than likely that it is also readily translated from its endogenous mRNA.

The observed nuclear SIRT2 activity must be a result of a catalytically active isoform. In light of our study, two mechanisms to promote nuclear SIRT2 localization appear most plausible: Absence of the NES (Ref. [21] and this study) or conditions of CRM1-dependent export inhibition [21,29]. Our analyses of the NES encoding region indicate that isoform 5 is the only splice variant that excludes the NES from the primary structure. On the other hand, the essentially exclusive cytoplasmic localization of isoforms 1 and 2 indicates highly active CRM1-dependent nuclear export. Consequently, it would appear that the nuclear SIRT2 activity is likely a result of low-level abundance of SIRT2 isoform(s) brought about either by constant shuttling or by masking of the NES, for example, in a nuclear complex.

Isoform 5 shows nuclear enrichment, however, is catalytically inactive

The absence of the NES from isoform 5 immediately suggested the possibility that it might be localized to the nucleus. Indeed, using both immunocytochemistry and cell fractionation, we observed a predominant nuclear localization of SIRT2 isoform 5. This pattern is distinct from isoforms 1 and 2, which are solely cytoplasmic. Considering the molecular size of SIRT2 isoform 5, an active transport mechanism either by a non-canonical NLS or "piggy-backing" in complex with other proteins seems likely. Computational NLS prediction using cNLS mapper [37] indicated the presence of a weak bipartite NLS containing an extended linker region (residues 342–375 in isoform 1). The weak score (2.8) is in accordance with the observed partial cytoplasmic localization of isoform 5 and, thus, may be a result of low NLS activity.

Given that the known SIRT2 isoforms 1 and 2 localized to the cytoplasm (Refs. [13–15] and this study), it appeared likely that the new nuclear isoform could account for the SIRT2-dependent deacetylation of nuclear proteins. Surprisingly, in contrast to isoforms 1 and 2, isoform 5 displayed no catalytic activity in our experiments. The absence of detectable activity in multiple approaches and experimental systems provides compelling evidence that the novel SIRT2 isoform has no deacetylase activity, at least toward known SIRT2 targets (Refs. [27,38–40] and confirmed here): When using isolated, recombinant SIRT2 isoform 5, it neither deacetylated the fluorogenic peptide nor histones or HATc of p300. Moreover, when expressed and directly analyzed in bacterial or human cells, isoform 5 exhibited no deacetylase activity, whereas isoforms 1 and 2 were active. Thus, even though isoform 5 provided an excellent candidate to account for nuclear SIRT2 activity, our results seem to rule out such a function.

The fold of the catalytic domain of SIRT2 isoform 5 is not substantially impaired

An obvious explanation for the catalytic inactivity of isoform 5 would have been the lack of the most N-terminal part of the catalytic domain (including α-helix α1). The absence of these 12 residues could either cause structural impairment or involve catalytic residues. Several lines of evidence suggest, however, that this is not the case. For example, isolation of recombinant isoform 5 after expression in bacteria resulted in a readily soluble protein. Moreover, analyses of the tryptophan fluorescence during GdmCl-dependent denaturation further indicated that isolated isoform 5 is properly folded. These experiments were also in line with our structural model that predicts the catalytic core of isoform 5 to resemble that of isoforms 1 and 2. All residues known to be essential for catalysis [41,42] are still present in isoform 5. However, comparison with the structure of SIRT2 isoform 1 revealed that α-helix α1 is missing in isoform 5. Since α1 is part of the NAD^+-binding Rossmann fold, the structural integrity of isoform 5 could be affected. However, the modeling using homology and threading approaches indicates that the general structure could still be maintained. This is supported by a crystallographic study of cobB, a bacterial sirtuin homologue [43]. The cobB protein used in that study lacked the equivalent α-helix in the Rossmann fold but was catalytically active.

Examination of the denaturation curves suggests that, at least, one of the tryptophans of isoform 1 is in labile environment created by the presence of the N-terminal region. Shortening of the N-terminus (isoform 2) or its removal (isoform 5) leads to an increased solvent exposure as indicated by the drop in the I_{330}/I_{360} ratio. Considering the positioning of the tryptophans within the structure, it is likely that either the N-terminus folds back onto the catalytic domain shielding the surface tryptophan W320 (isoform 1) or helix α15 separates from the core structure exposing W337 (isoform 1). Both changes could have an indirect influence on the substrate binding capability of SIRT2 without altering the major fold. An additional indication that the observed inactivity of isoform 5 is likely to be a result of more subtle conformational differences is its preserved ability to interact with the catalytic domain of p300. The latter feature is shared by isoforms 1 and 2. The strengthened interaction observed for all three isoforms in the presence of

either co-substrate (acetyl-CoA for p300 or NAD^+ for SIRT2) indicates that the interaction is partially due to the enzyme–substrate relationship of the two proteins. Moreover, the noticeably enhanced binding of SIRT2 isoform 5 to HATc in the presence of NAD^+ strongly suggests that isoform 5 has retained the capacity to bind NAD^+.

Together, these results indicate that subtle structural differences are responsible for the apparent catalytic inactivity of isoform 5. Still, there exists a possibility that isoform 5 has altered substrate specificity or that nuclear interaction partners restore its catalytic activity. It is interesting to note in this regard that deacetylation of tubulin appears to be mediated by a complex containing both SIRT2 and the NAD^+-independent deacetylase HDAC6 [15,44,45]. It has been proposed that HDAC6 is a constitutive active deacetylase, whereas the SIRT2 tubulin–deacetylase activity, but not its ability to interact with HDAC6, is regulated by phosphorylation of S368 (isoform 1) [15,44,46]. This would suggest that SIRT2 has an additional deacetylase activity-independent function within the complex. By analogy, it might be possible that isoform 5 mediates nuclear protein interactions, for example, with p300, perhaps, even in a NAD^+-dependent manner.

It is also interesting to note that a non-catalytic function has been described for SIRT1. Proteasomal cleavage of SIRT1 in the C-terminal region renders the enzyme catalytically inactive without affecting the structure of the conserved core domain. The resulting inactive fragment translocates from the nucleus to the mitochondria where it protects from apoptosis by interfering with apoptosome assembly [47]. The regulation of cellular processes by non-catalytic splice variants is, however, not limited to sirtuins but is a more common phenomenon observed for a variety of enzymes including DNA methyltransferase DNMT3B, protein phosphatase 2α and GTP cyclohydrolase I [48–50]. Future studies will have to explore the physiological roles of the novel SIRT2 isoform and thereby establish whether these include regulated catalytic activity or exclusively non-catalytic functions.

Materials and Methods

Antibodies

Rabbit polyclonal acetylated lysine antibody and rabbit monoclonal acetyl-α-tubulin (K40) antibody (D20G3) were from Cell Signaling Technology. Rabbit polyclonal GST (Z-5) antibody was from Santa Cruz Biotechnology, mouse monoclonal α-tubulin antibody (B-5-1-2) was from Sigma-Aldrich, rabbit polyclonal histone H3 antibody was from Millipore and mouse monoclonal V5-epitope antibody (1H6) was from MBL International. Fluorescence-conjugated secondary antibodies (Alexa Fluor 488-conjugated goat anti-mouse and anti-rabbit; Alexa Fluor 594-conjugated goat anti-mouse) were from Invitrogen/Life Technologies. Horseradish-peroxidase-conjugated secondary goat anti-mouse and anti-rabbit antibodies were from Pierce.

Cell culture

143B, 293 (HEK-293), A-431 and NIH-3T3 cells were cultivated in high glucose DMEM (*D*ulbecco's *m*odified *E*agle's *m*edium) supplemented with 10% FCS, 2 mM L-glutamine, penicillin (10,000 units/ml) and streptomycin (10 mg/ml). HeLa S3 cells were cultivated in HAM's F12 medium, HepG2 and U-87 cells were grown in EMEM and MCF-7 cells were grown in IMDM. All media were supplemented with 10% FCS and penicillin/streptomycin. SH-SY5Y cells were grown in a 1:1 mixture of high glucose DMEM and HAM's F12 medium supplemented with 15% FCS, penicillin/streptomycin, 2 mM L-glutamine and 1% non-essential amino acids solution. Cells were incubated at 37 °C in humidified atmosphere with 5% CO_2.

Transfection of cultured human cells

Cells were seeded 24 h prior transfection. HeLa S3 cells were transfected using Effectene (Qiagen), and 293 cells were transfected using CalPhos Mammalian transfection reagent (Clontech) according to the manufacturer's recommendations.

Preparation of cell lysates and immunoblot analysis

Cells were washed twice with PBS and lysed with 20 mM Tris–HCl (pH 7.4), 150 mM NaCl, 1 mM ethylenediaminetetraacetic acid and 1% (w/v) SDS. Genomic DNA was disrupted by sonication and insoluble material removed by centrifugation. Protein concentration of supernatant was determined by BCA protein assay (Pierce). After SDS-PAGE and protein transfer onto nitrocellulose membranes, immunoblot analyses were carried out using primary and secondary antibodies as indicated. Proteins were detected by enhanced chemiluminescence (Pierce) and images were taken with a ChemiDoc XRS+ system (Bio-Rad).

Reverse-transcription PCR analysis

Reverse transcription of total RNA, isolated from murine brain tissue, 293, 143B, A-431, HeLa S3, HepG2, MCF-7, NIH-3T3, SH-SY5Y and U-87 cells, was performed from oligo$(dT)_{17}$ primers using RevertAid Reverse Transcriptase (Fermentas). The composition of the 5′-ends of the isoform-specific cDNAs was analyzed by PCRs in the presence of primer pair 5′-GGGGCGCTCTGGGTGTTGTA (exon 1) and 5′-CATGAAGTAGTGACAGATGGTTGG (exon 8). Preparations of cDNA from murine brain tissue and NIH-3 T3 cells were subject to PCR analysis using primer pair 5′-AGAGCAGTCGGTGACAGTCC (exon 1) and 5′-CGAAAAACACGATATCAGGCTTTAC (exon 10/11 transition).

Amplification of the full-length ORFs of human *SIRT2* isoforms by nested-PCRs was performed using primer pair 5′-GCCCTTTACCAACATGGCTGC (exon 1) and 5′-GTCTCCAATAAGCAATGTCTTCTG (exon 16) in primary PCRs. Gel-purified products were used as template in secondary PCRs. The isoform 5-specific 5′-fragment was

amplified using primer pair 5′-GGGGCGCTCTG GGTGTTGTA (exon 1) and 5′-CAGATGACTCTGCCA CGGTC (exon 1/5 transition). The isoform 5-specific 3′-fragment was amplified using primer pair 5′-CATGGCA GAGCCAGACCGTC (exon 1/5 transition) and 5′-CTGC TGGTTAAGAGGGGGCC (exon 16). Full-length *SIRT2* ORFs were amplified using a non-discriminating primer pair 5′-GGGGCGCTCTGGGTGTTGTA (exon 1) and 5′-CTGCTGGTTAAGAGGGGGCC (exon 16).

Vector construction

The ORFs of the *SIRT2* isoforms were amplified from 293 cDNA using forward primer 5′-agttaagcttgccacc ATGGCAGAGCCAGACCG (isoforms 1 and 5) and 5′-agt taagcttgccaccATGGACTTCCTGCGGAAC (isoform 2) along with reverse primer 5′-atcgtctagaacaCTGGGGT TTCTCCCTCTC and ligated into eukaryotic expression vector pcDNA3.1/V5-His (Invitrogen/Life Technologies) via HindIII and XbaI sites.

For prokaryotic expression of the SIRT2 isoforms, the encoding ORFs were amplified from the corresponding eukaryotic vectors using forward primer 5′-gcatccATGGCA GAGCCAGACCCCTCTCACCC (isoform 1), 5′-cgtgccATG GACTTCCTGCGGAACTTATTC (isoform 2) and 5′-gcatcc ATGGCAGAGCCAGACCGTCGCAGAG (isoform 5) along with reverse primer 5′-ggacggatccTCAATGGTGATGGTGAT GATGACC. The DNA fragments were ligated into pET9d (Novagen) via NcoI and BamHI sites.

Mutation of the base triplet encoding the catalytic histidine (i.e., H187 in isoform 1) into a tyrosine codon and the mutation of the second ATG triplet in the ORF of isoform 1 into an alanine codon was performed by PCR-based site-directed mutagenesis.

For prokaryotic expression of the acetyltransferase domain of p300 (HATc), the encoding ORF (spanning residues 1284–1845) was subcloned from a pT7T vector containing the human p300 cDNA (pT7Ts-p300 [51])[§] by PCR amplification using forward primer 5′-gcgaattcagcggccgcAAAGAAAA TAAGTTTTCTGCT and reverse primer 5′- gcgtacgtcgac CCTGTTGCTGCCCAACCACACC. The DNA fragment was ligated into pSXG [52] via EcoRI and SalI restriction sites.

For expression of the SIRT2 isoforms in the context of their endogenous 5′-UTRs, isoform-specific 5′-UTRs were amplified from 293 cDNA using forward primer 5′-ctcgtttagt gaaAGAGTATTCGGGAGGACTACAACTCTC along with reverse primer 5′-GCGCGGTGCTGAAGCCC. The resulting PCR products were fused to the downstream ORFs and subsequently inserted into pFLAG-CMV4 via EcoICRI and BamHI sites.

Mutation of the base triplet encoding the start codon of isoform 1 into a non-transcription initiating AAG triplet was performed by PCR-based site-directed mutagenesis.

Immunocytochemistry and fluorescence microscopy

HeLa S3 cells grown on cover slips were fixed 24 h post transfection with 4% formaldehyde in PBS, permeabilized with 0.5% Triton X-100 in PBS and blocked for 1 h at room temperature using complete culture medium. Cells were incubated with primary antibodies overnight at 4 °C, washed twice with PBS and once with PBS containing 0.1% (v/v) Triton X-100 prior to adding secondary antibodies. Following 1 h incubation at room temperature, chromatin was stained with 4′,6-diamidino-2-phenylindole and cells were subjected to fluorescence microscopy. Images were acquired using an inverted Leica DMI 6000B fluorescence microscope equipped with a 100× oil immersion objective (numerical aperture, 1.4).

Cell fractionation

293 cells were grown in 60 mm dishes and transfected with SIRT2 encoding vectors. Twenty-four hours after transfection, cells were trypsinized and resuspended in DMEM medium. Cells were centrifuged (900 rpm, 5 min) and washed once with PBS. Nuclear extracts were prepared as described earlier [53] with following modifications: The supernatant, after NP-40 addition, was collected as cytoplasmic fraction and not further processed. Genomic DNA was removed by adding 2 units DNase I (Promega), 5 mM $MgCl_2$ and 5 mM $CaCl_2$ to the nuclear pellet followed by 20 min incubation at 37 °C. Fractions were subject to immunoblot analyses.

Protein expression and purification

Recombinant proteins were expressed in *Escherichia coli* strain BL21(DE3)-CodonPlus cells (Stratagene) grown in 2× YTG medium supplemented with appropriate antibiotics. Expression was induced at OD_{600nm} of 0.6 with 300 μM IPTG and 5 μM zinc acetate and conducted overnight at 18 °C.

Recombinant SIRT2 isoforms were purified by Ni^{2+}-NTA chromatography (Qiagen) according to the manufacturer's protocol using the following buffers: All buffer contained 50 mM Tris–HCl (pH 7.6) and 500 mM NaCl; additionally, the lysis/binding buffer contained 5 mM imidazole, the first washing buffer contained 20 mM imidazole, the second washing buffer contained 50 mM imidazole and the elution buffer contained 500 mM imidazole.

Recombinant GST and p300-HATs were affinity purified as described earlier [52].

All proteins were dialyzed (10,000 molecular weight cutoff) against deacetylation buffer [50 mM Tris–HCl (pH 7.6), 137 mM NaCl, 2.7 mM KCl and 10 mM $MgCl_2$] supplemented with 0.5 mM DTT.

Deacetylation assays

Deacetylation activity of recombinant SIRT2 isoforms was assayed using four different approaches.

The deacetylation activity of purified SIRT2 isoforms was measured using the CycLex SIRT2 Deacetylation Fluorometric Assay Kit (MBL International). Reactions were performed with 0.8 μM SIRT2 according to the manufacturer's protocol. All given values were blank corrected.

The deacetylation activity of purified SIRT2 isoforms toward specific targets was carried out in deacetylation buffer using 1 mM purified SIRT2, 1 mM NAD^+ and 0.4 mM target protein. Reactions were incubated at 30 °C for 2 h. Control samples were incubated in the presence of 20 mM nicotinamide (Nam). The reactions were terminated with SDS sample buffer and the acetylation state of target proteins was monitored by immunoblot analyses.

The deacetylation activity of SIRT2 isoforms in soluble fractions of lysates from bacteria expressing theses proteins

was carried out as described above with the following modification: The amount of the SIRT2 isoforms in the lysates was quantified by immunoblot analysis. Subsequently, the SIRT2 content in the bacterial lysates was adjusted by dilution with lysate from bacteria harboring the "empty" vector. Cell extracts containing a total of 20 μg protein were mixed with 20 μg of lysates from bacteria expressing p300-HATc or 5 μg of chemically acetylated histones[‖].

In living bacteria, the deacetylation activity of the three SIRT2 isoforms was monitored by co-expression with p300-HATc in *E. coli*. Bacteria were transformed with equimolar amounts of expression vectors and grown on agar plates in the presence of appropriate antibiotics. One colony was transferred into 15 ml of 2× YTG medium and expression was induced as described above. Subsequently, the bacteria were grown overnight at 18 °C. The OD_{600nm} of the cultures was determined and cells were harvested by centrifugation. Cells were lysed with SDS sample buffer and equal protein amounts (estimated by OD_{600nm} value) were subjected to immunoblot analyses.

SIRT2-p300 interaction assay

Proteins were purified as described above and dialyzed overnight against HAT buffer [50 mM Tris–HCl (pH 8), 137 mM NaCl, 2.7 mM KCl, 0.5 mM DTT and 10% (v/v) glycerol]. Protein concentrations were determined using BCA protein assay kit (Pierce). Proteins were mixed and diluted to reach 1:5 molar ratio (p300/GST:SIRT2). Acetyl-CoA, NAD^+ or buffer was added as indicated and samples were incubated at 30 °C for 2 h, followed by overnight incubation at 4 °C. Pulldown was performed by incubating samples with glutathione Sepharose in washing buffer [50 mM Tris–HCl (pH 8), 200 mM NaCl and 0.1% (v/v) NP-40] for 1 h at 4 °C. Samples were subsequently washed four times with washing buffer and once with 50 mM Tris–HCl (pH 8). Bound proteins were detected by immunoblot analyses.

Protein stability measurement

Bacterially expressed SIRT2 isoforms were purified by Ni^{2+}-NTA chromatography as described above and were eluted with low ionic strength elution buffer [50 mM Tris–HCl (pH 8), 50 mM NaCl and 500 mM imidazole]. Samples were diluted 1:2 with ion-exchange buffer A [50 mM Tris–HCl (pH 8)] and subjected to anion-exchange chromatography using MonoQ 5/50 column (GE Healthcare) on an automated ÄKTA purifier system (Amersham Bioscience) with a linear gradient from buffer A to buffer B (buffer A containing 1 M NaCl). Subsequently, the proteins were dialyzed overnight against denaturation buffer [50 mM Tris–HCl (pH 8) and 250 mM NaCl].

Samples were adjusted to indicate final concentrations of GdmCl by dilution with 8 M GdmCl in denaturation buffer and incubated for 1 h at 25 °C prior to measuring tryptophan fluorescence. Emission spectra were recorded from 300 to 400 nm (5 nm bandwidth) at 25 °C after excitation at 290 nm (5 nm bandwidth) using a LS 50B fluorescence spectrometer (Perkin Elmer). Data were blank corrected and the ratios of the fluorescence intensities at 330 and 360 nm calculated.

Protein structure prediction

Structural models of SIRT2 isoforms 1 and 5 were generated using the Web-based homology and threading server Swiss-Model (automated mode) [54–56], HHpred/MODELLER (best template mode) [57–60], M4T Server Version 3.0 [61,62], I-Tasser (restrain-free) [63,64] and RaptorX (multiple template refraining) [65]. Manual model–structure comparison and generation of electrostatic surface potential maps were performed using the PyMOL Molecular Graphics System, Version 1.3 Schrödinger, LLC.

Acknowledgments

We thank Gro E. K. Bjerga for the preparation of the pSXG-HATc expression vector and Marc Niere for critical reading of the manuscript. This work was financially supported by the European Community's Seventh Framework Programme (FP7/2007-2013) under grant agreement number 238176, the Norwegian Cancer Society (Kreftforeningen) and the Lauritz Meltzers Høyskolefond (Meltzerfondet).

Appendix A. Supplementary data

Supplementary data to this article can be found online at http://dx.doi.org/10.1016/j.jmb.2013.10.027.

Received 8 August 2013;
Received in revised form 19 October 2013;
Accepted 22 October 2013
Available online 29 October 2013

Keywords:
protein structure;
p300;
molecular genetics;
localization;
NAD+-dependent signaling

†The nucleotide sequences reported in this paper have been submitted to the GenBank database with accession numbers KF032392 (murine *Sirt2* transcript variant 3) and KF032391 (human *SIRT2* transcript variant 5).

‡The nucleotide sequence of human *SIRT2* transcript variant 3 can be accessed in the GenBank database under accession number NM_001193286.1 and that of the one of transcript variant 4 can be accessed under GenBank accession number NR_034146.1.

§The amino acid sequence of p300 can be accessed through the UniProtKB database under UniProt number Q09472.

‖Chemically acetylated *Xenopus laevis* histone octamers were a kind gift of Mariano Oppikofer and Susan Gasser from the Friedrich Miescher Institute for Biomedical Research in Basel.

Abbreviations used:
NES, nuclear export signal; NLS, nuclear localization signal; GdmCl, guanidinium hydrochloride; wt, wild type; ORF, open reading frame; UTR, untranslated region.

References

[1] Asher G, Schibler U. Crosstalk between components of circadian and metabolic cycles in mammals. Cell Metab 2011;13:125–37.

[2] Houtkooper RH, Pirinen E, Auwerx J. Sirtuins as regulators of metabolism and healthspan. Nat Rev Mol Cell Biol 2012;13:225–38.

[3] Kim HS, Vassilopoulos A, Wang RH, Lahusen T, Xiao Z, Xu X, et al. SIRT2 maintains genome integrity and suppresses tumorigenesis through regulating APC/C activity. Cancer Cell 2011;20:487–99.

[4] McBurney MW, Yang X, Jardine K, Hixon M, Boekelheide K, Webb JR, et al. The mammalian SIR2alpha protein has a role in embryogenesis and gametogenesis. Mol Cell Biol 2003;23:38–54.

[5] Vaquero A. The conserved role of sirtuins in chromatin regulation. Int J Dev Biol 2009;53:303–22.

[6] Wang RH, Sengupta K, Li C, Kim HS, Cao L, Xiao C, et al. Impaired DNA damage response, genome instability, and tumorigenesis in SIRT1 mutant mice. Cancer Cell 2008;14:312–23.

[7] Bao J, Lu Z, Joseph JJ, Carabenciov D, Dimond CC, Pang L, et al. Characterization of the murine SIRT3 mitochondrial localization sequence and comparison of mitochondrial enrichment and deacetylase activity of long and short SIRT3 isoforms. J Cell Biochem 2010;110:238–47.

[8] Flick F, Luscher B. Regulation of sirtuin function by posttranslational modifications. Front Pharmacol 2012;3:29.

[9] Matsushita N, Yonashiro R, Ogata Y, Sugiura A, Nagashima S, Fukuda T, et al. Distinct regulation of mitochondrial localization and stability of two human Sirt5 isoforms. Genes Cells 2011;16:190–202.

[10] Nemoto S, Fergusson MM, Finkel T. Nutrient availability regulates SIRT1 through a forkhead-dependent pathway. Science 2004;306:2105–8.

[11] Shah ZH, Ahmed SU, Ford JR, Allison SJ, Knight JR, Milner J. A deacetylase-deficient SIRT1 variant opposes full-length SIRT1 in regulating tumor suppressor p53 and governs expression of cancer-related genes. Mol Cell Biol 2012;32:704–16.

[12] Wang HF, Li Q, Feng RL, Wen TQ. Transcription levels of sirtuin family in neural stem cells and brain tissues of adult mice. Cell Mol Biol (Noisy-le-grand) 2012:OL1737–43.

[13] Afshar G, Murnane JP. Characterization of a human gene with sequence homology to *Saccharomyces cerevisiae* SIR2. Gene 1999;234:161–8.

[14] Michishita E, Park JY, Burneskis JM, Barrett JC, Horikawa I. Evolutionarily conserved and nonconserved cellular localizations and functions of human SIRT proteins. Mol Biol Cell 2005;16:4623–35.

[15] North BJ, Marshall BL, Borra MT, Denu JM, Verdin E. The human Sir2 ortholog, SIRT2, is an NAD^+-dependent tubulin deacetylase. Mol Cell 2003;11:437–44.

[16] Hisahara S, Chiba S, Matsumoto H, Tanno M, Yagi H, Shimohama S, et al. Histone deacetylase SIRT1 modulates neuronal differentiation by its nuclear translocation. Proc Natl Acad Sci U S A 2008;105:15599–604.

[17] Tanno M, Sakamoto J, Miura T, Shimamoto K, Horio Y. Nucleocytoplasmic shuttling of the NAD^+-dependent histone deacetylase SIRT1. J Biol Chem 2007;282:6823–32.

[18] Iwahara T, Bonasio R, Narendra V, Reinberg D. SIRT3 functions in the nucleus in the control of stress-related gene expression. Mol Cell Biol 2012;32:5022–34.

[19] Scher MB, Vaquero A, Reinberg D. SirT3 is a nuclear NAD^+-dependent histone deacetylase that translocates to the mitochondria upon cellular stress. Genes Dev 2007;21:920–8.

[20] Vaquero A, Scher MB, Lee DH, Sutton A, Cheng HL, Alt FW, et al. SirT2 is a histone deacetylase with preference for histone H4 Lys 16 during mitosis. Genes Dev 2006;20:1256–61.

[21] North BJ, Verdin E. Interphase nucleo-cytoplasmic shuttling and localization of SIRT2 during mitosis. PLoS One 2007;2: e784.

[22] Beirowski B, Gustin J, Armour SM, Yamamoto H, Viader A, North BJ, et al. Sir-two-homolog 2 (Sirt2) modulates peripheral myelination through polarity protein Par-3/atypical protein kinase C (aPKC) signaling. Proc Natl Acad Sci U S A 2011;108:E952–61.

[23] Jiang W, Wang S, Xiao M, Lin Y, Zhou L, Lei Q, et al. Acetylation regulates gluconeogenesis by promoting PEPCK1 degradation via recruiting the UBR5 ubiquitin ligase. Mol Cell 2011;43:33–44.

[24] Zhu H, Zhao L, Wang E, Dimova N, Liu G, Feng Y, et al. The QKI-PLP pathway controls SIRT2 abundance in CNS myelin. Glia 2012;60:69–82.

[25] Serrano L, Martinez-Redondo P, Marazuela-Duque A, Vazquez BN, Dooley SJ, Voigt P, et al. The tumor suppressor SirT2 regulates cell cycle progression and genome stability by modulating the mitotic deposition of H4K20 methylation. Genes Dev 2013;27:639–53.

[26] Vempati RK, Jayani RS, Notani D, Sengupta A, Galande S, Haldar D. p300-mediated acetylation of histone H3 lysine 56 functions in DNA damage response in mammals. J Biol Chem 2010;285:28553–64.

[27] Black JC, Mosley A, Kitada T, Washburn M, Carey M. The SIRT2 deacetylase regulates autoacetylation of p300. Mol Cell 2008;32:449–55.

[28] Han Y, Jin YH, Kim YJ, Kang BY, Choi HJ, Kim DW, et al. Acetylation of Sirt2 by p300 attenuates its deacetylase activity. Biochem Biophys Res Commun 2008;375:576–80.

[29] Inoue T, Hiratsuka M, Osaki M, Yamada H, Kishimoto I, Yamaguchi S, et al. SIRT2, a tubulin deacetylase, acts to block the entry to chromosome condensation in response to mitotic stress. Oncogene 2007;26:945–57.

[30] Maxwell MM, Tomkinson EM, Nobles J, Wizeman JW, Amore AM, Quinti L, et al. The Sirtuin 2 microtubule deacetylase is an abundant neuronal protein that accumulates in the aging CNS. Hum Mol Genet 2011;20:3986–96.

[31] Frye RA. Phylogenetic classification of prokaryotic and eukaryotic Sir2-like proteins. Biochem Biophys Res Commun 2000;273:793–8.

[32] Hamamori Y, Sartorelli V, Ogryzko V, Puri PL, Wu HY, Wang JY, et al. Regulation of histone acetyltransferases p300 and PCAF by the bHLH protein twist and adenoviral oncoprotein E1A. Cell 1999;96:405–13.

[33] Thompson PR, Wang D, Wang L, Fulco M, Pediconi N, Zhang D, et al. Regulation of the p300 HAT domain via a novel activation loop. Nat Struct Mol Biol 2004;11:308–15.

[34] Banik U, Saha R, Mandal NC, Bhattacharyya B, Roy S. Multiphasic denaturation of the lambda repressor by urea and its implications for the repressor structure. Eur J Biochem 1992;206:15–21.

[35] North BJ, Verdin E. Mitotic regulation of SIRT2 by cyclin-dependent kinase 1-dependent phosphorylation. J Biol Chem 2007;282:19546–55.
[36] Kozak M. Point mutations define a sequence flanking the AUG initiator codon that modulates translation by eukaryotic ribosomes. Cell 1986;44:283–92.
[37] Kosugi S, Hasebe M, Tomita M, Yanagawa H. Systematic identification of cell cycle-dependent yeast nucleocytoplasmic shuttling proteins by prediction of composite motifs. Proc Natl Acad Sci U S A 2009;106:10171–6.
[38] Borra MT, O'Neill FJ, Jackson MD, Marshall B, Verdin E, Foltz KR, et al. Conserved enzymatic production and biological effect of *O*-acetyl-ADP-ribose by silent information regulator 2-like NAD^+-dependent deacetylases. J Biol Chem 2002;277:12632–41.
[39] Dan L, Klimenkova O, Klimiankou M, Klusman JH, van den Heuvel-Eibrink MM, Reinhardt D, et al. The role of sirtuin 2 activation by nicotinamide phosphoribosyltransferase in the aberrant proliferation and survival of myeloid leukemia cells. Haematologica 2012;97:551–9.
[40] Dryden SC, Nahhas FA, Nowak JE, Goustin AS, Tainsky MA. Role for human SIRT2 NAD-dependent deacetylase activity in control of mitotic exit in the cell cycle. Mol Cell Biol 2003;23:3173–85.
[41] Finnin MS, Donigian JR, Pavletich NP. Structure of the histone deacetylase SIRT2. Nat Struct Biol 2001;8:621–5.
[42] Moniot S, Schutkowski M, Steegborn C. Crystal structure analysis of human Sirt2 and its ADP-ribose complex. J Struct Biol 2013;182:136–43.
[43] Zhao K, Chai X, Marmorstein R. Structure and substrate binding properties of cobB, a Sir2 homolog protein deacetylase from *Escherichia coli*. J Mol Biol 2004;337:731–41.
[44] Nahhas F, Dryden SC, Abrams J, Tainsky MA. Mutations in SIRT2 deacetylase which regulate enzymatic activity but not its interaction with HDAC6 and tubulin. Mol Cell Biochem 2007;303:221–30.
[45] Rual JF, Venkatesan K, Hao T, Hirozane-Kishikawa T, Dricot A, Li N, et al. Towards a proteome-scale map of the human protein–protein interaction network. Nature 2005;437:1173–8.
[46] Pandithage R, Lilischkis R, Harting K, Wolf A, Jedamzik B, Luscher-Firzlaff J, et al. The regulation of SIRT2 function by cyclin-dependent kinases affects cell motility. J Cell Biol 2008;180:915–29.
[47] Oppenheimer H, Gabay O, Meir H, Haze A, Kandel L, Liebergall M, et al. 75-kd sirtuin 1 blocks tumor necrosis factor alpha-mediated apoptosis in human osteoarthritic chondrocytes. Arthritis Rheum 2012;64:718–28.
[48] Gordon CA, Hartono SR, Chedin F. Inactive DNMT3B splice variants modulate de novo DNA methylation. PLoS One 2013;8:e69486.
[49] Migueleti DL, Smetana JH, Nunes HF, Kobarg J, Zanchin NI. Identification and characterization of an alternatively spliced isoform of the human protein phosphatase 2Aalpha catalytic subunit. J Biol Chem 2012;287:4853–62.
[50] Pandya MJ, Golderer G, Werner ER, Werner-Felmayer G. Interaction of human GTP cyclohydrolase I with its splice variants. Biochem J 2006;400:75–80.
[51] Li Q, Herrler M, Landsberger N, Kaludov N, Ogryzko VV, Nakatani Y, et al. *Xenopus* NF-Y pre-sets chromatin to potentiate p300 and acetylation-responsive transcription from the *Xenopus* hsp70 promoter *in vivo*. EMBO J 1998;17:6300–15.
[52] Ragvin A, Valvatne H, Erdal S, Arskog V, Tufteland KR, Breen K, et al. Nucleosome binding by the bromodomain and PHD finger of the transcriptional cofactor p300. J Mol Biol 2004;337:773–88.
[53] Schreiber E, Matthias P, Muller MM, Schaffner W. Rapid detection of octamer binding proteins with "mini-extracts", prepared from a small number of cells. Nucleic Acids Res 1989;17:6419.
[54] Arnold K, Bordoli L, Kopp J, Schwede T. The SWISS-MODEL workspace: a Web-based environment for protein structure homology modelling. Bioinformatics 2006;22:195–201.
[55] Kiefer F, Arnold K, Kunzli M, Bordoli L, Schwede T. The SWISS-MODEL repository and associated resources. Nucleic Acids Res 2009;37:D387–92.
[56] Peitsch MC. Protein modeling by e-mail. Bio-Technology 1995;13:658–60.
[57] Eswar N, Webb B, Marti-Renom MA, Madhusudhan MS, Eramian D, Shen MY, et al. Comparative protein structure modeling using Modeller. Curr Protoc Bioinformatics 2006 [Chapter 5, Unit 5 6].
[58] Sali A, Blundell TL. Comparative protein modelling by satisfaction of spatial restraints. J Mol Biol 1993;234:779–815.
[59] Soding J. Protein homology detection by HMM-HMM comparison. Bioinformatics 2005;21:951–60.
[60] Soding J, Biegert A, Lupas AN. The HHpred interactive server for protein homology detection and structure prediction. Nucleic Acids Res 2005;33:W244–8.
[61] Fernandez-Fuentes N, Madrid-Aliste CJ, Rai BK, Fajardo JE, Fiser A. M4T: a comparative protein structure modeling server. Nucleic Acids Res 2007;35:W363–8.
[62] Fernandez-Fuentes N, Rai BK, Madrid-Aliste CJ, Fajardo JE, Fiser A. Comparative protein structure modeling by combining multiple templates and optimizing sequence-to-structure alignments. Bioinformatics 2007;23:2558–65.
[63] Roy A, Kucukural A, Zhang Y. I-TASSER: a unified platform for automated protein structure and function prediction. Nat Protoc 2010;5:725–38.
[64] Zhang Y. I-TASSER server for protein 3D structure prediction. BMC Bioinformatics 2008;9:40.
[65] Kallberg M, Wang H, Wang S, Peng J, Wang Z, Lu H, et al. Template-based protein structure modeling using the RaptorX Web server. Nat Protoc 2012;7:1511–22.

Constitutive nuclear localization of an alternatively spliced sirtuin-2 isoform

Johannes G.M. Rack, Magali R. VanLinden, Timo Lutter, Rein Aasland, and Mathias Ziegler

Department of Molecular Biology
University of Bergen
Postbox 7803
5020 Bergen
Norway

Supplementary Material

Figures S1 SIRT2 isoform 5 is composed of exon 1 and exons 5-16. Nested PCR analysis of cDNAs derived from 293 and SH-SY5Y cells. The exon composition and length of the amplified DNA fragments is shown below the agarose gels, triangles indicate the location of primer sequences. The size of selected marker bands (bp) is indicated. The major product of the primary reactions is a ~2000 bp fragment. Secondary PCRs were carried out with gel purified primary PCR products using three different primer pairs: (i) for isoform 5- specific amplification of the 5' region, (ii) for isoform 5-specific amplification of the 3' region, and (iii) for non-discriminative amplification of all *SIRT2* cDNAs. Reactions (i) and (ii) resulted in a specific amplicon that originated from a splice event linking exon 1 and exons 5-16 as revealed by DNA sequence analysis. Reaction (iii) resulted in the amplification of three specific products corresponding to isoforms 1, 2, and 5 as revealed by DNA sequence analyses.

Figures S2 Multiple sequence alignment of SIRT2 isoforms. Isoform 2 is a truncated form of isoform 1 lacking the first 37 residues, whereas in isoform 5 residues 6-76 are substituted for an arginine. The structurally resolved residues of isoform 1 are highlighted in blue. The NES within the N-terminal region is indicated in red, the NLS predicted by cNLS mapper in violet, α-helices in orange and β-sheets in grayblue. The catalytic domain as defined by multiple sequence alignment and structural data is framed: the black frame indicates the Rossmann-fold and the gray frame the small zinc-

containing subdomain. Residues involved in cosubstrate binding and catalytic mechanism are indicated by (#), zinc- coordinating cysteine by (◊), and tryptophans by (‡).

Figures S3 Structural models of SIRT2 isoform 5 are similar to the solved structure. (a) Summary of the obtained models and comparison of their structural divergence to the solved structure (pdb: **3zgo**). (b) Overlay of SIRT2 structure and isoform 5 models in ribbon representation. The positions of α-helices α0, α1 (red) and α15 are indicated. Note, that the loop between α0 and α1 is not resolved in the structure (purple line; upper panel). Both α0 and α1 are not present in isoform 5. Secondary structure elements are colored: α-helices in bluegray, β-sheets in orange, and loop regions in black. The coordinated zinc atom is displayed in dark red and the catalytic histidine (H187, isoform 1) in stick representation. The C- and N-termini (N_{i1}: isoform 1, N_{i5}: isoform 5) are indicated. All obtained models adopt the SIRT2 catalytic domain structure and display most structural conservation within the secondary structure elements as well as most divergence within the loop regions.

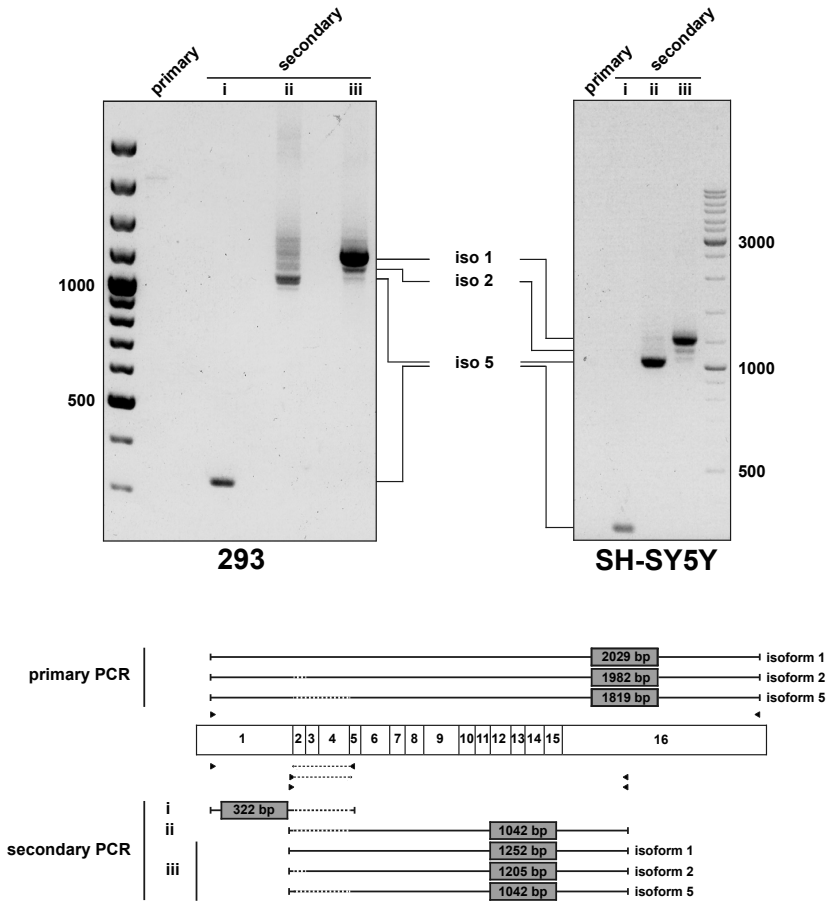

Supplementary Figure S1

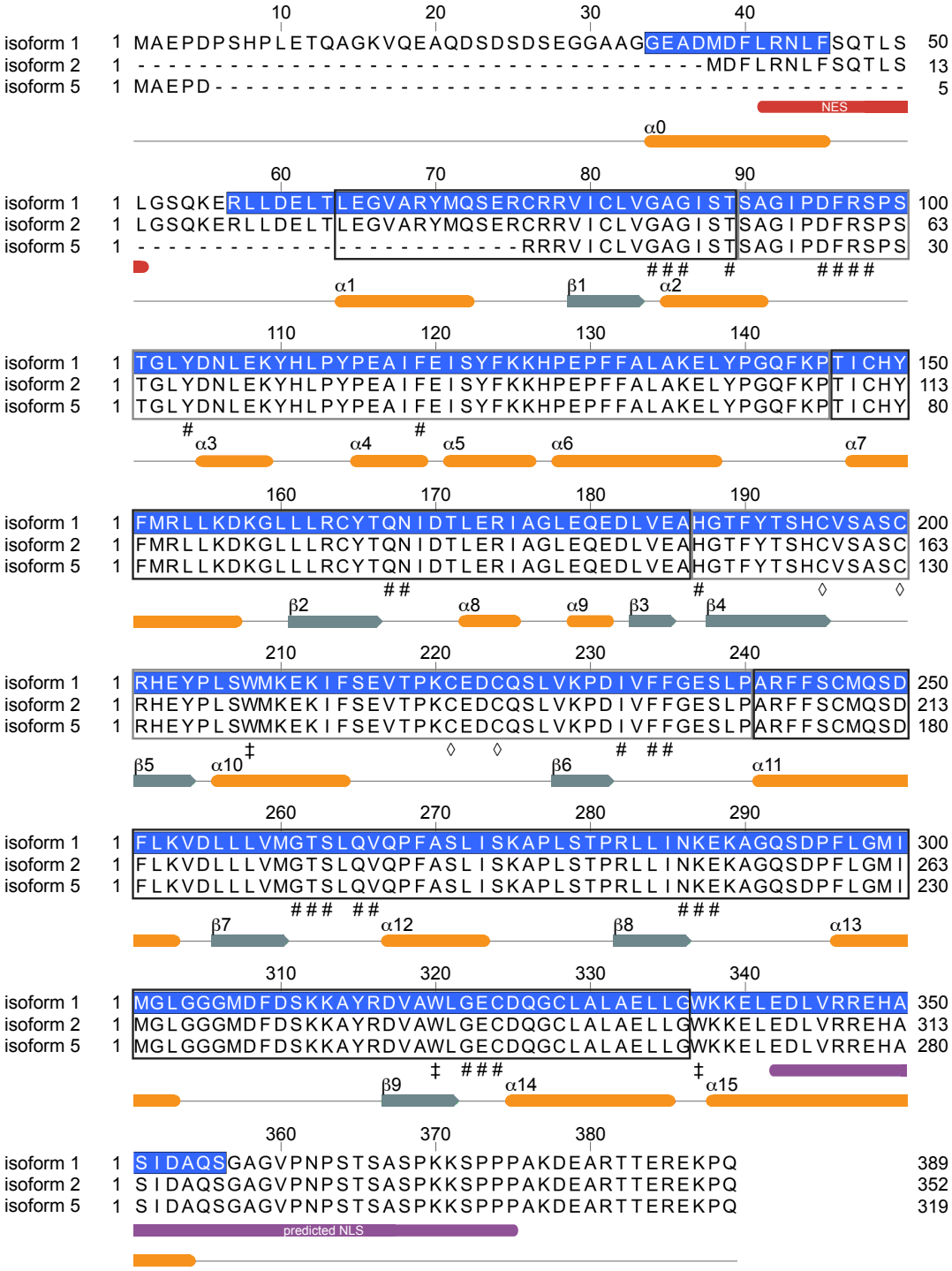

Supplementary Figure S2

(a)

modeling program		RMSD (Å)	atoms aligned
HHpred/MODELLER		0.201	221
M4T		0.196	215
RaptorX		0.139	217
I-Tasser	model 1	0.698	238
	model 2	0.568	243
	model 3	0.722	248
	model 4	0.446	240
	model 5	0.885	248

(b)

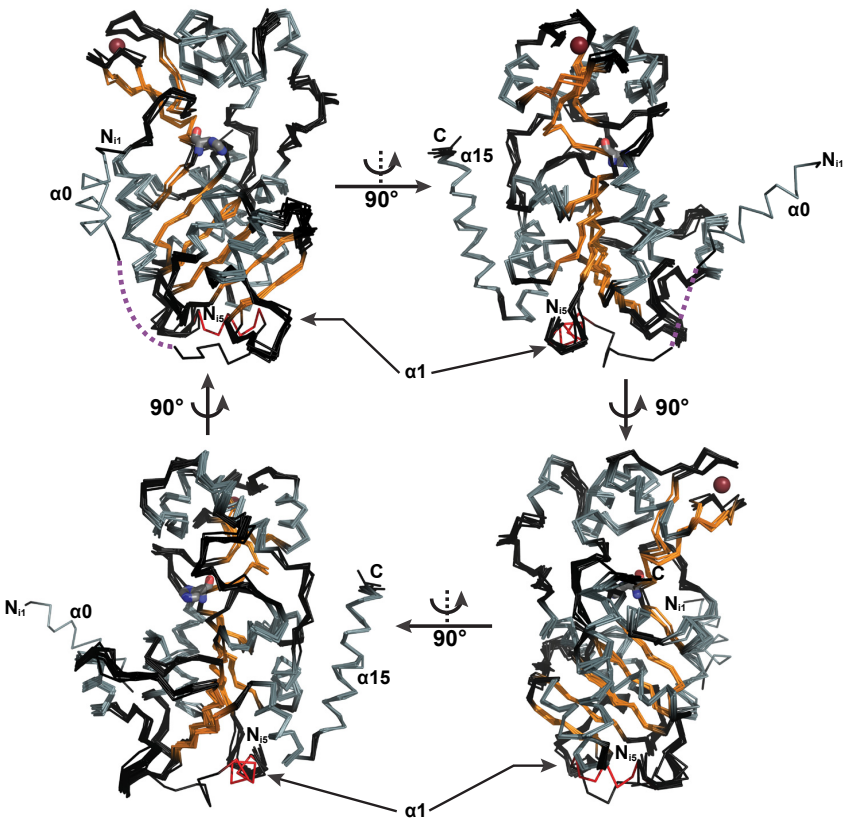

Supplementary Figure S3